INTENSITY LIMITATIONS FROM COHERENT

INSTABILITIES IN STORAGE RINGS

by

Xiao-tong Yu

B.S., University of Science and Technology of China
(1986)

M.S., Institute of Theoretical Physics, Academia Sinica
(1988)

Submitted to the Department of Physics
in Partial Fulfillment of the
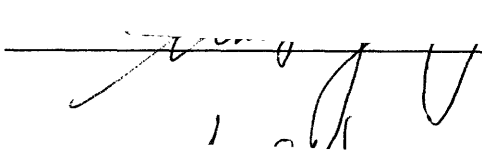Requirements for the
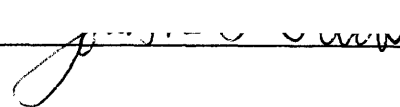Degree of

DOCTOR OF PHILOSOPHY
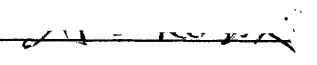
at the

Massachusetts Institute of Technology

March 1994

Signature of Author _____
Department of Physics
March 17, 1994

Certified by _____
Jonathan S. Wurtele
Thesis Supervisor

Accepted by _____
George F. Koster
Cha. ..an, Graduate Committee

INTENSITY LIMITATIONS FROM

COHERENT INSTABILITIES

IN STORAGE RINGS

by

Xiao-tong Yu

ABSTRACT

The performance of modern synchrotron light sources and circular colliders relies on sustaining very short bunches of high-peak currents. The bunch lengthening instability, i.e., the sudden increase of both the bunch length and the energy spread at a threshold current, can be a serious limitation. For short (electron) bunches, the bunch lengthening instability has traditionally been explained by the coupling of two adjacent synchrotron modes. However, mode coupling has not been observed experimentally when the bunch current reaches the threshold. In this thesis, we propose a new instability mechanism for bunch lengthening which occurs with an uncoupled synchrotron mode. We found that a critical role is played by the nonlinearity of the static wake force: Without it, the system is described by the Sacherer equation, and does not have an unstable eigenmode. The nonlinearity of the static wake force distorts the electron bunch's equilibrium density from its Gaussian shape. By including this phenomenon we derived an improved Sacherer equation which has unstable eigenmodes when the bunch current exceeds a threshold value. While the Sacherer equation is linear in the bunch current, the new terms in our equation are propor-

tional to the square of the bunch current. Since the Sacherer equation can be written as an eigenvalue problem for a symmetric operator, the correction terms, which are asymmetric operators, push the real eigenvalues into the complex plane when the current reaches some threshold value. Analytical expressions for these correction terms are obtained with a parameterization scheme for the equilibrium density. For short bunches ($\omega_r \sigma < 0.7$), where σ is the equilibrium bunch length and ω_r is the frequency of the broadband resonator impedance, the four lowest order cummulants are sufficient to construct a density function, which approximates the equilibrium bunch distribution to great accuracy. We also develop a multiparticle multiperiod simulation code, which has three major improvements over the existing codes. The simulation verifies the theoretical predictions based on the instability analysis of our improved Sacherer equation. We study the SPEAR II parameters analytically and numerically. Approximating the SPEAR impedance by a $Q = 1$ resonator, the simulation gives a threshold current around 45mA. The instability analysis based on the improved Sacherer equation gives dipole and quadrupole modes as the first unstable modes at 50mA. In the experiment, the quadrupole mode was observed to go unstable first. We also compare our theoretical model with the observations made at LEP. Both the experiment and our instability analysis identify the dipole mode as the first to become unstable for a threshold of 0.113mA, comparing well with the observed threshold at 0.1mA. Since the bunch lengthening instability is determined by $\omega_r \sigma$ and a dimensionless coupling parameter ξ, we also calculate the critical coupling ξ_c as a function of $\omega_r \sigma$, and the result agrees very well with the numerical multimode Vlasov analysis of Oide and Yokoya for short bunches.

Thesis Supervisor: Dr. Jonathan S. Wurtele

Title: Associate Professor of Physics

3

Acknowledgments

I would like to thank Prof. Jonathan Wurtele for his continuous support throughout my graduate study at MIT. His guidance and encouragement have made this thesis possible. Special thanks are also due to the following persons from whom I have learned a great deal of accelerator physics: Dr. Alex Chao, Dr. Bo Chen, Prof. Senyu Chen, Dr. Samir Dutt, Dr. Ken Jacobs, Dr. David Whittum. I would also like to thank Prof. Ulrich Becker and Prof. Stanley Kowalski for reading the manuscript and giving me valuable comments.

To Shien-chi Chen, Ronson Chu, Jun Feng, Bob Gormley, Chi-tien Hsu, Chi-kang Li, Leon Lin, Dominic Sartorio, Shuang-he Shi, Gennady Shvets, Gerasimos Tinios, Sam Tsui, James Wei, Lin Wang, Yin Wang, Song Zhao and many others, who have made the Plasma Fusion Center a friendly working environment, I would like to express my appreciation. I am grateful to Ronson Chu for giving me the latex template for writing my thesis and to Leon Lin for various his help in using NCAR graphics packages. I would like to thank James Wei, Mike Huang and Shirley Chi for making my life at Cambridge tolerable, and to my long time friends from the University of Science and Technology of China for their insights and generous help during various critical moments of my life.

I like to thank my parents Kong-ming Yu, Hui-ming Lin and my sister Shonnon Yu for their love, care and support throughout the years. I like to thank my uncles Hui-zhong Lin and Dong-hai Yu for their generosity. Finally I would like to thank my grandmother Nü-zuo Huang for her unfailing love and to her this dissertation is dedicated.

Contents

List of Figures

List of Tables

Chapter 1

Introduction

1.1 Coherent Instabilities in Accelerators

The subject of collective instabilities in high-energy accelerators has been studied since the late 1950s and early 1960s. The importance of the subject lies in the fact that it is one of the main factors that determine the ultimate performance of the accelerator. The advancement of this subject over the years is evidenced by the discovery and curing of several collective instability mechanisms. Each accelerator, when pushed to the limit for its for its performance, will encounter some intensity limit. As this limit is analyzed, understood, and possibly cured, a new limit emerges. The process repeats, and the end result is the improved understanding and higher performance of the accelerator. The confidence gained by understanding and controlling collective instabilities in turn provides a basis for ever more advanced accelerators. Without this knowledge, there could be no linear colliders, high-luminosity circular colliders, B-factories, free-electron laser drivers, modern synchrotron light sources, inertial fusion drivers, etc. Today, the study of the collective instabilities has grown into a large field of activities: methods to measure the impedance of the ring or linac, novel beam diagnostic techniques, beam cooling techniques, numerical simulation methods, calculation of the wake fields and impedances of complex objects, impedance budgeting in accelerator design, feedback systems and numerous theo-

retical studies. Each activity constitutes an important research area; each must be understood or implemented in the accelerators of the future.

Accelerators must control and manipulate the motion of charged particles. To design an accelerator, one starts by considering the motion of a single particle. To describe the dynamics of a beam of particles, one first regards the beam as a collection of noninteracting single particles moving in the environment determined by the accelerator design. This environment is defined by the electric and magnetic fields of the various accelerator components. Given these fields, the linear and nonlinear dynamics of a single particle or a group of non-interacting particles can be studied in detail. In the accelerator physics terminology, this area of research is known as beam optics.

Many accelerator applications, however, require beams of medium or high intensities. The electromagnetic fields generated by the beam itself increase with increasing beam intensity. Eventually, the fields generated by the beam interacting with its immediate surroundings will perturb the externally prescribed fields. Small perturbations of the beam can grow exponentially, thus the beam becomes unstable. To describe this collective behavior of the beam, the single particle motion must be modified to include the important self-generated fields. Often in such a study, the detailed nonlinear dynamics studied in connection with long-time single particle motion is omitted or simplified.

To be more specific, consider an intense particle beam contained in a metallic vacuum chamber of an accelerator. The beam interacts electromagnetically with its surroundings to generate an electromagnetic field, known as the wake field. This field then acts back on the beam, perturbing its motion. Under unfavorable conditions, the perturbation of the beam further enhances the wake field, and this leads to an instability, known as a collective instability, and subsequent beam degradation. The

beam and its surroundings form a self-consistent dynamical system. It is a particular coherent instability of this system, one that places a major limit on machine performance, that we investigate theoretically and numerically in this thesis.

There are many excellent references regarding the physics of collective beam instabilities. The book by Chao [1] of SLAC introduces and analyzes various collective instabilities in high-energy accelerators. The presentation is theoretically oriented, and the emphasis is on the underlying physical principles of these instabilities, typically using models and soluble examples as illustrations. The discussion is lucid and penetrating. The most significant feature of this book is that the author focuses his attention on establishing a solid intuitive picture first using macroparticle models. The conventional treatment of the subject using Vlasov techniques is postponed to a later part of the book. Another excellent reference is the ZAP User's Manual [2] by Zisman, et al. The authors developed a very good accelerator physics code, ZAP, which calculates the performance of a storage ring in terms of the limitation from beam-intensity-dependent phenomena. In the ZAP User's Manual, the authors summarize the theoretical foundations behind ZAP, providing the relevant formulations, physical models and particularly the equations used in the code in evaluating the various effects of collective instability. Other sources on the beam collective instabilities can be found in many conference proceedings, accelerator physics school publications, etc. One particularly useful source is the proceedings [3] of the topical course on intensity limitations in 1990.

1.2   Bunch Lengthening Instability

In this thesis, we focus our attention on a particular collective instability resulting from the interaction of beam particles with vacuum chambers: the bunch lengthening instability.

13

In modern storage rings, bunch length is a crucial parameter. Consider, for example, the B-factories planned both in the United States and Japan. In order to reach the high luminosities desired, one needs to apply strong focusing to compress the beam to very low beta values at the interaction point. However, due to the increase of transverse beam size at the bunch edges (the hour-glass effect, explained in Fig 1.1), the luminosity increases only so long as the bunch length is smaller than the beta value. Another example of a system where bunch length has limited performance is the damping ring at the Stanford Linear Collider.

In both examples, high bunch currents are strongly desired. Unfortunately, when the bunch current reaches a critical value, known as the "turbulent threshold", an instability appears. The effect of this instability in an electron storage ring is to increase both the bunch length and the energy spread of the beam, compared to its equilibrium value below the threshold. This is obviously a dynamic process. As the bunch length increases, the bunch peak current decreases, which in turn, decreases the longitudinal forces. Radiation damping then serves to reduce the bunch length. The competition between radiation damping and quantum excitation, together with longitudinal instability, leads to some new dynamic "equilibrium". This instability is the bunch lengthening instability, (also known as turbulent bunch lengthening or anomalous bunch lengthening), and it limits the performance of the B-factories, synchrotron light sources and other applications of storage rings.

1.2.1 Background

The lengthening of electron bunches in storage rings and circular accelerators was first observed experimentally [4, 5, 6, 7, 8]. The first analytical studies [9, 10, 11] identified the mechanism as a deformation of the potential well, formed by the external RF voltage, due to the induced voltage in the wall impedances. The problem was analyzed by Pellegrini and Sessler [12] and scaling laws were obtained which were in
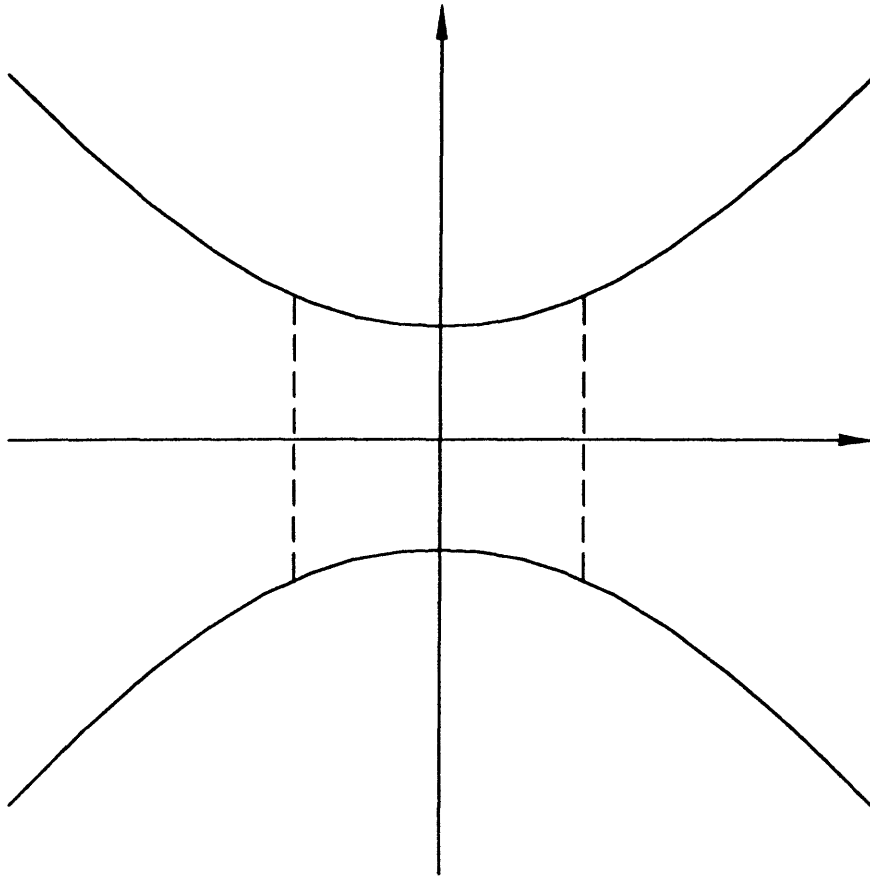
Figure 1.1: Hour-glass effect: Horizontal axis corresponds to axial direction of motion, vertical axis corresponds to transverse displacement. Solid line is the beta function. In order for the bunch's transverse dimension to be as small as possible, the whole bunch should be inside the area of dashed line. This requires the bunch length to be smaller than the minimum β.

good agreement with observations at low currents.

The induced voltage $V(t)$ seen by the bunch due to wake fields is

$$V(t) = -L_0 \int_{-\infty}^{+\infty} dt' W(t' - t) I(t') = -\int_{-\infty}^{+\infty} d\omega Z(\omega) \tilde{I}(\omega) \exp(-i\omega t). \qquad (1.1)$$

Here, $W(t)$ is the wake field, $Z(\omega)$ is the Fourier transform of the wake field; $I(t)$ is the bunch current, $\tilde{I}(\omega)$ is its Fourier transform; L_0 is the ring circumference. The concept of the wake field will be discussed in greater detail in Ch. 2. It characterizes the interaction between particles mediated through the wall impedances. In the low-current limit, Pellegrini and Sessler were able to assume the bunch shape was basically Gaussian with bunch length σ. Keeping terms only to linear order in t, they obtained:

$$V(t) = -\frac{Ne}{\pi} \int_{-\infty}^{+\infty} d\omega Re Z(\omega) \exp(-\frac{\omega^2\sigma^2}{2})$$
$$- \frac{Ne}{\pi} t \int_{-\infty}^{+\infty} d\omega Im Z(\omega) \omega \exp(-\frac{\omega^2\sigma^2}{2}). \qquad (1.2)$$

Here, N is the number of electrons in a bunch. The first term gives the shift of equilibrium phase. The second term gives a derivative of RF voltage and changes the synchrotron frequency. Since energy spread is determined by the synchrotron radiation below the threshold of bunch lengthening instability, the change in bunch length $\Delta\sigma$ is directly related to the change in synchrotron tune $\Delta\nu_s$:

$$\frac{\Delta\sigma}{\sigma} = -\frac{\Delta\nu_s}{\nu_{s0}} = -\frac{e^2 \varsigma_c}{2\pi\omega_0^2} \int_0^{+\infty} d\omega Im Z(\omega) \omega \exp(-\frac{\omega^2\sigma^2}{2}). \qquad (1.3)$$

Here,

$$\varsigma_c = \frac{\eta I}{\nu_{s0}^2 E_0}. \qquad (1.4)$$

is the scaling parameter of Chao and Gareyte [13], ω_0 is the angular revolution frequency, η is the momentum compaction factor, I is the bunch current, ν_{s0} is the synchrotron tune and E_0 is the bunch energy.

As will be explained in Sec. 2.2.4 impedances for many rings are actually described by a broadband resonator. For a broadband resonator, $Im Z(\omega)$ is negative below ω_r

and positive above. When the natural bunch length σ is large, small ω contributes, the effective wall impedance is inductive, and in this circumstance the bunch lengthens. When σ is small, large ω contributes, the effective wall impedance may become capacitive and the bunch shortens.

However, this analysis is valid above transition, which is always the case for electrons in high-energy storage rings, but not necessarily true for protons. For low-energy protons (or ions), the dominant space-charge or "negative mass" effect always leads to bunch lengthening, since it has the negative sign of a capacitance. At higher energies the space-charge impedance becomes much smaller, and the usual resistive wall impedance dominates.

Bunch shortening had been observed in SPEAR [8] at low currents, probably mainly due to the strong capacitive impedance of a number of RF cavities installed to reach high energies. However, after several years of operation below the peak energy, some RF cavities were removed and the free space was utilized for the installation of other equipment. The bunches became longer, which presented no problem until an attempt was made to increase the luminosity with a mini-beta insertion. A shorter bunch length would have been needed again in order to avoid the hour-glass effect, but the space for the old cavities was no longer available.

Bane [14] of SLAC described the so-called SPEAR capacitor, a section of disk-loaded waveguide with deep slots and varying iris apertures following the beam size, designed to increase the capacitive impedance as much as possible in the available space of only two meters. After installation of the waveguide section, shorter bunches were indeed observed at low currents. However, in order to reach a high luminosity, the current had to be increased. When it was increased above the turbulent threshold, the potential-well bunch-shortening was no longer effective and the bunches became almost as long as before.

17

Burov [15] proposed an idea along similar lines to achieve the bunch shortening. Dielectric walls were proposed for storage rings, whose essentially capacitive impedance should shorten the bunches. While this would probably work at low current levels, it will not prevent the onset of bunch lengthening at higher currents.

The theory of potential well distortion [17, 18, 19] (see Sec. 2.3) provides the complete equation to determine the equilibrium electron phase space distribution, without making the small current assumption. In this theory, the particle distribution in the energy deviation remains Gaussian while the particle distribution in the arrival time is given by a self-consistent integral equation, known as the Haissinski equation [17]. However, the theory failed to predict the appearance of the turbulent threshold which was observed experimentally as the onset of stronger bunch lengthening, accompanied by an increase of the energy spread.

1.2.2 Coasting Beams and the Boussard Criterion

Turbulent bunch lengthening is often explained by the Boussard criterion [20, 21]. Boussard conjectured that the longitudinal instability in a bunched beam is due to a coasting beam-like instability within the bunch. Qualitatively, the argument goes as follows: Consider an impedance which induces an instability that has a small wavelength compared to the bunch length. If the growth time of the instability is short compared to a synchrotron oscillation period, then the center of the bunch looks like a coasting beam–except, of course, that it has a high peak current. Therefore, to estimate the threshold for instability one might use the coasting beam threshold [22, 23] but replace the coasting beam current and the average energy spread with the highest local values for bunched beams [20].

We consider a longitudinal phase space and take θ and W as canonical variables.

Here θ is the angular position in the storage ring and W is defined as

$$W = \int^E \frac{dE}{f(E)},$$ (1.5)

where $f(E)$ is the revolution frequency. The coasting beam analysis is based on the linearization of the Vlasov equation [24]:

$$\frac{\partial \psi}{\partial t} + \dot{\theta}\frac{\partial \psi}{\partial \theta} + \dot{W}\frac{\partial \psi}{\partial W} = 0,$$ (1.6)

where $\psi(\theta, W, t)$ is a distribution function in phase space. Then

$$\frac{d\theta}{dt} = \omega_0 = 2\pi f(E),$$ (1.7)

$$\frac{dW}{dt} = eV(\theta, t);$$ (1.8)

where $V(\theta, t)$ is the induced voltage given by Eq. 1.1. We divide $\psi(\theta, W, t)$ into a stationary distribution $\psi_0(W)$ and a small perturbed part $\psi_1(n, W, \omega)$ as

$$\psi(\theta, W, t) = \psi_0(W) + \sum_{-\infty}^{+\infty} \int d\omega \psi_1(n, W, \omega) \exp(in\theta - i\omega t),$$ (1.9)

where ψ is normalized as

$$\int d\theta dW \psi(\theta, W) = Ne.$$ (1.10)

The bunch current is given by:

$$I(t) = \omega_0 \int dW \psi.$$ (1.11)

Inserting Eqs. 1.7, 1.8 and 1.9 into the Vlasov equation 1.6 and keeping only linear terms in ψ_1 yields

$$i(n\dot{\theta} - \omega)\psi_1 = e\omega_0 Z(\omega)\frac{d\psi_0}{dW} \int dW \psi_1.$$ (1.12)

We note that ψ_1 is the Fourier amplitude of the n'th azimuthal mode, and that the azimuthal modes are uncoupled. This is an important consequence of linearization in ψ_1 which is valid for a coasting beam. As we shall see later, this simplification

19

does not occur for a bunched beam. Dividing each term of Eq. 1.12 by $i(n\dot{\theta} - \omega)$ and integrating over W gives the very important relation:

$$1 = i\epsilon\omega_0 Z(\omega) \int_{-\infty}^{+\infty} dW \frac{d\psi_0}{dW} \frac{1}{\omega - n\dot{\theta}}. \tag{1.13}$$

The equation is called a dispersion relation and it plays an essential role in determining the turbulent threshold. However, it is difficult to handle the dispersion integral in Eq. 1.13 because of the singularity at $\omega = n\dot{\theta}$. This singularity is a result of the use of the Fourier transform in Eq. 1.9. A prescription for solving similar problems was given by Landau [25], who formulated the stability analysis as an initial-value problem and used a Laplace transform. He showed that the energy spread of the beam can damp the collective mode. We will not go into the details of this Landau damping problem. An excellent treatment of Landau damping for the bunched and unbunched beams in circular accelerators can be found in the book by Chao [1]. It can be shown that in order to include the Landau damping, we need only make the substitution:

$$\omega \Rightarrow \omega + i\epsilon, \tag{1.14}$$

where ϵ is an infinitesimal small positive quantity. Then the dispersion relation 1.13 can be solved analytically for several equilibrium distributions $\psi_0(W)$: Lorentzian, rectangular, parabolic, elliptical, bi-Lorentzian and Gaussian distribution. Ruggiero and Vaccaro [26], among other authors, calculated the stability limit diagram. Keil and Schnell [23] summarized their results in a very simple formula

$$\left| \frac{Z(n\omega_0)}{n} \right| < F \frac{\eta(\Delta E)_{FWHM}}{ecI_0}, \tag{1.15}$$

where F is a form factor which depends on the distribution and is roughly equal to unity, I_0 is the current and $(\Delta E)_{FWHM}$ is the energy full width at half maximum of the stationary distribution $\psi_0(W)$.

Boussard [20] applied this formula to a bunched beam (though without including the effects of synchrotron oscillations) in the process of debunching. He used local values of I_0 and ΔE and explained the increase of the energy spread and the appearance of microwave signals. He named this the "microwave instability". Later his argument was also applied to bunched beams with synchrotron oscillations.

The criterion 1.15 is usually called the Keil-Schnell-Boussard criterion. However, some years earlier, Laslett, Neil and Sessler [22] derived the same criterion with a form factor relevant to a Lorentzian distribution and with $Z(n\omega_0)$ interpreted as the shunt impedance of a cavity. Thus the same criterion is sometimes also called the LNS criterion.

The issue of the applicability of a coasting beam instability criterion to a bunched beam was studied in detail by Wang and Pellegrini [27]. They found that one obtains a coasting beam-like instability condition provided that:

1. The impedance is broad-band relative to the bunch spectrum (Fourier transform of the bunch density).

2. The growth rate is much greater than ω_{s0}.

3. The instability occurs at wavelengths much shorter than the bunch length.

The third point of this condition is obvious: For bunches which are long compared to the wavelength of the oscillation (e.g. protons), the bunch can be approximated by a coasting-beam and the Keil-Schnell criterion can be applied locally. For short bunches (e.g. electrons) these wavelengths usually correspond to frequencies well beyond the cut-off of the vacuum chamber. There impedances are much smaller, since energy cannot be stored in cavities and propagates with the wrong phase velocity in the beam pipes. Experimentally, the Boussard criterion has been used successfully to estimate the instability threshold for proton beams. It does not work well for

short electron bunches, and other more complicated theories have been put forward to explain bunch lengthening in electron rings.

1.2.3 Mode Coupling Theory

Sacherer [28] initiated a mode coupling theory for the bunch lengthening instability in electron beams. Since we go into the details of the mode coupling theory à la Sacherer in Ch. 3, here we will only outline its results and comment on some other recent work on the bunch lengthening based on the mode coupling theory. The basic idea is as follows: Before the turbulent threshold, the equilibrium state of the bunch is given by the theory of the potential well distortion. We assume that the onset of the turbulent bunch lengthening corresponds to the instability of the equilibrium given by the theory of the potential well distortion. The Vlasov technique [24, 29] can be used to analyze the stability of the equilibrium. Sacherer showed that the system becomes unstable when two adjacent higher order modes couple together. However, the required strong impedances at frequencies well beyond the vacuum chamber cutoff make the model less plausible [30].

Chao and Gareyte [13] considered the mode coupling theory for the waterbag beam. In this model, all the radial modes degenerate and the coupling of synchrotron modes lead to a scaling law for the bunch length. They showed that the bunch length is a function of ς_c only, where ς_c is given by Eq. 1.4, and they were able to test this qualitative conclusion with the experiment of Wilson et al. [8], and the agreement was surprisingly good.

Theories based on the coupling of the dipole mode with its mirror image ($l = 1$ and $l = -1$) were published a few years later [45, 46]. They did away with the requirement for large impedances, but comparison of predictions for the turbulent threshold with measurements at SPEAR [8] were unsatisfactory. Theoretical predictions were usually too high.

1.3 Motivation and Outline

The most severe blow to any theory of bunch lengthening based on the coupling of synchrotron modes is that both the experiment by Wilson et al. [8], and the more recent experiment by Rivkin et al. [33], did not observe the coupling of lower-order synchrotron modes at the bunch lengthening threshold. Our multiparticle multiperiod numerical simulation also confirms this observation. As we mentioned earlier, the impedances corresponding to the higher order synchrotron modes are very small, it is unlikely that the bunch lengthening instability is driven by the coupling of high-order synchrotron modes.

By examining the existing mode coupling theories closely, we have found out that the nonlinear contribution from the static potential well has not been properly included. By linearizing the wake force from the static potential well, previous authors were able to incorporate all of the effects of a deformed potential well into the incoherent frequency shift and the shift of the center of the bunch. As a result (see Ch. 3), the equilibrium bunch shape remains Gaussian. This approximation significantly simplifies the Vlasov instability analysis but, unfortunately, it also misses the bunch lengthening instability mechanism. In Sec. 3.5, we will show that the nonlinearity of the static wake force distorts the equilibrium density from its Gaussian shape, which results in asymmetric corrections to the ordinary single-mode Sacherer equation. This modified Sacherer equation will have unstable eigenmodes when the beam current reaches a threshold value.

The only work to carefully include potential well distortion is a recent eigenvalue analysis by Oide and Yokoya [34]. Rather than parameterize the equilibrium bunch shape by several parameters, Oide and Yokoya used the numerical solution of the Haissinski equation directly and introduced the action-angle variables for the Vlasov equation. Although Oide and Yokoya's method is, in some ways, more rigorous than

23

ours, they can not go too far before plunging into full-fledged numerical computations. Thus the real instability mechanism is not clear from their analysis. However, Oide and Yokoya's work serves a good reference to our work and we will compare our results with theirs in Ch. 5.

This thesis focuses on developing a new theory of the bunch lengthening instability based on the nonlinearity of the static wake force. Fig. 1.2 highlights various steps of this new theory and their correspondence with different chapters of this thesis. The detailed outline of this thesis is listed below.

In Ch. 2, we start from a brief introduction of the longitudinal dynamics of a charged particle in a circular accelerator without the wake field. Then we introduce the longitudinal wake field and its Fourier transform, the longitudinal impedance. We calculate the longitudinal shunt impedance for a localized cavity analytically and argue that the longitudinal impedance of a storage ring can be approximated by a broadband resonator. It is this broadband resonator impedance that will be used in our subsequent analysis of the bunch lengthening instability. In the last part of this chapter, we develop the potential well distortion theory by solving the bunch-environment system self-consistently.

Ch. 3 is devoted exclusively to the development of our new theory of the bunch lengthening instability, and presents a significant new contribution to this field. We start this chapter by reviewing the SPEAR results of Wilson et al. [8] on the bunch lengthening instability. Based on the experimental observations and simulation results, we assume that different synchrotron modes do not couple each other at the turbulent threshold. Using a Vlasov formalism we derive the single mode Sacherer equation by linearizing the static wake force and we show that this equation is indeed stable. In Sec. 3.5 we demonstrate that, by including the nonlinearity of the static wake force, there will be correction terms to the Sacherer equation. This improved
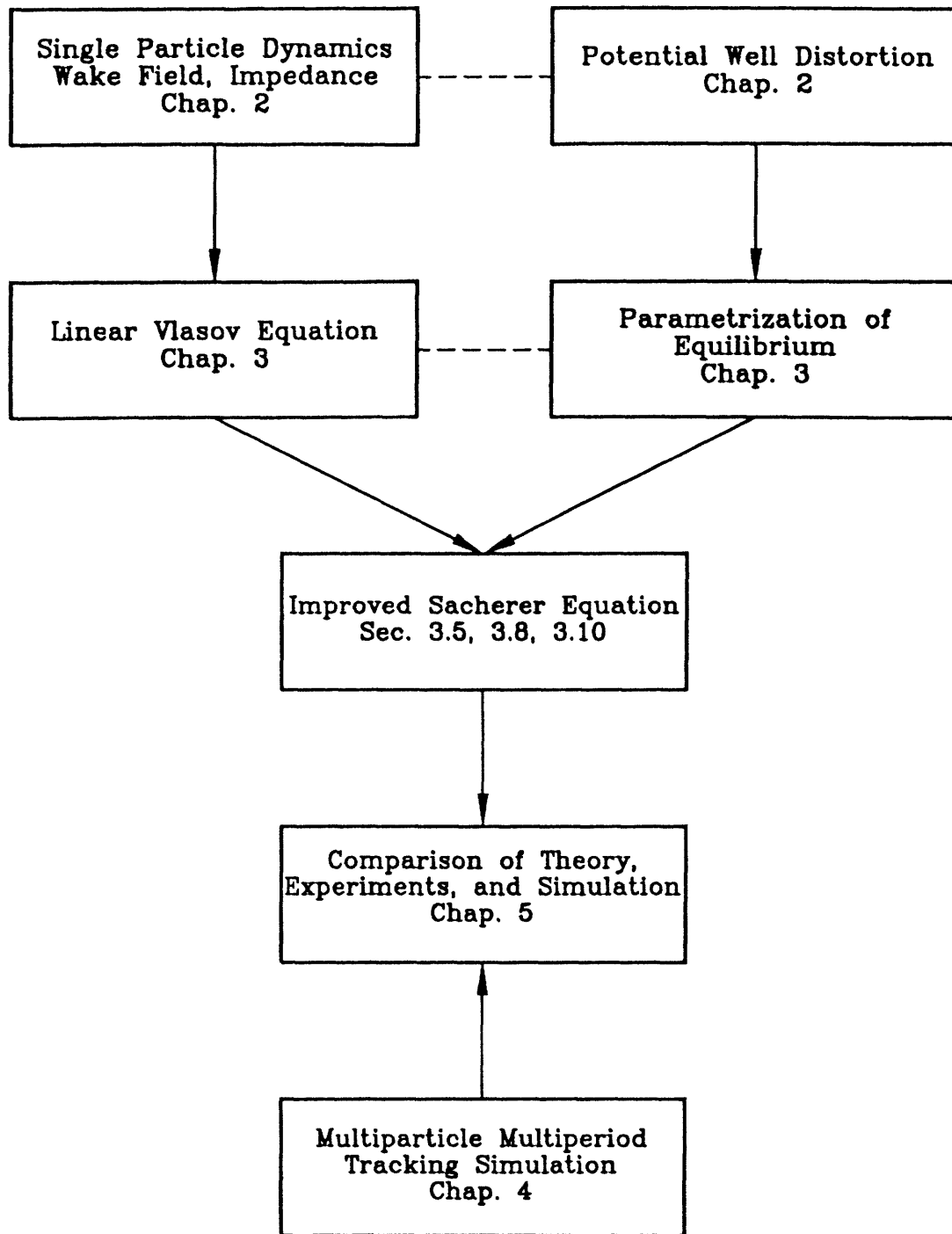
Figure 1.2: Relations between the key steps in developing new bunch lengthening theory and different chapters in which these steps are discussed.

Sacherer equation will have unstable eigenmodes when the bunch current reaches some threshold value. This section is the key part of this thesis. Using cummulant expansion techniques, the equilibrium bunch shape can be approximated fairly well by four parameters: The center of the bunch $< \tau >$, the bunch length σ, the skewness γ_1 and the excess γ_2. With this approximation, explicit forms for the correction terms can be analytically derived. In the last section of this chapter, we develop a numerical algorithm to transform the improved Sacherer equation into an eigenvalue problem. All numerical results based on the SPEAR parameter will be discussed in Ch. 5.

In Ch. 4, the physics behind our multiparticle multiperiod tracking simulation is explained. We start from the iteration equations for the longitudinal synchrotron motion of a single particle and add three terms corresponding to the wake force, the radiation damping and the energy fluctuation due to the quantum nature of the synchrotron radiation. We also point out two important characteristics of the iteration equations, which have not been noticed by other researchers. The first is related to the phase space trajectory of a single particle executing a synchrotron oscillation. We show that the trajectory is a tilted ellipse. This knowledge enables us to load the particle along this tilted ellipse, which reduces the noise that is generated from the dipole oscillation of the bunch when particles are loaded along an ordinary ellipse. The second is related to the localized kick that is used in the multiparticle tracking simulation. The equilibrium distribution of a bunch experiencing a localized wake force is drastically different from that of a bunch experiencing a distributed wake force. (Detailed analysis of the equilibrium phase space distribution following the formalism of Hirata [35] is provided in App. A.) In order to approximate the real wake field, which is distributed along the ring, we distribute the wake force into many periods in our multiparticle simulation code. Finally we introduce several new diagnostics into our multiparticle multiperiod simulation code. These new diagnostics

are more powerful than most of the widely used diagnostics.

In Ch. 5, we compare the results from our multiparticle multiperiod simulation with the instability analysis based on the improved Sacherer equation and the experimental measurements of Wilson et al. [8] on the SPEAR II ring and Brandt et al. [36] on the LEP ring. The agreements are excellent. Since the instability threshold is determined by two dimensionless scaling parameters, $\omega_r \sigma$ and ξ, we have also run our instability code to determine the critical coupling ξ_c as a function of $\omega_r \sigma$ and compare our result with the full-scale numerical Vlasov analysis of Oide and Yokoya [34]. For short bunches, the agreements are excellent.

Throughout this thesis, cgs units have been adopted.

Chapter 2

Longitudinal Dynamics, Wake Fields and Equilibrium Bunch Shape

A charged particle bunch propagating through an accelerator vacuum chamber interacts electromagnetically with its environment (beam pipe, bellows, RF cavities, etc.) to create a wake field. This field then acts back on the bunch, perturbing the motion of the particles within the bunch. For sufficiently intense bunch currents, this feedback may lead to collective instabilities and to subsequent beam loss or degradation of the performance of the accelerator. In this chapter, we will first discuss the longitudinal dynamics for a charged particle in a storage ring, without complications from the wake. Next, we will parameterize the effect of the wake field from a rigid bunch, i.e., in the approximation that the action of the wake field on the particle distribution in the bunch can be neglected. Finally this self-consistent bunch shape, including the wake field effect, will be determined.

2.1 Single Particle Longitudinal Dynamics

Before investigating the collective motion of a charged particle bunch, we will examine the single particle dynamics. It is convenient to describe the motion of a particle in the bunch by examining how its motion differs from that of a reference, or designed

particle. The revolution time for the design particle in a storage ring is

$$t_0 = \frac{L_0}{v_0},$$
(2.1)

where L_0 is the ring circumference and v_0 is the particle's average speed. Another particle, with a slightly different energy, $E_0 + \delta E$, will have a revolution time $t_0 + \delta t$, with

$$\frac{\delta t}{t_0} = \frac{\delta L}{L_0} - \frac{\delta v}{v_0} = \eta \frac{\delta E}{E_0}.$$
(2.2)

The change in revolution time δt is composed of two contributions, one from δL, the change of traveling distance compared to the design particle, and the other from δv, the change of the average velocity. Both these terms are proportional to δE, as seen in the second equality in Eq. 2.2. The constant of proportionality η is related to the momentum compaction factor of the ring, α, and the relativistic gamma factor $\gamma_0 = 1/\sqrt{1 - v_0^2/c^2}$ through:

$$\eta = \alpha - \frac{1}{\gamma_0^2}.$$
(2.3)

Let τ_n be the arrival time displacement of the particle at the accelerating cavity in the nth revolution, measured relative to the design particle, and δE_n the corresponding energy displacement. The longitudinal motion of a particle with charge e, where e is the positron's charge, is given by the mapping [38]:

$$\tau_{n+1} = \tau_n - \frac{\eta T_0}{E_0} \delta E_{n+1}.$$
(2.4)

$$\delta E_{n+1} = \delta E_n - \text{wake field loss}$$

$$+ \underbrace{eV \sin(\phi_s - \omega_{rf}\tau_n)}_{\text{gain from RF cavity}}$$

$$- \underbrace{eV \sin(\phi_s)}_{\text{synchrotron radiation loss}}.$$
(2.5)

Eq. 2.4 is identical to Eq. 2.2. Eqs. 2.5 shows that the loss of energy due to the synchrotron radiation and wake field is compensated by the gain from the RF cavity.
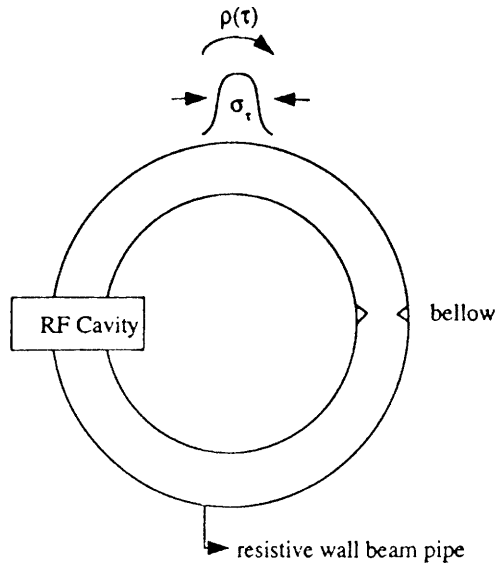
Electron bunch circulating in accelerator

bunch lengthening threshhold
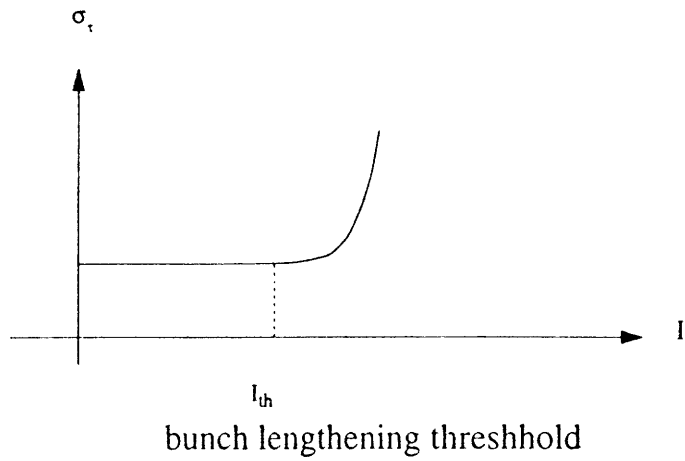
Figure 2.1: (a) Electron bunch circulating in a ring. (b) Bunch length as a function of current (sketch) showing threshold behavior near $I = I_{th}$.

The synchrotron phase ϕ_s is chosen to guarantee that particles execute stable synchrotron oscillations: When a particle arrives after the design particle, it must receive less RF kick. For a ring operating above transition (positive η), a particle with less energy requires a shorter time to complete a revolution, thus reducing the delay with respect to the design particle. In the same way, a particle arrival before the design particle must receive a larger RF kick so that it requires a longer time to complete a revolution. The operating frequency of the RF cavity is ω_{rf}, which is usually slightly above a multiple of the revolution frequency ω_0 to avoid the Robinson instability [10].

Wake field losses result from the interaction of a charged particle with its vacuum chamber environment. When a charged particle is traveling through an accelerator, it will excite an electromagnetic field from the RF cavities, the resistive walls of the vacuum chamber and many small discontinuities: bellows, masks, transitions, etc. This electromagnetic field is called the wake field and it will lead to energy loss or gain of the trailing particle. In Sec. 2.2 we will discuss in great detail how to model the wake field and how to calculate the energy loss associated with it.

For the next generation of advanced light sources and colliders, short bunches are crucial to the performance of the machine. A clear theoretical understanding of the bunch lengthening instability has not been achieved in the short bunch length parameter regime. The focus of this thesis will be on revealing the physics mechanism driving the bunch lengthening instability. Thus, we assume the equilibrium bunch length is much shorter than the RF wavelength. Linearizing the RF bucket in Eq. 2.5 produces a simpler set of equations:

$$\tau_{n+1} = \tau_n - \frac{\eta T_0}{E_0} \delta E_{n+1}, \tag{2.6}$$

$$\delta E_{n+1} = \delta E_n - \text{wake field loss}$$

$$-eV \cos(\phi_s) \omega_{rf} \tau_n. \tag{2.7}$$

Eqs. 2.6 and 2.7, when completed by including radiation damping, quantum emission
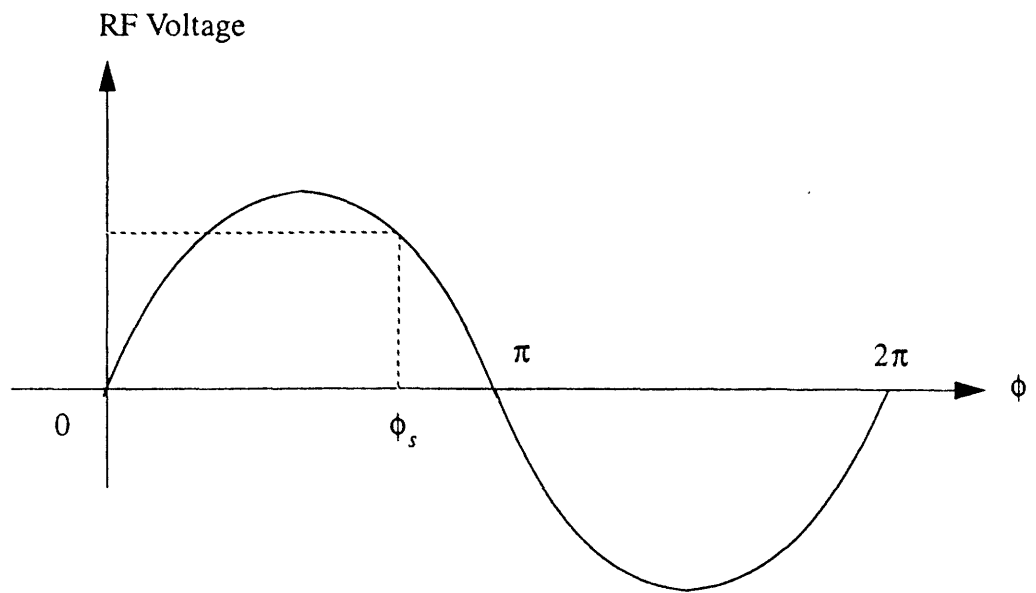
Figure 2.2: Sinusoidal RF accelerating voltage. Here ϕ_s is the synchrotron phase.

and wake field, form the basis of the multiple particle tracking simulation to be discussed in Ch. 4.

We can make one more approximation. Observing that changes for τ_n and δE_n are very small in one iteration and the wake field loss is distributed throughout the ring, we can approximate difference equations 2.6 and 2.7 by differential equations:

$$\frac{d\tau}{dt} = -\eta\delta, \tag{2.8}$$

$$\frac{d\delta}{dt} = \frac{\omega_{s0}^2}{\eta}\tau - \text{wake field loss}. \tag{2.9}$$

Here,

$$\delta = \frac{\delta E}{E_0}, \tag{2.10}$$

and ω_{s0} is given by:

$$\omega_{s0}^2 = -\frac{\eta eV}{E_0 T_0}\cos(\phi_s)\omega_{rf}. \tag{2.11}$$

Without the wake field losses, the particle executes simple harmonic oscillations with frequency ω_{s0}. We will show in Sec. 2.2 that the effect of the wake field loss can be described by an external force acting on a harmonic oscillator:

$$\frac{d\tau}{dt} = -\eta\delta, \tag{2.12}$$

$$\frac{d\delta}{dt} = \frac{\omega_{s0}^2}{\eta}\tau - \frac{1}{E_0 T_0}F(\tau). \tag{2.13}$$

If we identify τ as the generalized coordinate and δ as the corresponding generalized momentum, Eqs. 2.12 and 2.13 can be derived from the Hamiltonian:

$$H = \frac{\delta^2}{2} + \frac{\omega_{s0}^2\tau^2}{2\eta^2} - \frac{1}{\eta E_0 T_0}\int_0^\tau d\tau' F(\tau'). \tag{2.14}$$

2.2 Wake Field and Impedance

In this section we consider how to model the wake field of a localized cavity and then generalize the result to the wake field of a vacuum beam pipe.

33

2.2.1 Cavity Response to a Relativistic Charged Particle

The electric field $\mathbf{E}$ and magnetic field $\mathbf{B}$ can be written in terms of a vector potential $\mathbf{A}$ and scalar potential Φ as [39]

$$
\begin{aligned}
\mathbf{E} &= -\nabla\Phi - \frac{1}{c}\frac{\partial \mathbf{A}}{\partial t}, \\
\mathbf{B} &= \nabla \times \mathbf{A}.
\end{aligned}
\tag{2.15}
$$

Substituting Eq. 2.15 into Maxwell's equations [39]:

$$
\begin{aligned}
\nabla \cdot \mathbf{E} &= 4\pi\rho, \\
\nabla \times \mathbf{B} &= \frac{4\pi}{c}\mathbf{j} + \frac{1}{c}\frac{\partial \mathbf{E}}{\partial t}.
\end{aligned}
\tag{2.16}
$$

we have

$$
\nabla^2\Phi = -4\pi\rho.
\tag{2.17}
$$

$$
\nabla^2\mathbf{A} - \frac{1}{c^2}\frac{\partial^2 \mathbf{A}}{\partial t^2} = -\frac{4\pi}{c}\mathbf{j}.
\tag{2.18}
$$

when the Coulomb gauge $\nabla \cdot \mathbf{A} = 0$ has been used.

It is convenient to expand Φ in terms of normal modes,

$$
\Phi(\mathbf{x}, t) = \sum_\mu f_\mu(t)\phi_\mu(\mathbf{x}).
\tag{2.19}
$$

The normal mode ϕ_μ is real and satisfies

$$
\nabla^2\phi_\mu + \frac{\omega_\mu'^2}{c^2}\phi_\mu = 0.
\tag{2.20}
$$

along with the orthogonality requirement:

$$
\int d^3x\, \nabla\phi_\mu(\mathbf{x}) \cdot \nabla\phi_{\mu'}(\mathbf{x}) = 0 \quad \text{if } \mu \neq \mu'.
\tag{2.21}
$$

The integral is over the cavity volume. Equation 2.17 can be solved:

$$
f_\mu(t) = 4\pi \frac{\int d^3x\, \phi_\mu(\mathbf{x})\rho(\mathbf{x}, t)}{\int d^3x\, \nabla\phi_\mu(\mathbf{x}) \cdot \nabla\phi_\mu(\mathbf{x})}.
\tag{2.22}
$$

Next, we expand both $\mathbf{A}$ and $\mathbf{j}$ in terms of the normal modes:

$$\mathbf{A}(\mathbf{x}, t) = \sum_\lambda q_\lambda(t) \mathbf{a}_\lambda(\mathbf{x}), \tag{2.23}$$

$$\mathbf{j}(\mathbf{x}, t) = \sum_\lambda j_\lambda(t) \mathbf{a}_\lambda(\mathbf{x}). \tag{2.24}$$

The normal mode $\mathbf{a}_\lambda(\mathbf{x})$ is real and satisfies

$$\nabla^2 \mathbf{a}_\lambda + \frac{\omega_\lambda^2}{c^2} \mathbf{a}_\lambda = 0, \tag{2.25}$$

and the orthogonality condition,

$$\int d^3x \, \mathbf{a}_\lambda(\mathbf{x}) \cdot \mathbf{a}_{\lambda'}(\mathbf{x}) = 0 \quad \text{if } \lambda \neq \lambda'. \tag{2.26}$$

Inserting Eqs. 2.23 and 2.24 into Eqs. 2.17 and 2.18, leads to the equation for the mode amplitude $q_\lambda(t)$:

$$\frac{d^2 q_\lambda}{dt^2} + \frac{\omega_\lambda}{Q_\lambda} \frac{dq_\lambda}{dt} + \omega_\lambda^2 q_\lambda(t) = 4\pi c j_\lambda(t), \tag{2.27}$$

where $j_\lambda(t)$ is related to the bunch current $\mathbf{j}(\mathbf{x}, t)$ by

$$j_\lambda(t) = \frac{\int d^3x \, \mathbf{a}_\lambda(\mathbf{x}) \cdot \mathbf{j}(\mathbf{x}, t)}{\int d^3x \, \mathbf{a}_\lambda(\mathbf{x}) \cdot \mathbf{a}_\lambda(\mathbf{x})}. \tag{2.28}$$

2.2.2   Green Function Solution for the Mode Amplitude

The solution of the homogeneous equation

$$\frac{d^2 q_\lambda}{dt^2} + \frac{\omega_\lambda}{Q_\lambda} \frac{dq_\lambda}{dt} + \omega_\lambda^2 q_\lambda(t) = 0, \tag{2.29}$$

is

$$q_\lambda(t) = A' \sin \Omega_\lambda t e^{-v_\lambda t} + B' \cos \Omega_\lambda t e^{-v_\lambda t}, \tag{2.30}$$

where

$$\Omega_\lambda^2 = \omega_\lambda^2 - v_\lambda^2,$$

$$v_\lambda = \frac{\omega_\lambda}{2Q_\lambda}. \tag{2.31}$$

Since our initial condition assumes a zero field inside the cavity before the bunch enters, namely $q_\lambda(0) = 0$, $\dot{q}_\lambda(0) = 0$, we have

$$A' = B' = 0. \tag{2.32}$$

Thus the homogeneous solution does not contribute to the Green function. It remains to find a special solution to the equation

$$\frac{d^2 q_\lambda}{dt^2} + \frac{\omega_\lambda}{Q_\lambda} \frac{dq_\lambda}{dt} + \omega_\lambda^2 q_\lambda(t) = \delta(t). \tag{2.33}$$

The solution for both $t > 0$ and $t < 0$ is obvious:

$$q_\lambda(t) = A \sin \Omega_\lambda t e^{-v_\lambda t} + B \cos \Omega_\lambda t e^{-v_\lambda t} \quad t > 0, \tag{2.34}$$

$$q_\lambda(t) = C \sin \Omega_\lambda t e^{-v_\lambda t} + D \cos \Omega_\lambda t e^{-v_\lambda t} \quad t < 0. \tag{2.35}$$

Continuity of the function $q_\lambda(t)$ around $t = 0$ implies

$$B = D, \tag{2.36}$$

and the discontinuity of the function $\dot{q}_\lambda(t)$ around $t = 0$,

$$\dot{q}(t = 0^+) - \dot{q}(t = 0^-) = 1, \tag{2.37}$$

implies

$$(\Omega_\lambda A - v_\lambda B) - (\Omega_\lambda C - v_\lambda D) = 1. \tag{2.38}$$

From Eqs. 2.36 and 2.38, we find

$$q_\lambda(t) = (\tfrac{1}{\Omega_\lambda} + C) \sin \Omega_\lambda t e^{-v_\lambda t} + D \cos \Omega_\lambda t e^{-v_\lambda t} \quad t > 0, \tag{2.39}$$

$$q_\lambda(t) = C \sin \Omega_\lambda t e^{-v_\lambda t} + D \cos \Omega_\lambda t e^{-v_\lambda t} \quad t < 0. \tag{2.40}$$

Furthermore, C and D must be zero because of the causality. Thus we get the Green function of Eq. 2.27:

$$G_\lambda(t) = \begin{cases} \frac{1}{\Omega_\lambda} \sin \Omega_\lambda t e^{-v_\lambda t} & t > 0, \\ 0 & t < 0. \end{cases} \tag{2.41}$$

2.2.3 Longitudinal Wake Function and Impedance

We assume that a bunch carrying unit charge enters the cavity at $t = 0$ along the center of the cavity. Inside the cavity, we assume that the bunch moves with the speed of light c. The charge density and the current density can therefore be represented as

$$\rho(\mathbf{x}, t) = \delta(x)\delta(y)\delta(z - ct), \tag{2.42}$$

$$\mathbf{j}(\mathbf{x}, t) = c\delta(x)\delta(y)\delta(z - ct)\hat{\mathbf{z}}. \tag{2.43}$$

Using Eqs. 2.42 and 2.43 in Eq. 2.22 yields

$$f_\mu(t) = \frac{4\pi}{\int d^3x \, |\nabla\varphi_\mu(\mathbf{x})|^2}\phi_\mu(0, 0, ct) \quad 0 < t < L/c, \tag{2.44}$$

$$f_\mu(t) = 0 \quad \text{otherwise.} \tag{2.45}$$

The amplitude equation 2.27 then simplifies to

$$\frac{d^2q_\lambda}{dt^2} + \frac{\omega_\lambda}{Q_\lambda}\frac{dq_\lambda}{dt} + \omega_\lambda^2 q_\lambda(t) = \frac{4\pi c^2}{\int d^3x \, |\mathbf{a}_\lambda(\mathbf{x})|^2}a_{\lambda z}(0, 0, ct). \tag{2.46}$$

Using the Green function $G_\lambda(t)$ (Eq. 2.41), we find the solution of Eq. 2.46:

$$q_\lambda(t) = \frac{4\pi c}{\int d^3x \, |\mathbf{a}_\lambda(\mathbf{x})|^2}\int_0^L dz' \, G_\lambda(t - \frac{z'}{c})a_{\lambda z}(0, 0, z'). \tag{2.47}$$

Here we assume that the mode is not sensitive to the transverse position of the bunch. For convenience, we drop the index λ and calculate the average wake force acting on a unit charge test particle which moves with the speed of light c and arrives at the cavity at time $t = t_0$:

$$F_z = E_z = -\frac{\partial\Phi}{\partial z} - \frac{1}{c}\frac{\partial A_z}{\partial t} = -f(t)\frac{\partial\phi}{\partial z}(0, 0, z) - \frac{1}{c}\frac{dq}{dt}a_z(0, 0, z). \tag{2.48}$$

The longitudinal wake function $W_0'(t_0)$ is readily calculated by averaging the wake force experienced by the test charge inside the cavity:

$$W_0'(t_0) = -\frac{c}{L}\int_{t_0}^{t_0 + L/c} dt \, F_z(t) =$$

37

$$\frac{4\pi}{L}\frac{1}{\int d^3x\,|\nabla\phi(\mathbf{x})|^2}\int_0^L dz\,\phi(0,0,ct_0+z)\frac{\partial\phi}{\partial z}(0,0,z)$$

$$+\frac{4\pi}{L}\frac{1}{\int d^3x\,|\mathbf{a}(\mathbf{x})|^2}\int_0^L\int_0^L dz\,dz'\,G'(t_0+\frac{z-z'}{c})a_z(0,0,z)a_z(0,0,z').$$

$$(2.49)$$

First consider the case $t_0 > L/c$. Only the current response contributes to the wake function. Neglecting decay of the wake field during the transit of the test charge through the cavity,

$$W_0'(t_0) = \frac{4\pi}{L}\frac{|\int_0^L dz\,e^{-ikz}a_z(0,0,z)|^2}{\int d^3x\,|\mathbf{a}(\mathbf{x})|^2}G'(t_0). \qquad (2.50)$$

For $0 < t_0 < L/c$, we break $W_0'(t_0)$ into two parts: The charge density response, $W_{0\rho}'(t_0)$, and the current response, $W_{0j}'(t_0)$. Then,

$$\begin{aligned}
W_{0\rho}'(t_0) &= \frac{4\pi}{L}\frac{1}{\int d^3x\,|\nabla\phi(\mathbf{x})|^2}\int_0^L dz\,\phi(0,0,ct_0+z)\frac{\partial\phi}{\partial z}(0,0,z)\\
&= \frac{4\pi}{L}\frac{1}{\int d^3x\,|\nabla\phi(\mathbf{x})|^2}\int_0^{L-ct_0} dz\,\phi(0,0,ct_0+z)\frac{\partial\phi}{\partial z}(0,0,z)\\
&= \frac{4\pi}{L}\frac{1}{\int d^3x\,|\nabla\phi(\mathbf{x})|^2}\int_{ct_0}^L dz\,\phi(0,0,z)\frac{\partial\phi}{\partial z}(0,0,z-ct_0). \qquad (2.51)
\end{aligned}$$

The current response is

$$W_{0j}'(t_0) = \frac{4\pi}{L}\frac{1}{\int d^3x\,|\mathbf{a}(\mathbf{x})|^2}\int_0^L\int_0^L dz\,dz'\,G'(t_0+\frac{z-z'}{c})a_z(0,0,z)a_z(0,0,z'). \quad (2.52)$$

Rewriting the two-dimensional integration, we have

$$W_{0j}'(t_0) =$$

$$\frac{4\pi}{L}\frac{1}{\int d^3x\,|\mathbf{a}(\mathbf{x})|^2}r_0\int_0^L\int_0^L dz\,dz'\,g'(t_0+\frac{z-z'}{c})a_z(0,0,z)a_z(0,0,z')$$

$$-\frac{4\pi}{L}\frac{1}{\int d^3x\,|\mathbf{a}(\mathbf{x})|^2}\int_{ct_0}^L dz'\int_0^{z'-ct_0} dz\,g'(t_0-\frac{z'-z}{c})a_z(0,0,z')a_z(0,0,z).$$

$$(2.53)$$

Let us prove the sum of $W_{0\rho}'(t_0)$ and the second term of Eq. 2.53 is zero by considering $W_0'(t_0)$ for t_0 in the range of $-L/c < t_0 < 0$. In this range

$$W_{0\rho}'(t_0) = \frac{4\pi}{L}\frac{1}{\int d^3x\,|\nabla\phi(\mathbf{x})|^2}\int_{|ct_0|}^L dz\,\phi(0,0,z-|ct_0|)\frac{\partial\phi}{\partial z}(0,0,z)$$

$$= -\frac{4\pi}{L}\frac{1}{\int d^3x\,|\nabla\phi(\mathbf{x})|^2}\int_{|ct_0|}^{L} dz\,\phi(0,0,z)\frac{\partial\phi}{\partial z}(0,0,z-|ct_0|), \quad (2.54)$$

and

$$W_{0j}'(t_0) =$$
$$\frac{4\pi}{L}\frac{1}{\int d^3x\,|\mathbf{a}(\mathbf{x})|^2}\int_{|ct_0|}^{L} dz\int_0^{z-|ct_0|} dz'\,g'(|t_0| - \frac{z-z'}{c})a_z(0,0,z)a_z(0,0,z').$$

$$(2.55)$$

Combining Eq. 2.51 with Eq. 2.54, and Eq. 2.53 with Eq. 2.55, we obtain, for $0 < t_0 < L/c$,

$$W_{0\rho}'(t_0) + W_{0j,2}'(t_0) = -W_0'(-t_0) = 0, \qquad (2.56)$$

where $W_{0j,2}'(t_0)$ is the second term in Eq. 2.53. Finally the longitudinal wake function for any t is,

$$W_0'(t) = \frac{4\pi}{L}\frac{|\int_0^L dz\,e^{-ikz}a_z(0,0,z)|^2}{\int d^3x\,|\mathbf{a}(\mathbf{x})|^2}G'(t). \qquad (2.57)$$

The longitudinal impedance $Z(\omega)$ is defined by

$$Z(\omega) = L\int_{-\infty}^{\infty} dt\,e^{i\omega t}W_0'(t) = 4\pi\frac{|\int_0^L dz\,e^{-ikz}a_z(0,0,z)|^2}{\int d^3x\,|\mathbf{a}(\mathbf{x})|^2}(-i\omega)\tilde{G}(\omega)$$

$$= 4\pi\frac{|\int_0^L dz\,e^{-ikz}a_z(0,0,z)|^2}{\int d^3x\,|\mathbf{a}(\mathbf{x})|^2}\frac{Q}{\omega_\lambda}\frac{1}{1+iQ(\frac{\omega_\lambda}{\omega}-\frac{\omega}{\omega_\lambda})}. \qquad (2.58)$$

The frequency insensitive part of Eq. 2.58 is known as the longitudinal shunt impedance of the cavity,

$$\frac{R}{Q} = 4\pi\frac{|\int_0^L dz\,e^{-ikz}a_z(0,0,z)|^2}{\omega_\lambda\int d^3x\,|\mathbf{a}(\mathbf{x})|^2}. \qquad (2.59)$$

With this definition, we arrive at the well-known expression [40]

$$Z(\omega) = R\frac{1}{1+iQ(\frac{\omega_\lambda}{\omega}-\frac{\omega}{\omega_\lambda})}. \qquad (2.60)$$

The most important result of Eq. 2.60 is that the effect of the wake field for a localized cavity can be described by three parameters: the longitudinal shunt impedance,

39

R, expressed in ohms, the quality factor Q of the cavity, and the resonant frequency ω_λ of the higher-order mode. Although impedance $Z(\omega)$ can have more complicated frequency dependence for other structures, it is often well approximated by one or more resonator impedances. These impedances are generally complex quantities, with their real parts characterizing the dissipative effects of the beam storage ring system (growth or damping rates of instabilities, parasitic mode energy loss, etc.) and their imaginary parts characterizing the effects on the reactive, oscillatory part of the system (coherent oscillation frequency shifts, etc.).

Fig. 2.3 shows the frequency dependence of both the real and imaginary parts of a resonator impedance.

2.2.4 Ring Broadband Impedance

The impedance of the RF cavities consists mainly of sharp peaks at frequencies corresponding to the cavity modes. Besides being powered at the fundamental longitudinal accelerating mode by klystrons, the cavities will also be driven by the beam at higher-order longitudinal parasitic modes. These higher-order modes usually lie at frequencies higher than that of the fundamental mode. The cutoff frequency, $\omega_c = c/b$, is an upper bound for the higher-order mode frequencies. Here, b is the beam pipe radius. These higher-order resonances often have high Q, corresponding to wake fields that ring in the cavity for a large number of RF oscillations. They can couple bunches to each other and lead to the coupled-bunch instability.

For the machines operating at the short bunch length parameter regime, equilibrium bunch length is often equal to, or shorter than, the beam pipe radius. Since the frequency spectrum of the impedance of the RF cavities ranges from zero all the way to the cutoff frequency ω_c, while the frequency spectrum of the bunch internal structure starts from $c/\sigma_{t0} > \omega_c$, the wake field due to the RF cavities does not have much effect on the single bunch collective instabilities. (Here, σ_{t0} is the equilibrium
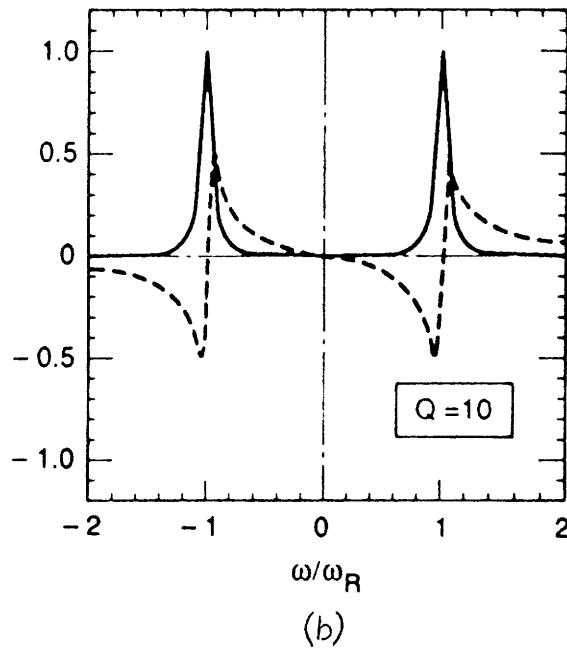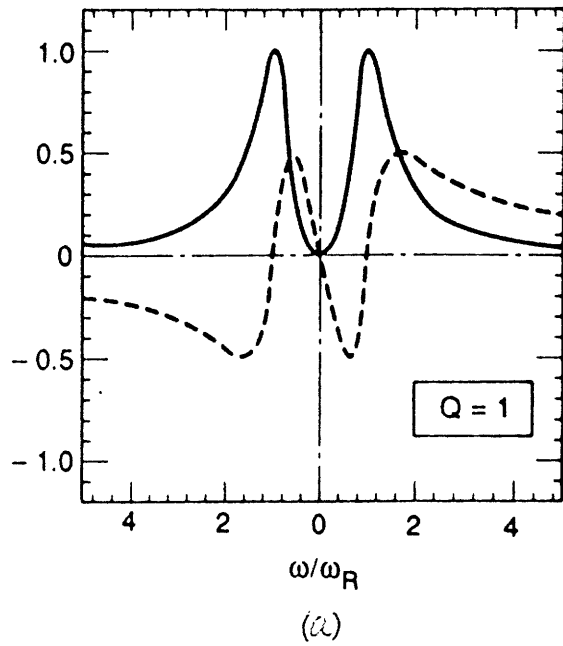
Figure 2.3: Resonator impedances. The solid curves plot the real part and the dashed curves the imaginary part of the impedances. (a) $Q = 1$. (b) $Q = 10$.

bunch length.)

The overall electromagnetical environment of the remainder of the storage ring is typically described by a broadband impedance [41]. This broadband impedance gives rise to a short-ranged wake field that induces coherent motion mainly within a single bunch. Except for the contributions from the resistive wall of a smooth vacuum chamber, it is very difficult to calculate or to precisely quantify this broadband impedance. It varies from ring to ring, and is generated by a large number of electromagnetic elements in the storage ring. Discontinuities in the vacuum chamber, such as bellows and beam collimators, other vacuum chamber cross-section variations, as well as beam instrumentation, such as beam position monitors, feedback loop pickups and kickers, and beam injection and abort kickers, all contribute to this broadband impedance.

It is nearly impossible to calculate analytically or to measure the detailed frequency dependence of the ring broadband impedance. In this work, we will model the ring broadband impedance mostly by a $Q = 1$ resonator [41] centered at the characteristic resonance frequency ω_c. We will also model the ring broadband impedance by a few resonators with Q close to one. This will enable us to obtain a qualitatively correct picture of the bunch lengthening instability; a more precise impedance model may change the threshold current slightly.

Fig. 2.4 illustrates the crossover from narrow band impedances to broadband impedance at the cutoff frequency ω_c.

The above considerations can be summarized as follows. For the bunch lengthening instability, we need only consider the ring broadband impedance. This broadband impedance can often be approximated by one (or at most a few) resonator impedance:

$$Z(\omega) = R\frac{1}{1 + iQ(\frac{\omega_r}{\omega} - \frac{\omega}{\omega_r})},$$
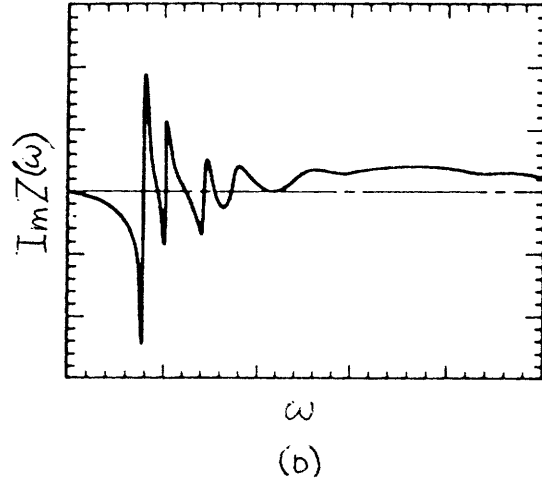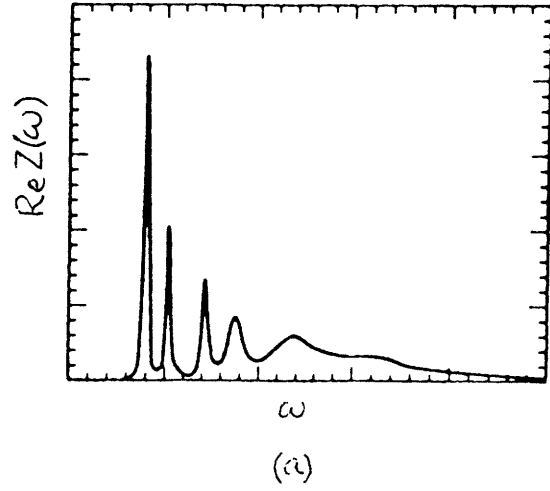(2.61)

Figure 2.4: Sketch of the impedance for a small number of cavities in series. (a) Real part. (b) Imaginary part.

with Q close to one. The longitudinal wake function of this impedance is given by

$$W(t)L_0 = \int_{-\infty}^{\infty} \frac{d\omega}{2\pi} \exp(-i\omega t)Z(\omega).$$ (2.62)

Here we have changed the notation of the longitudinal wake function to $W(t)$. Performing the Fourier transform. we obtain

$$W(t)L_0 = \begin{cases} 0 & \text{if } t < 0, \\ \frac{\omega_r R}{Q} \exp(-vt)(\cos\Omega t - \frac{v}{\Omega}\sin\Omega t) & \text{if } t > 0. \end{cases}$$ (2.63)

Here, v and Ω are related to the resonator frequency ω_r and Q through:

$$v = \frac{\omega_r}{2Q},$$
$$\Omega^2 = \omega_r^2 - v^2.$$ (2.64)

The wake vanishes for $t < 0$. This is the result of the causality: A particle only experiences the wake field from those particles traveling ahead of it.

2.2.5 $F(\tau)$: Wake Field Energy Loss per Turn

In the paragraph preceding Eq. 2.13, we mention that the effect of the wake field energy loss can be described by a force-like term $F(\tau)$. We are now in a position to give an explicit expression of $F(\tau)$ in terms of the wake function $W(\tau)$. Introducing the longitudinal particle distribution $\rho(\tau)$, normalized by

$$\int d\tau \rho(\tau) = 1,$$ (2.65)

the loss of the energy due to the wake field of a bunch with particle distribution $\rho(\tau)$ is given by:

$$F(\tau) = Ne^2 L_0 \int_{\tau}^{+\infty} d\tau' \rho(\tau')W(\tau' - \tau).$$ (2.66)

Substituting Eq. 2.66 into the Hamiltonian, Eq. 2.14, yields

$$H = \frac{\delta^2}{2} + \frac{\omega_{s0}^2 \tau^2}{2\eta^2} - \frac{Ne^2 L_0}{\eta E_0 T_0} \int_0^{\tau} d\tau' \int_{\tau'}^{+\infty} d\tau'' \rho(\tau'')W(\tau'' - \tau').$$ (2.67)

44

The first term in this Hamiltonian corresponds to a kinetic energy. The second and the third terms correspond to a potential energy. In the absence of the wake field, the potential is parabolic, as expected for simple harmonic motion. The potential well is distorted when wake fields are included. We shall investigate this distortion in the next section.

2.3 Potential Well Distortion

We will use the Vlasov technique [24] to study the longitudinal dynamics of a bunch of charged particles. Sacherer was the first to apply this technique to investigate collective instabilities in accelerator physics [29]. The book by Chao [1] provide a good introduction to this subject.

In this section, we will focus on the time-independent solution of the Vlasov equation to get the equilibrium bunch shape. While a wake field does not have any effect on the energy spread, it distorts the equilibrium bunch shape $\rho(\tau)$.

The evolution of the particle distribution function, $\psi(\tau, \delta, t)$, in the phase space of τ and δ is governed by the Vlasov equation

$$\frac{\partial \psi}{\partial t} + \frac{d\tau}{dt} \frac{\partial \psi}{\partial \tau} + \frac{d\delta}{dt} \frac{\partial \psi}{\partial \delta} = 0. \tag{2.68}$$

Here $\dot{\tau}$ and $\dot{\delta}$ are given by the single particle dynamics:

$$-\frac{1}{\eta} \dot{\tau} = \frac{\partial H}{\partial \delta}, \tag{2.69}$$

$$-\frac{1}{\eta} \dot{\delta} = -\frac{\partial H}{\partial \tau}, \tag{2.70}$$

where H is given by Eq. 2.67. It is easy to verify that Eqs. 2.69 and 2.70 are the same as Eqs. 2.12 and 2.13 for the longitudinal synchrotron motion.

Since the left hand side of Eq. 2.68 can also be written as $d\psi/dt = 0$, the time independent solution (the equilibrium solution of the Eq. 2.68) must be a constant of motion. When ψ does not depend on time explicitly, the Hamiltonian is the only

constant of motion for this one-dimensional dynamical system. Thus, the stationary solution of the Vlasov equation must be a function of H: $\psi = f(H)$.

In order to determine the exact functional form of $f(H)$, we need to consider the damping and diffusion processes in the phase space. To understand the damping process, we reexamine Eq. 2.5, where the synchrotron radiation loss $U = \epsilon V \sin(\phi_s)$ is a constant. In reality, U is a function of the particle energy: $U(E_0 + \delta E)$, with $U(E_0) = \epsilon V \sin(\phi_s)$. Expanding $U(E_0 + \delta E)$ around E_0, we add a damping term to Eq. 2.70:

$$\dot{\delta} = \eta \frac{\partial H}{\partial \tau} - \frac{2}{t_r}\delta, \qquad (2.71)$$

where $t_r = 2T_0 / \frac{dU}{dE}$ is the radiation damping time [38]. The diffusion process in phase space is the result of the quantum nature of synchrotron radiation. It can be described by an energy diffusion constant D. With these additions, the Vlasov equation 2.68 becomes the Fokker-Planck equation [43]:

$$\frac{\partial \psi}{\partial t} - \eta \frac{\partial H}{\partial \delta}\frac{\partial \psi}{\partial \tau} + (\eta \frac{\partial H}{\partial \tau} - \frac{2}{t_r}\delta)\frac{\partial \psi}{\partial \delta} = \frac{2}{t_r}\psi + D\frac{\partial^2 \psi}{\partial \delta^2}. \qquad (2.72)$$

Substituting the time-independent solution $\psi = f(H)$ into the Fokker-Planck equation, noting that H is a constant of motion and $\partial H/\partial \delta = \delta$, we have

$$\frac{2}{t_r}f + Df' + \delta^2(\frac{2}{t_r}f' + Df'') = 0. \qquad (2.73)$$

The condition that Eq. 2.73 must valid for all δ leads us to

$$\frac{2}{t_r}f + Df' = 0. \qquad (2.74)$$

Thus, we conclude that ψ is an exponential function of H:

$$\psi \propto \exp(-\frac{H}{\sigma_{\delta 0}^2}), \qquad (2.75)$$

where $\sigma_{\delta 0}$, the equilibrium energy spread, is determined by balancing the radiation damping and the quantum diffusion:

$$\sigma_{\delta 0}^2 = \frac{Dt_r}{2}. \qquad (2.76)$$

46

Since the Hamiltonian of Eq. 2.67 is a quadratic function of the energy deviation δ, the equilibrium energy distribution of the bunch is always Gaussian, regardless of the wake field. Without the wake field, the equilibrium distribution in τ is also Gaussian. This τ distribution will be distorted from a Gaussian shape when the longitudinal wake field is included. In general, the τ distribution $\rho(\tau)$ is related to the distribution function ψ by:

$$\psi(\tau, \delta) = \frac{1}{\sqrt{2\pi}\sigma_{\delta 0}} \exp(-\frac{\delta^2}{2\sigma_{\delta 0}^2})\rho(\tau). \tag{2.77}$$

Substituting Eq. 2.77 into Eq. 2.75 with the explicit form of the Hamiltonian given by Eq. 2.67, we obtain a transcendental integral equation for $\rho(\tau)$:

$$\rho(\tau) = A_0 \exp\left(-\frac{\omega_{s0}^2\tau^2}{2\eta^2\sigma_{\delta 0}^2} - \frac{Ne^2L_0}{\eta E_0 T_0 \sigma_{\delta 0}^2} \int_0^\tau d\tau' \int_{\tau'}^{+\infty} d\tau'' \rho(\tau'')W(\tau'' - \tau')\right). \tag{2.78}$$

Here A_0 is determined by the normalization of ρ, $\int d\tau \rho = 1$. This equation is sometimes called the Haissinski equation; it was derived independently by many people [17, 18, 19]. The double integral in Eq. 2.78 can be simplified further. Consider the double integral

$$A(\tau) = \int_0^\tau d\tau' \int_{\tau'}^{+\infty} d\tau'' \rho(\tau'')W(\tau'' - \tau'). \tag{2.79}$$

Changing the variable of integration τ'' to $t = \tau'' - \tau'$ gives

$$A(\tau) = \int_0^\tau d\tau' \int_0^{+\infty} dt \rho(t + \tau')W(t). \tag{2.80}$$

From Eq. 2.80, $A(\tau)$ satisfies the following differential equation:

$$\frac{dA}{d\tau} = \int_0^{+\infty} dt \rho(t + \tau)W(t). \tag{2.81}$$

Now, consider

$$B(\tau) = -\int_0^{+\infty} dt \rho(t + \tau)g(t), \tag{2.82}$$

where $g(t)$ is related to the wake function $W(t)$ by

$$g(t) = \int_0^t dt' W(t'). \tag{2.83}$$

47

Evaluating the derivative of $B(\tau)$, we find

$$
\begin{aligned}
\frac{dB}{d\tau} &= -\int_0^{+\infty} dt \left[\frac{\partial}{\partial t} \rho(t+\tau) \right] g(t) \\
&= \int_0^{+\infty} dt \rho(t+\tau) W(t).
\end{aligned} \tag{2.84}
$$

In deriving Eq. 2.84, we have used a partial integration with $\rho(+\infty) = 0$ and $g(0) = 0$. Comparing it with Eq. 2.81, we conclude that

$$
A(\tau) = B(\tau) + \text{constant.} \tag{2.85}
$$

Substituting the double integral $A(\tau)$ in Eq. 2.78 with the single integral $B(\tau)$, and absorbing the constant into the normalization constant A_0, we get [44]

$$
\rho(\tau) = A_0 \exp\left(-\frac{\omega_{s0}^2 \tau^2}{2\eta^2 \sigma_{\delta0}^2} - \frac{Ne^2 L_0}{\eta E_0 T_0 \sigma_{\delta0}^2} \int_0^{+\infty} dt \rho(t+\tau) g(t) \right). \tag{2.86}
$$

Obviously, this equation is not easily solvable analytically and often needs to be approached numerically. Due to the causality of the wake field, it is rather straightforward to obtain a numerical solution. Since the right hand side of Eq. 2.86 contains only the values of $\rho(\tau')$ at $\tau' > \tau$, Eq. 2.86 can be sequentially solved from the front to the back of the bunch under the assumption that $\rho(\tau)$ vanishes for $\tau \to +\infty$. For a fixed A_0, we can calculate $b(A_0) = \int d\tau \rho(\tau)$. Then we solve the equation $b(A_0) = 1$ to determine the correct normalization constant.

Another interesting point from Eq. 2.86 is the relationship between the energy spread and the equilibrium bunch length. When the current is zero, we have

$$
\sigma_{\tau0} = \frac{\eta}{\omega_{s0}} \sigma_{\delta0}. \tag{2.87}
$$

Figure 2.5 shows the numerical solution of Eq 2.86 for the SPEAR II ring impedance for various currents. The bunch shape is Gaussian at low bunch currents, but clearly distorts as bunch current is increased. Another feature is that the center of the

bunch shifts forward, so that the parasitic energy losses are compensated for by the RF voltage.

If a static solution of Eq. 2.86 exists, will it always describe the synchrotron motion of the bunch? In other words, as we increase the beam current, will the distribution in energy always be Gaussian with a energy spread independent of the current? The answer is no. The wake field starts to drive the bunch lengthening instability when the bunch current reaches some threshold value. The static solution of Eq. 2.86 is no longer stable and can not describe the motion of the bunch. Both the experimental observations and theoretical analysis of bunch lengthening will be given in the next chapter.

Fig. 2.6 plots the measured bunch shapes vs. distributions calculated based on a modified Haissinski equation for the electron damping ring in SLAC. The agreements are excellent.

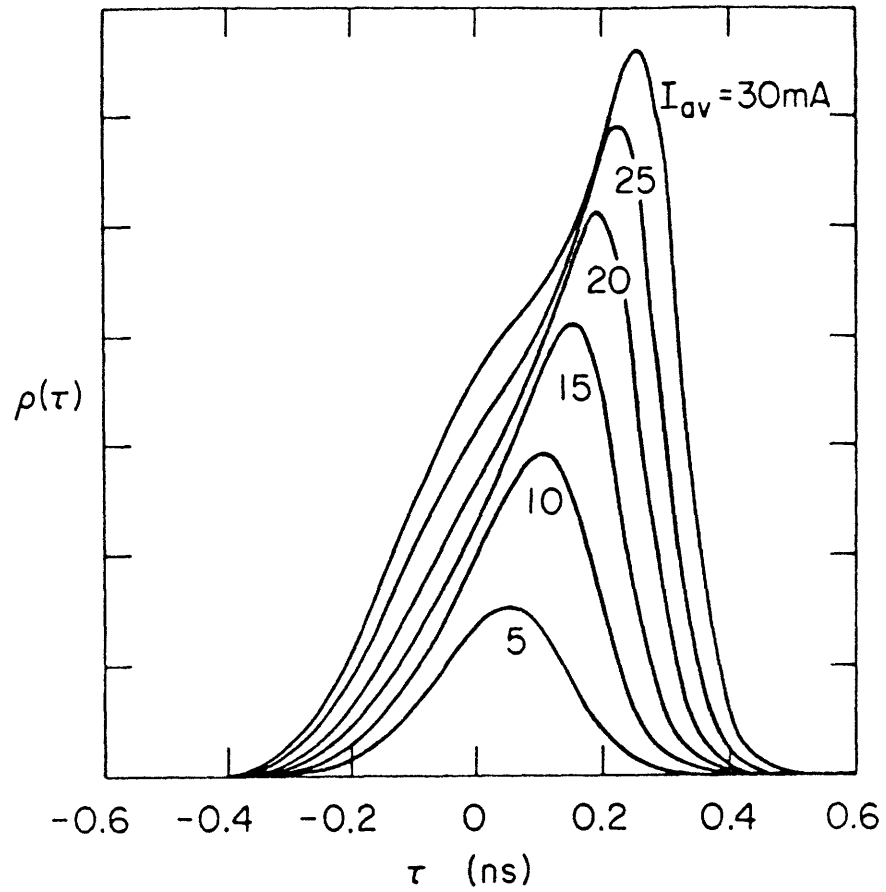Figure 2.5: Potential well distorted bunch shape for various beam intensities calculated for the storage ring SPEAR II parameters based on Haissinski equation 2.86. (from Bane, Chao and Lee, 1978.)
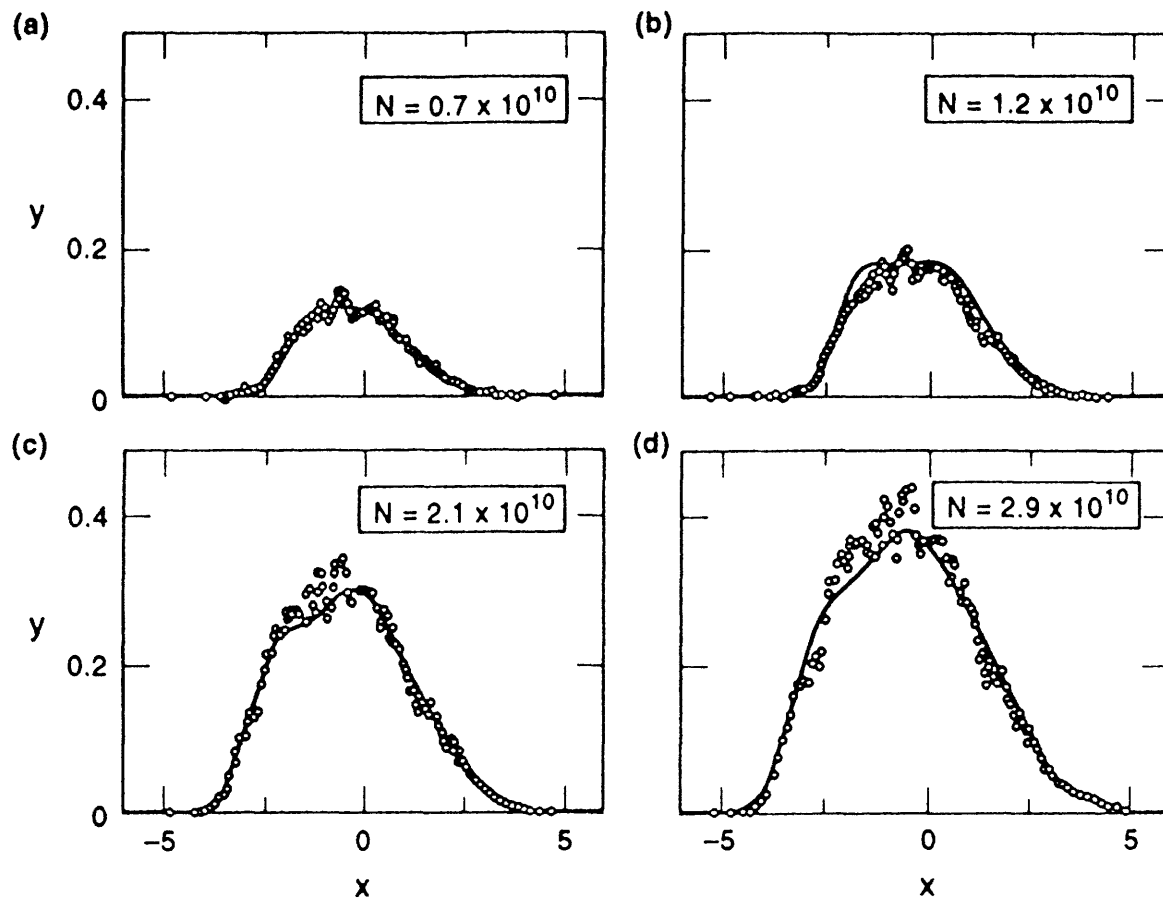
Figure 2.6: Potential well distortion of bunch shape for various beam intensities for the SLC damping ring. Plotted points are data; solid curves are calculations based on Haissinski equation 2.86. (from Bane and Ruth, 1992.)

Chapter 3

Theoretical Analysis of the Bunch Lengthening Instability

In the last section of Ch. 2, we solved the bunch-environment system self-consistently and determined the equilibrium bunch shape. In this chapter, we will study the stability of this equilibrium. First, we will summarize the detailed experimental measurements obtained by Wilson et al. in 1977 [8]. These revealed that, as the bunch current exceeded a threshold value, the bunch behaved differently from predictions of the static potential well distortion theory. Most prominently, both the bunch length and energy spread were observed to increase. They also observed the strong excitation of several coherent synchrotron modes above the threshold current. These observations suggest that the equilibrium determined by the static potential well distortion is unstable when the current reaches a threshold. We will apply the Vlasov [24] technique to study the bunch lengthening instability perturbatively. Since most experiments and numerical simulations give no clear evidence of mode coupling at threshold, we will abandon the mode-coupling approach and search for an instability which occurs for a single synchrotron mode. Our approach is to include the nonlinear static wake force. We will show that if we ignore this nonlinearity, the bunch will always be stable. Nonlinearity of the static wake force gives rise to a non-Gaussian distortion of the bunch, which in turn drives the bunch lengthening

instability.

3.1 Experimental Results

In 1977, Wilson et at. [8] reported an extensive measurements of the bunch length and the energy spread in the storage ring SPEAR II. Some of their results are shown in Figure. 3.1. Their findings are summarized by:

1. At a threshold current, both the bunch length and the energy spread increase abruptly. Since the static potential well distortion theory dictates that the energy spread remains constant. this gives a strong indication that the bunch motion is no longer described by the equilibrium solution of the Vlasov equation above this threshold current.

2. Bunch lengthening thresholds coincide with the growth of longitudinal modes. The quadrupole mode appears at the lowest current, corresponding to the onset of an abrupt increase in bunch length. Other modes contribute less strongly at higher currents. This also supports the observation that some synchrotron modes become unstable at the threshold.

3. The energy width of the bunch core follows the bunch length very closely in the various current regimes.

4. Below the threshold, there is a nearly linear relation between the shift of the synchrotron phase angle and the current. This indicates the parasitic mode resistance must be almost constant. However, this linearity breaks down as the current reaches the threshold.
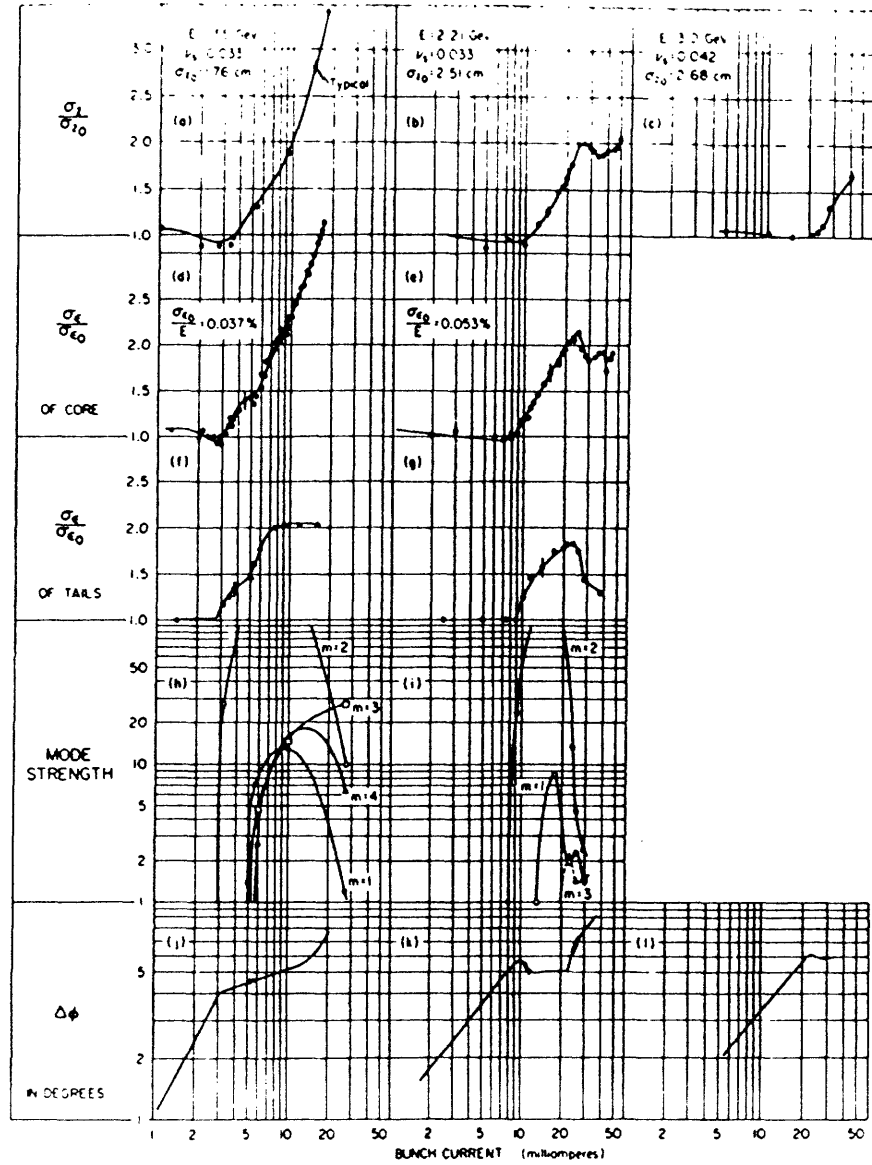
Figure 3.1: Bunch lengthening measurements on SPEAR II. Bunch length, energy spread, mode strength and phase shift data plotted as a function of bunch current. (from Wilson et al., 1977.)

5. There is a scaling behavior of the dependence of the bunch length on the machine parameters after the current reaches the threshold. This scaling parameter is

$$\varsigma_c = \frac{I\eta}{\nu_{s0}^2 E_0} \qquad (3.1)$$

There are other good measurements of the bunch lengthening instability, most notably the one done on the SLC damping ring by Rivkin et al. [33]. The conclusions are the same as Wilson's. Rivkin et al. also measured synchrotron oscillation frequencies as a function of the bunch current and observed no coupling of lower-order modes at the threshold current.

3.2   Longitudinal Modes

From this section onwards, we investigate the stability of the static potential well distorted equilibrium. The Vlasov equation 2.68 for the particle distribution $\psi(\tau, \delta, t)$ is given by

$$\frac{\partial \psi}{\partial t} + \frac{d\tau}{dt}\frac{\partial \psi}{\partial \tau} + \frac{d\delta}{dt}\frac{\partial \psi}{\partial \delta} = 0. \qquad (3.2)$$

The single particle dynamics are (Eqs. 2.12 and 2.13)

$$\frac{d\tau}{dt} = -\eta\delta, \qquad (3.3)$$

$$\frac{d\delta}{dt} = \frac{\omega_{s0}^2}{\eta}\tau - \frac{1}{E_0 T_0}F(\tau). \qquad (3.4)$$

Substituting Eqs. 3.3 and 3.4 into Eq. 3.2 yields

$$\frac{\partial \psi}{\partial t} - \eta\delta\frac{\partial \psi}{\partial \tau} + \frac{\omega_{s0}^2}{\eta}\tau\frac{\partial \psi}{\partial \delta} - \frac{F(\tau)}{E_0 T_0}\frac{\partial \psi}{\partial \delta} = 0. \qquad (3.5)$$

In order to understand the mode structure clearly, we will investigate Eq. 3.5 in increasing complexity. First, we consider Eq. 3.5 without the wake field

$$\frac{\partial \psi}{\partial t} - \eta\delta\frac{\partial \psi}{\partial \tau} + \frac{\omega_{s0}^2}{\eta}\tau\frac{\partial \psi}{\partial \delta} = 0. \qquad (3.6)$$

In the polar coordinates,

$$\tau = r\cos\phi,$$

$$\frac{\eta}{\omega_{s0}}\delta = r\sin\phi, \tag{3.7}$$

the Vlasov equation takes the much simpler form

$$\frac{\partial\psi}{\partial t} + \omega_{s0}\frac{\partial\psi}{\partial\phi} = 0. \tag{3.8}$$

The equilibrium, or the time-independent solution of the Vlasov equation must not depend on ϕ:

$$\psi_0 = \psi_0(r). \tag{3.9}$$

From the arguments in Sec. 2.3, we know that

$$\psi_0(r) = \frac{\omega_{s0}}{2\pi\eta\sigma_{\delta 0}^2}\exp\left(-\frac{\omega_{s0}^2 r^2}{\eta^2\sigma_{\delta 0}^2}\right). \tag{3.10}$$

The time-dependent solutions of the Vlasov equation, known as coherent synchrotron modes are

$$\psi_l = R_l(r)\exp(il\phi - i\Omega t). \tag{3.11}$$

Substituting Eq. 3.11 into the Vlasov equation in the polar coordinate Eq. 3.8, we get the eigenvalues:

$$\Omega^{(l)} = l\omega_{s0} \tag{3.12}$$

Here l is any integer.

In conclusion, we have the longitudinal modes of the system. Their frequencies are multiples of the synchrotron frequency ω_{s0}. For a particular synchrotron mode $\Omega^{(l)} = l\omega_{s0}$, the distribution is

$$\psi = R_l(r)\exp(il\phi - il\omega_{s0}t). \tag{3.13}$$

Since we did not include the wakefield, the internal structure of each synchrotron mode is degenerate. Thus the eigenfunction $R_l(r)$ is arbitrary.

3.3 Sacherer Equation

In this section, we will start to consider the effect of the wake field on the equilibrium by investigating the Vlasov equation perturbatively:

$$\psi = \psi_0 + \psi_1 + \cdots. \tag{3.14}$$

The zero'th order Vlasov equation is:

$$-\eta\delta\frac{\partial\psi_0}{\partial\tau} + \frac{\omega_{s0}^2}{\eta}\tau\frac{\partial\psi_0}{\partial\delta} - \frac{F_0(\tau)}{E_0T_0}\frac{\partial\psi_0}{\partial\delta} = 0. \tag{3.15}$$

Here the subscript 0 denotes a zero'th order quantity. In this section, we will only keep the linear order terms in the zero'th order wake force:

$$F_0(\tau) = F_0(0) + \frac{dF_0}{d\tau}\tau + O(\tau^2). \tag{3.16}$$

Substituting Eq. 3.16 into Eq. 3.15, it is evident that all the wake field effects can be incorporated into an incoherent frequency shift,

$$\omega_{s0}^2 \rightarrow \omega_s^2[1 - \frac{\eta}{E_0T_0\omega_{s0}^2}\frac{dF_0}{d\tau}], \tag{3.17}$$

and a shift of the center of the bunch:

$$\tau \rightarrow \tau' = \tau - \tau_0, \tag{3.18}$$

with

$$\tau_0 = \frac{\eta}{E_0T_0\omega_s^2}F_0(0). \tag{3.19}$$

Thus the zero'th order solution of the Vlasov equation, i.e. the equilibrium distribution, is still given by Eq. 3.10 with the shifted synchrotron frequency ω_s to replacing ω_{s0} and the center of the bunch shifted to τ_0 ($\tau \rightarrow \tau'$):

$$\psi_0(r) = \frac{\omega_s}{2\pi\eta\sigma_{\delta0}^2}\exp\left(-\frac{\omega_s^2r^2}{\eta^2\sigma_{\delta0}^2}\right). \tag{3.20}$$

It is interesting to note that this linear dependence of the shift of the center of the bunch on the bunch current has been clearly identified in the experiment of Wilson described in Sec. 3.1 (see Fig. 3.1).

Now consider the first order Vlasov equation:

$$\frac{\partial \psi_1}{\partial t} - \eta\delta\frac{\partial \psi_1}{\partial \tau} + \frac{\omega_{s0}^2}{\eta}[\tau - \frac{\eta F_0(\tau)}{E_0 T_0 \omega_{s0}^2}]\frac{\partial \psi_1}{\partial \delta} - \frac{F_1(\tau)}{E_0 T_0}\frac{\partial \psi_0}{\partial \delta} = 0. \qquad (3.21)$$

Using the linearized zero'th order wake force approximation, we have

$$\frac{\partial \psi_1}{\partial t} - \eta\delta\frac{\partial \psi_1}{\partial \tau'} + \frac{\omega_s^2}{\eta}\tau'\frac{\partial \psi_1}{\partial \delta} - \frac{F_1(\tau')}{E_0 T_0}\frac{\partial \psi_0}{\partial \delta} = 0. \qquad (3.22)$$

Note we have shifted the zero point of the arrival time to the center of the bunch by using τ'. Change now into the polar coordinates

$$\tau' = r\cos\phi,$$

$$\frac{\eta}{\omega_s}\delta = r\sin\phi. \qquad (3.23)$$

Note the difference between Eq. 3.7 and Eq. 3.23. In Eq. 3.7, corresponding to the case of zero bunch current, the center of the polar coordinate is chosen to be the same as the position of the synchronous electron. In Eq. 3.23, corresponding to the more general case of non-zero bunch current, we have shifted the center of the polar coordinate to the center of the bunch, which is different from the position of the synchronous electron when the bunch current is not zero. We have also used the shifted synchrotron frequency ω_s in Eq. 3.23. Equation 3.22 can be further simplified:

$$\frac{\partial \psi}{\partial t} + \omega_s\frac{\partial \psi}{\partial \phi} - \frac{F_1(\tau')}{E_0 T_0}\frac{\partial \psi_0}{\partial \delta} = 0. \qquad (3.24)$$

where τ' and δ are to be regarded as functions of (r, ϕ). Next, Fourier expand ψ_1 in terms of the synchrotron modes:

$$\psi_1 = \sum_{l=-\infty}^{+\infty} R_l(r)\exp(il\phi - i\Omega t). \qquad (3.25)$$

This is always possible since ψ_1 must be periodic in ϕ with period 2π. We have used l as the summation index in anticipation that it actually is the longitudinal mode index discussed in Sec. 3.2 in the limit of weak beam intensities.

Substituting Eq. 3.25 into Eq. 3.24 yields

$$-i\sum_{l'}(\Omega - l'\omega_s)R_{l'}(r)\exp(il'\phi) - \frac{\eta e^2}{E_0 T_0 \omega_s}\sin\phi\psi_0'(r)$$

$$\times \int d\omega \tilde{\rho}_1(\omega)\exp(i\omega\tau')Z(\omega) = 0. \qquad (3.26)$$

Here $\tilde{\rho}$ is the Fourier transform of the density

$$\tilde{\rho}_1(\omega) = \int \frac{d\tau'}{2\pi}\exp(-i\omega\tau')\rho_1(\tau). \qquad (3.27)$$

Multiply Eq. 3.26 by $\exp(-il\phi)$ and integrate over ϕ from 0 to 2π, using the integral identity

$$\int \frac{d\phi}{2\pi}\exp(-il\phi + i\omega r\cos\phi)\sin\phi = -i^l\frac{l}{\omega r}J_l(\omega r), \qquad (3.28)$$

to obtain the eigenvalues equations

$$-i(\Omega - l\omega_s)R_l(r) + \frac{\eta e^2}{E_0 T_0 \omega_s}l i^l\frac{\psi_0'(r)}{r}\int d\omega \tilde{\rho}_1(\omega)\frac{Z(\omega)}{\omega}J_l(\omega r) = 0.$$

$$l = 0, \pm 1, \pm 2, \cdots \qquad (3.29)$$

In Eq. 3.29, $J_l(x)$ is the Bessel function. We will need to express $\tilde{\rho}_1(\omega)$ in terms of the longitudinal synchrotron modes:

$$\tilde{\rho}_1(\omega) = \int \frac{d\tau}{2\pi}\exp(-i\omega\tau)\rho_1(\tau)$$

$$= \frac{1}{2\pi}\int d\tau \int d\delta \exp(-i\omega\tau')\psi_1(r,\psi)$$

$$= \frac{\omega_s}{2\pi\alpha}\int_0^{2\pi} d\phi \int_0^{+\infty} rdr\exp(-i\omega r\cos\phi)\sum_{l'}R_{l'}\exp(il'\phi)$$

$$= \frac{\omega_s}{\eta}\sum_{l'}i^{-l'}\int_0^{+\infty} rdr R_{l'}(r)J_{l'}(\omega r). \qquad (3.30)$$

59

Substituting Eq. 3.30 into Eq. 3.29, we have

$$(\Omega - l\omega_s)R_l(r) = -i\frac{e^2}{E_0T_0}l\frac{\psi_0'(r)}{r}\sum_{l'}\int r'dr'$$

$$\times\, i^{l-l'}R_{l'}(r')\int d\omega\frac{Z(\omega)}{\omega}J_l(\omega r)J_{l'}(\omega r'). \tag{3.31}$$

Given the impedance Z and the initial distribution ψ_0, we can in principle solve this eigenvalue problem to get the eigenvalues and eigenfunctions. We can calculate the bunch lengthening threshold by determine the bunch current such that the system first has complex eigenvalues. Many researchers have used this formalism to investigate the bunch lengthening instability. The coupling of two adjacent (higher) modes was first proposed by Sacherer [28]. However, the required strong impedances at frequencies well beyond the vacuum chamber cutoff made the model unconvincing. The theory of the coupling of the dipole mode ($l = 1$) with its mirror image ($l = -1$) was published a few years later [45, 46]. This eliminated the requirement for large impedances at very high frequencies, but the comparison of predictions for the threshold with measurements at SPEAR were unsatisfactory. Chao and Gareyte [13] developed a scaling theory for the bunch length and energy spread. Their qualitative result fits experiment well. However, their theory does not predict the threshold.

The most important objections to any theory based on the coupling of two low order synchrotron modes come from experiments. Both the experiment by P. Wilson et al. [8] and the more recent experiment by L. Rivkin et al. [33] did not observe mode coupling at the bunch lengthening threshold. For example, in Fig. 3.2, the frequency of the dipole mode and half the frequency of the quadrupole mode are plotted as a function of the number of particles in the SLC damping ring. These two modes are well-separated at the threshold $N=1.5\times10^{10}$. Our numerical simulations also seem to suggest this conclusion (see Ch. 4). Based on this, we will abandon the coupling of synchrotron modes in search for the instability mechanism and try to find the instability within a single synchrotron mode.
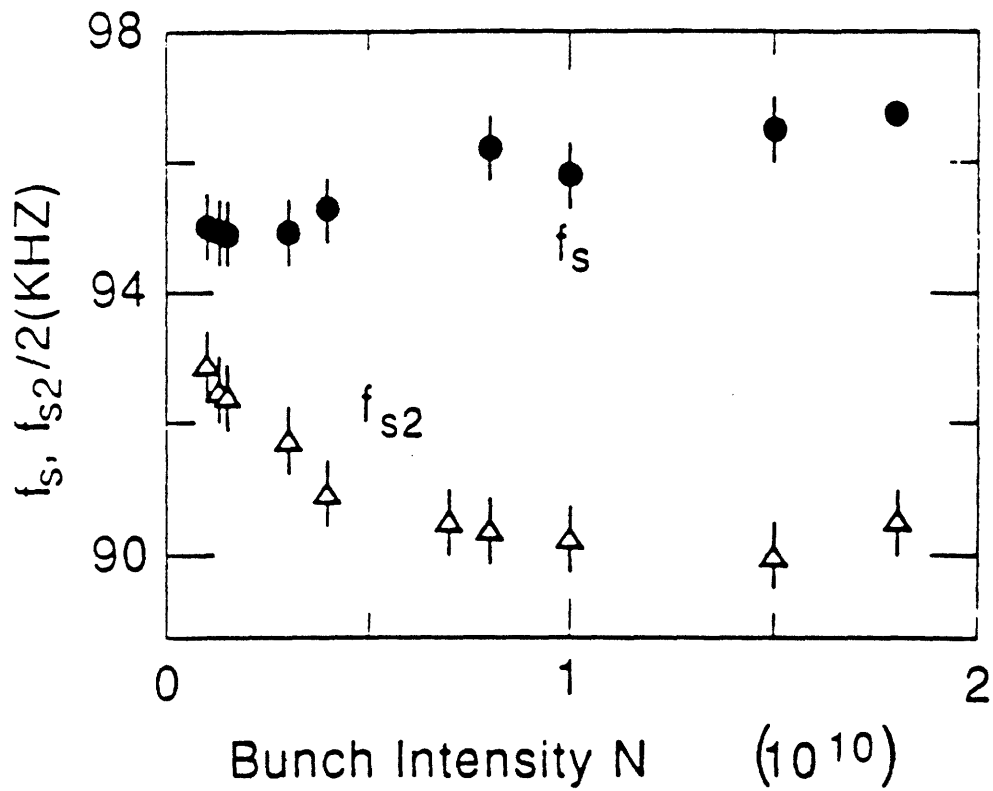
60

Figure 3.2: The longitudinal dipole and half the quadrupole mode frequencies as functions of beam intensity. Bunch lengthening threshold is at $N = 1.5 \times 10^{10}$. (from Rivkin et al., 1988.)

Neglecting the coupling of different synchrotron modes, Eq. 3.31 simplifies to:

$$(\Omega - l\omega_s)R_l(r) = \frac{Ne^2}{E_0 T_0} l \frac{\psi_0'(r)}{r} \int r'dr' G_l(r,r')R_l(r').$$

(3.32)

This is the Sacherer equation [29]. Here the kernel

$$G_l(r,r') = \int d\omega \frac{Im Z(\omega)}{\omega} J_l(\omega r) J_l(\omega r')$$

(3.33)

is real and symmetric and is determined by the imaginary part of the impedance $Z(\omega)$. In the next section, we will show that this equation only has real eigenvalues.

3.4 Stability of the Single Mode Sacherer Equation

We begin by examining the slightly generalized eigenvalue problem:

$$\Omega R(r) = \int dr' f_1(r) f_2(r') G(r,r') R(r').$$

(3.34)

We will assume that $G(r,r')$ is real and symmetric and all other quantities are real. Define

$$F(r) = R(r)/f_1(r),$$

(3.35)

the eigenvalue problem changes into:

$$\Omega F(r) = \int dr' w(r') G(r,r') F(r').$$

(3.36)

$w(r)$ is the weight function and is given by

$$w(r) = f_1(r) f_2(r).$$

(3.37)

Usually $w(r)$ is a positive function. Define the inner product for the Hilbert space spanned by the eigenfunctions of the Eq. 3.36 as

$$(u, v) = \int dr w(r) u(r) v(r),$$

(3.38)

Consider the right hand side of Eq. 3.36 as the action of integral operator I_{op} acting on the function $F(r)$:

$$I_{op}F(r) = \int dr' w(r')G(r,r')F(r'). \tag{3.39}$$

We can prove that the operator I_{op} is symmetric, i.e.

$$(u, I_{op}v) = (I_{op}u, v). \tag{3.40}$$

Since

$$(u, I_{op}v) = \int dr\, w(r)u(r)I_{op}v(r)$$

$$= \int dr\, w(r)u(r) \int dr'\, w(r')G(r,r')v(r')$$

$$= \int dr\, dr'\, w(r)w(r')u(r)v(r')G(r,r')$$

$$= \int dr\, dr'\, w(r)w(r')u(r')v(r)G(r',r),$$

and since $G(r,r')$ is symmetric, we find

$$(u, I_{op}v) = \int dr\, dr'\, w(r)w(r')u(r')v(r)G(r,r')$$

$$= \int dr\, w(r) \left[\int dr'\, w(r')G(r,r')u(r') \right] v(r)$$

$$= \int dr\, w(r)I_{op}u(r)v(r) = (I_{op}u, v). \tag{3.41}$$

The operator I_{op} is also real, and thus it only has real eigenvalues.

We conclude that the single mode Sacherer equation 3.32 only has real eigenvalues. All synchrotron modes will always be stable. In order to explain the bunch lengthening instability within the single mode framework, we need to look for new instability mechanism.

3.5 Improved Sacherer Equation, Part 1.

Left out in our derivation of the single mode Sacherer equation 3.32 were nonlinear terms in the zero'th order wake force. This is a poor approximation, as seen in Fig. 3.3, where the zero'th order wake force and the equilibrium bunch shape are plotted for a bunch current near threshold. It is clear from Fig. 3.3 that the bunch experiences significant nonlinearity of the wake force.

When the nonlinearity of the wakefield is included, the arguments following Eq. 3.16 are no longer valid. Substitution of Eq. 3.16 with full nonlinearity into Eq. 3.15 shows that the effect of the wake field on the equilibrium can not be fully described by the synchrotron frequency shift and the shift of the center of the bunch. Although the distribution in the energy spread is still Gaussian in the static potential well theory (i.e. below threshold), the arrival time distribution $\rho(\tau)$ is distorted from a Gaussian. Transforming to polar coordinates, the equilibrium distribution will, in general, be a function of both r and ϕ: $\psi_0(r, \phi)$.

Fourier expanding $\psi_0(r, \phi)$ in the ϕ variable gives

$$\psi_0(r, \phi) = f_0(r) + f_1(r) \cos\phi + f_2(r) \cos 2\phi + \cdots. \tag{3.42}$$

Since $\delta \propto \sin\phi$ and ψ_0 is an even function of δ, there are no $\sin n\phi$ terms in the expansion Eq. 3.42.

When the current $I = 0$, we only get a ϕ-independent term: $f_0(r) = \psi_0(r)$. This will lead us to the real and symmetric operator (which is proportional to the current), found in the single mode Sacherer equation. When the current is not zero, we get $f_1(r)$, $f_2(r)$, etc. These terms are proportional to the current and they introduce asymmetric perturbations to the Sacherer equation which are proportional to the square of the current. Thus, we anticipate deriving a new, improved, Sacherer-like
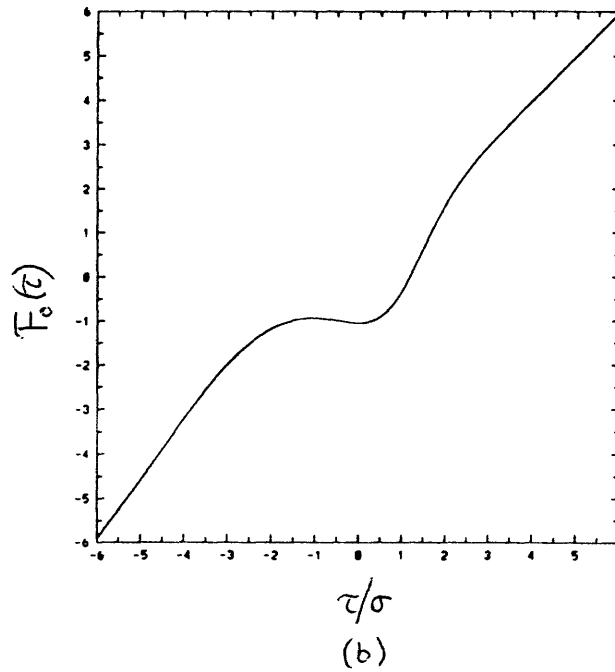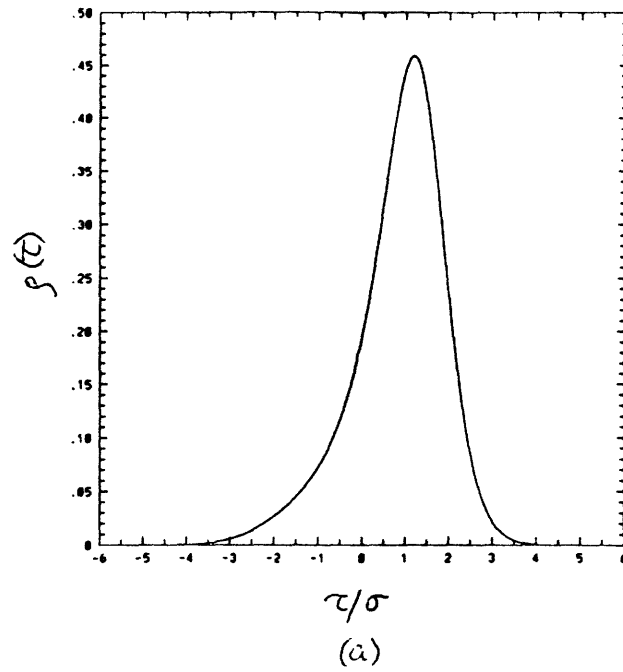
(a)

(b)

Figure 3.3: Nonlinearity of static wake force from calculations based on SPEAR II data. Bunch current is at the threshold current of 45mA. (a) Density profile $\rho(\tau)$. (b) Static wake force $F_0(\tau)$ (given by Eq. 2.66).

equation of the form

$$(\Omega - l\omega_s)R_l(r) = I \times \quad \text{symmetric operator on } R_l$$

$$+ \quad I^2 \times \quad \text{asymmetric operator on } R_l. \tag{3.43}$$

An equation in the form of 3.43 has the property: When the current I is small, the symmetric operator dominates and the system has only real eigenvalues, and when I reaches some critical value, the asymmetric perturbations are big enough to push the eigenvalues into the complex plane. For currents greater than this critical current, the system is unstable.

3.6 Parameterization of the Equilibrium

We will now investigate the formalisms of the previous section in greater detail and develop an efficient computational algorithm for the computation of the threshold current.

In principle, we need to know all the functions $f_n(r)$, $n = 1, \ldots \infty$, in the Fourier expansion of the equilibrium Eq. 3.42. In order to develop a fast numerical scheme for studying the bunch lengthening instability, we need to truncate the series at as small n as possible. In this problem, we use the cummulant expansion technique to systematically truncate the series.

For an arbitrary distribution $\rho(\tau)$, consider its generating function

$$f(x) = \sum_{n=0}^{+\infty} \frac{x^n}{n!} <\tau^n> = 1 + x <\tau> + \frac{x^2}{2!} <\tau^2> + \frac{x^3}{3!} <\tau^3> + \frac{x^4}{4!} <\tau^4> + \cdots. \tag{3.44}$$

Here $<a>$ denotes the average by the distribution function $\rho(\tau)$:

$$<a> = \int d\tau \rho(\tau) a(\tau). \tag{3.45}$$

66

$< \tau^n >$ is usually called the nth order moment of the distribution $\rho(\tau)$. The cummulant expansion for the generating function is defined by:

$$g(x) = \log f(x) = \log \left(1 + x < \tau > + \frac{x^2}{2!} < \tau^2 > + \frac{x^3}{3!} < \tau^3 > + \frac{x^4}{4!} < \tau^4 > + \cdots \right)$$

$$= 1 + x < \tau >_c + \frac{x^2}{2!} < \tau^2 >_c + \frac{x^3}{3!} < \tau^3 >_c + \frac{x^4}{4!} < \tau^4 >_c + \cdots . \qquad (3.46)$$

Here $< \tau^n >_c$ is the n'th order cummulant for the distribution ρ. Performing the Taylor expansion in Eq. 3.46 and equating terms of the same order in x gives the relationship between the ordinary moments and the cummulant moments:

$$< \tau >=< \tau >_c, \qquad (3.47)$$

$$< \tau^2 >_c =< \tau^2 > - < \tau >^2, \qquad (3.48)$$

$$< \tau^3 >_c =< \tau^3 > -3 < \tau >< \tau^2 >_c - < \tau >^3, \qquad (3.49)$$

$$< \tau^4 >_c =< \tau^4 > -3 < \tau^2 >_c^2 -4 < \tau >< \tau^3 >_c -6 < \tau >^2< \tau^2 >_c - < \tau >^4,$$

$$(3.50)$$

with the extension to higher-order moments straightforward. Note that $\sigma = \sqrt{< \tau^2 >_c}$ is the standard deviation, $\gamma_1 =< \tau^3 >_c /\sigma^3$ is the skewness and $\gamma_2 =< \tau^4 >_c /\sigma^4$ is the excess of the distribution.

Our strategy for the construction of the truncation is the following: First, we develop a numerical solver for the Haissinski equation 2.78. Due to the causality of the wake, this turns out to be relatively easy and the required computation time is very short. Second, after obtaining the distribution $\rho(\tau)$ numerically, we evaluate the average $< \tau >$, standard deviation σ, skewness γ_1 and excess γ_2. In principle, we can keep arbitrarily high order moments. But we will show later that for the SPEAR parameters, it is a sufficiently good approximation to keep the first four lowest order cummulants. Third, we need to construct an analytical functional form of the distribution ρ from these four cummulants. This is the task we describe below.

Consider

$$f(ik) = \sum_{n=0}^{+\infty} \frac{(ik)^n}{n!} < \tau^n > = \int d\tau \rho(\tau) \exp(ik\tau). \tag{3.51}$$

The distribution $\rho(\tau)$ can be found by the inverse Fourier transformation:

$$\rho(\tau) = \int \frac{dk}{2\pi} \exp(-ik\tau) f(ik)$$

$$\rho(\tau) = \int \frac{dk}{2\pi} \exp(-ik\tau) \exp\left(g(ik)\right)$$

$$= \int \frac{dk}{2\pi} \exp\left(-ik\tau + \sum_{n=1}^{+\infty} \frac{(ik)^n}{n!} < \tau^n >_c\right)$$

$$= \int \frac{dk}{2\pi} \exp\left(-ik(\tau - <\tau>) - \frac{k^2\sigma^2}{2} + \sum_{n\geq 3}^{+\infty} \frac{(ik)^n}{n!} < \tau^n >_c\right)$$

$$= \exp\left(\sum_{n\geq 3}^{+\infty} \frac{(-D)^n}{n!} < \tau^n >_c\right) n(\tau - <\tau>). \tag{3.52}$$

Here,

$$D = \frac{\partial}{\partial\tau}, \tag{3.53}$$

is a differential operator and

$$n(\tau) = \int \frac{dk}{2\pi} \exp\left(-ik\tau - \frac{k^2\sigma^2}{2}\right) = \frac{1}{\sqrt{2\pi}\sigma} \exp\left(-\frac{\tau^2}{2\sigma^2}\right), \tag{3.54}$$

is a normal distribution centered at the origin with standard deviation of σ.

In conclusion,

$$\rho(\tau) = \exp\left(\sum_{n\geq 3}^{+\infty} < \tau^n >_c \frac{(-D)^n}{n!}\right) n(\tau - <\tau>). \tag{3.55}$$

Now we are ready to start our truncation procedure: Keep only the skewness and excess moments in Eq. 3.55 and, since both the skewness and excess moments are proportional to the current, we can linearize with respect to them. Then

$$\rho(\tau) \approx \left[1 - \frac{\gamma_1\sigma^3}{6}D^3 + \frac{\gamma_2\sigma^4}{24}D^4\right] n(\tau - <\tau>). \tag{3.56}$$

68

Generally, differentiation j times with respect to τ of the normal distribution, $n(\tau)$, results in a j'th order polynomial $P_j(\tau)$ multiplied by the distribution $n(\tau)$ itself:

$$D^j n(\tau) = P_j(\tau) n(\tau). \tag{3.57}$$

We find

$$\rho(\tau) \approx \left[1 - \frac{\gamma_1 \sigma^3}{6} P_3(\tau') + \frac{\gamma_2 \sigma^4}{24} P_4(\tau') \right] n(\tau'). \tag{3.58}$$

Here $\tau' = \tau - <\tau>$. Substituting the explicit form of the polynomial P_2 and P_4 into Eq. 3.58 gives the desired expression for the distribution function $\rho(\tau)$ in terms of the first four moments of a cummulant expansion.

$$\rho(\tau) \approx \left[1 + \frac{\gamma_1}{6} \left(\frac{\tau'^3}{\sigma^3} - 3\frac{\tau'}{\sigma} \right) + \frac{\gamma_2}{24} \left(\frac{\tau'^4}{\sigma^4} - 6\frac{\tau'^2}{\sigma^2} + 3 \right) \right] n(\tau'). \tag{3.59}$$

There are a few properties of this approximate distribution Eq. 3.59 that are worth noting. First,

$$\int d\tau \rho(\tau) = \int d\tau' \left[1 + \frac{\gamma_1}{6} \left(\frac{\tau'^3}{\sigma^3} - 3\frac{\tau'}{\sigma} \right) + \frac{\gamma_2}{24} \left(\frac{\tau'^4}{\sigma^4} - 6\frac{\tau'^2}{\sigma^2} + 3 \right) \right] n(\tau')$$

$$= 1 + \frac{\gamma_2}{24} \int d\tau' \left(\frac{\tau'^4}{\sigma^4} - 6\frac{\tau'^2}{\sigma^2} + 3 \right) n(\tau'). \tag{3.60}$$

It is easy to verify the integral in Eq. 3.60 is zero, so that

$$\int d\tau \rho(\tau) = 1, \tag{3.61}$$

and the approximate distribution Eq. 3.59 satisfies the normalization condition.

Second, since the center of the distribution is defined by

$$\int d\tau \rho(\tau) \tau = <\tau> + \int d\tau \rho(\tau) \tau'$$

$$= <\tau> + \frac{\gamma_1}{6} \int d\tau' \left(\frac{\tau'^4}{\sigma^3} - 3\frac{\tau'^2}{\sigma} \right) n(\tau'), \tag{3.62}$$

and the integral in Eq. 3.62 is again zero, we conclude that neither skewness nor excess will change the center of the distribution.

69

Third, consider the variance of the distribution,

$$\int d\tau \rho(\tau)\tau'^2 = \sigma^2 + \frac{\gamma_2}{24} \int d\tau' \left(\frac{\tau'^6}{\sigma^4} - 6\frac{\tau'^4}{\sigma^2} + 3\tau'^2 \right) n(\tau'). \qquad (3.63)$$

Since the integral on the right hand side of Eq. 3.63 is once again zero, the variance is not affected by the skewness and excess moments.

Finally, we want to graphically compare the distribution given numerically by the Haissinski equation 2.86 with the distribution given by Eq. 3.59 with the same lowest four cummulants: $< \tau >$, σ, γ_1 and γ_2. We use the SPEAR II parameters with a bunch energy of 3GeV. In Fig. 3.4, the bunch current is 25mA. The solid line is the distribution given by the numerical solution of the Haissinski equation and the dashed line is the approximate distribution given by Eq. 3.59. We can hardly tell the difference between the two. In Fig. 3.4, we plot the wake field energy loss per turn. Since it is the convolution of the wake function and the distribution, the difference between two distributions has been further reduced. In Fig. 3.5, the current is at the threshold value of 45mA. Although the difference between the approximate distribution and the numerical distribution is getting bigger, it is still less than 5 percent. We conclude that it is a reasonable to use only the lowest four cummulants in our approximation of the equilibrium. For other cases, we might need to include higher order moments, and the principles and procedures of this section can be extended straightforwardly.

3.7 Determination of $f_n(r)$

Since we have the analytic form of the equilibrium in the Eq. 3.59, we are in a position to determine the functions $f_n(r)$. Substituting Eq. 3.59 into Eq. 2.77 gives the approximate equilibrium distribution function:

$$\psi_0(r, \phi) = \frac{\omega_s}{2\pi\sigma_{\delta 0}^2} \exp\left(-\frac{\delta^2}{2\sigma_{\delta 0}^2} - \frac{\tau'^2}{2\sigma^2} \right)$$

Figure 3.4: SPEAR II data with bunch current 20mA. Solid lines are computed from Haissinski equation 2.86. Dashed lines are from our approximate distribution 3.60. (a) Density profile $\rho(\tau)$. (b) Static wake force $F_0(\tau)$ (given by Eq. 2.66).
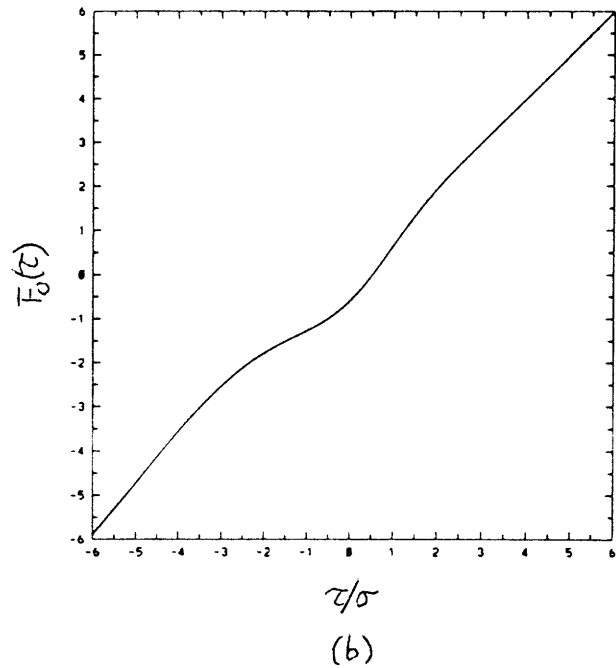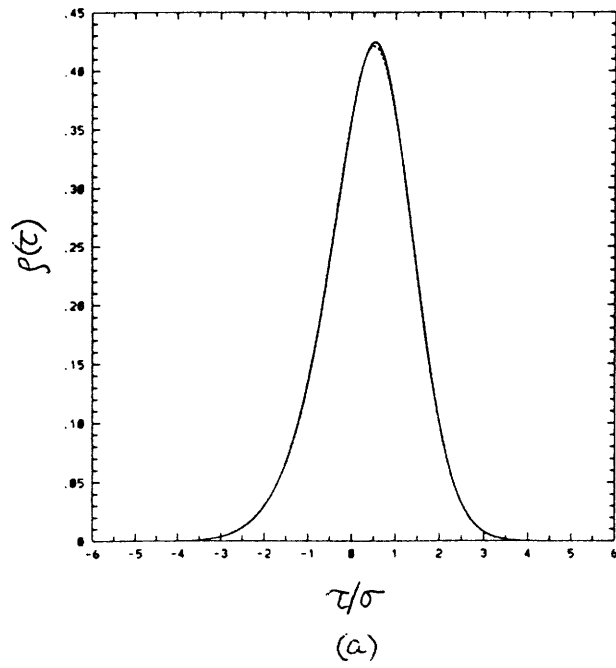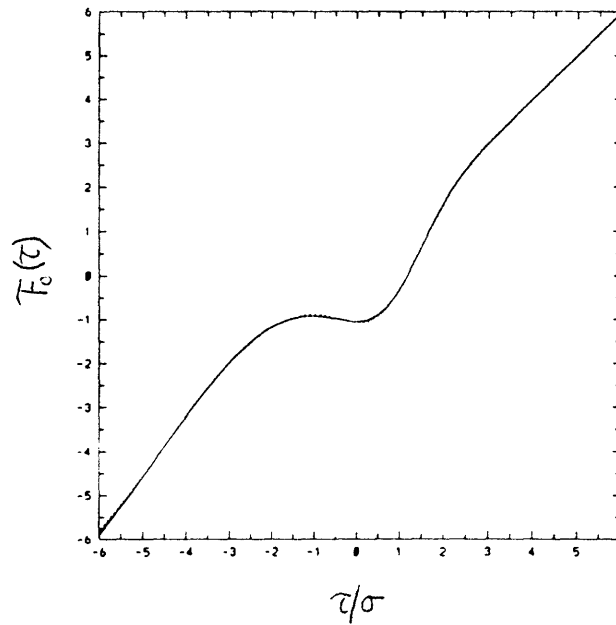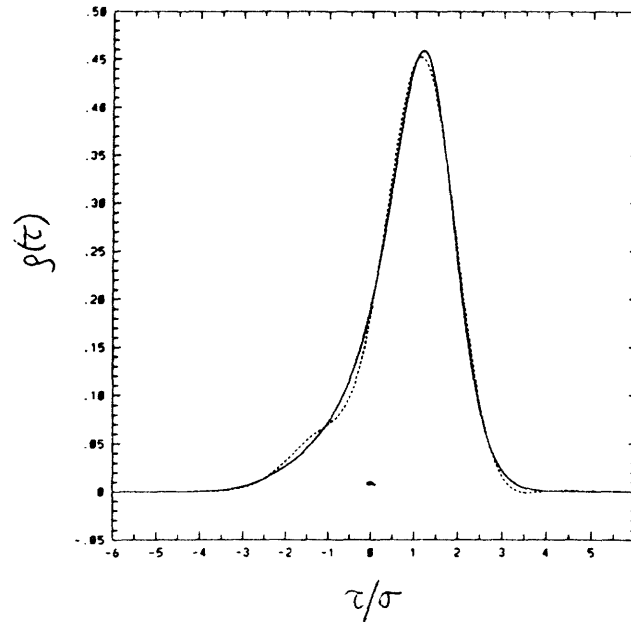
Figure 3.5: SPEAR II data with bunch current 45mA. Solid lines are computed from Haissinski equation 2.86. Dashed lines are from our approximate distribution 3.60. (a) Density profile $\rho(\tau)$. (b) Static wake force $F_0(\tau)$ (given by Eq. 2.66).

72

$$\times \left[1 + \frac{\gamma_1}{6} \left(\frac{\tau'^3}{\sigma^3} - 3\frac{\tau'}{\sigma} \right) + \frac{\gamma_2}{24} \left(\frac{\tau'^4}{\sigma^4} - 6\frac{\tau'^2}{\sigma^2} + 3 \right) \right]. \tag{3.64}$$

Transforming into the polar coordinates

$$\tau' = r\cos\phi,$$

$$\frac{\eta}{\omega_s}\delta = r\sin\phi,$$

results in

$$\psi_0(r,\phi) = \psi_0(r)$$

$$\times \left[1 + \frac{\gamma_1}{6} \left(\frac{r^3}{\sigma^3}\cos^3\phi - 3\frac{r}{\sigma}\cos\phi \right) + \frac{\gamma_2}{24} \left(\frac{r^4}{\sigma^4}\cos^4\phi - 6\frac{r^2}{\sigma^2}\cos^2\phi + 3 \right) \right]. \tag{3.65}$$

Here $\psi_0(r)$ is given by Eq. 3.20:

$$\psi_0(r) = \frac{\omega_s}{2\pi\sigma_{\delta0}^2} \exp\left(-\frac{\omega_s^2 r^2}{2\eta^2\sigma_{\delta0}^2} \right).$$

Next substitute the trigonometric identities

$$\cos^2\phi = \frac{1}{2} + \frac{1}{2}\cos 2\phi, \tag{3.66}$$

$$\cos^3\phi = \frac{3}{4}\cos\phi + \frac{1}{4}\cos 3\phi, \tag{3.67}$$

$$\cos^4\phi = \frac{3}{8} + \frac{1}{2}\cos 2\phi + \frac{1}{8}\cos 4\phi, \tag{3.68}$$

into Eq. 3.65, and regroup terms so that the constant term is $f_0(r)$, the coefficient of $\cos\phi$ is $f_1(r)$, the coefficient of $\cos 2\phi$ is $f_2(r)$, etc. Then

$$f_0(r) = \psi_0(r) \left[1 + \frac{\gamma_2}{8} \left(\frac{r^4}{8\sigma^4} - \frac{r^2}{\sigma^2} + 1 \right) \right], \tag{3.69}$$

$$f_1(r) = \frac{\gamma_1}{8}\psi_0(r) \left(\frac{r^3}{\sigma^3} - 4\frac{r}{\sigma} \right), \tag{3.70}$$

$$f_2(r) = \frac{\gamma_2}{48}\psi_0(r) \left(\frac{r^4}{\sigma^4} - 6\frac{r^2}{\sigma^2} \right), \tag{3.71}$$

$$f_3(r) = \frac{\gamma_1}{24}\psi_0(r)\frac{r^3}{\sigma^3}, \tag{3.72}$$

73

$$f_4(r) = \frac{\gamma_2}{192} \psi_0(r) \frac{r^4}{\sigma^4}. \tag{3.73}$$

Substituting Eqs. 3.69– 3.73 into Eq. 3.42 gives the equilibrium distribution in terms of cummulants calculated from Haissinski equation 2.86. The next section shows how to study Vlasov equation with this equilibrium.

3.8 Improved Sacherer Equation, Part 2.

In Sec. 3.5, we demonstrated that the nonlinearity of the wake field will distort the equilibrium density from its Gaussian shape, and that this, in turn, will result in asymmetric corrections to the Sacherer equation. We also showed that the symmetric operator in the Sacherer equation is proportional to the current and the asymmetric operator correction terms are proportional to the square of the current. So we expect the asymmetric terms will push the eigenvalues of the system into complex plane when the current reaches some threshold value. In the previous two sections, we developed an efficient way to approximate the non-Gaussian equilibrium by cummulant expansions. With only four parameters, the center of the bunch, $< \tau >$, the bunch length, σ_τ, the skewness, γ_1 and the excess, γ_2, we can approximate the potential well distorted bunch shape very accurately even when the bunch current is close to the threshold value. With this approximation, we can obtain the analytic form of the equilibrium distribution. In this section, the results of the previous sections are used to derive our complete improved Sacherer Equation.

We start from the first order Vlasov equation 3.21:

$$\frac{\partial \psi_1}{\partial t} - \eta \delta \frac{\partial \psi_1}{\partial \tau} + \frac{\omega_{s0}^2}{\eta}[\tau - \frac{\eta F_0(\tau)}{E_0 T_0 \omega_{s0}^2}]\frac{\partial \psi_1}{\partial \delta} - \frac{F_1(\tau)}{E_0 T_0}\frac{\partial \psi_0}{\partial \delta} = 0. \tag{3.74}$$

Changing the zero point of the arrival time τ to the center of the bunch:

$$\tau' = \tau - < \tau >, \tag{3.75}$$

74

gives

$$\frac{\partial \psi_1}{\partial t} - \eta \delta \frac{\partial \psi_1}{\partial \tau'} + \frac{\omega_{s0}^2}{\eta} f(\tau') \frac{\partial \psi_1}{\partial \delta} - \frac{F_1(\tau')}{E_0 T_0} \frac{\partial \psi_0}{\partial \delta} = 0. \qquad (3.76)$$

Here $f(\tau')$ is given by

$$f(\tau') = \tau' + <\tau> - \frac{\eta F_0(\tau')}{E_0 T_0 \omega_{s0}^2}. \qquad (3.77)$$

We have retained all the nonlinear terms in the wake force. Next, define the shifted synchrotron frequency by

$$\frac{\omega_s}{\omega_{s0}} = \frac{\sigma_{\tau 0}}{\sigma_\tau}, \qquad (3.78)$$

and write the first order Vlasov equation as

$$\frac{\partial \psi_1}{\partial t} - \eta \delta \frac{\partial \psi_1}{\partial \tau'} + \frac{\omega_s^2}{\eta} \tau' \frac{\partial \psi_1}{\partial \delta} + g(\tau') \frac{\partial \psi_1}{\partial \delta} - \frac{F_1(\tau')}{E_0 T_0} \frac{\partial \psi_0}{\partial \delta} = 0. \qquad (3.79)$$

Here

$$g(\tau') = \frac{\omega_{s0}^2}{\eta} \left[f(\tau') - \frac{\omega_s^2}{\omega_{s0}^2} \tau' \right],$$

$$= \frac{\omega_{s0}^2}{\eta} \left[\left(1 - \frac{\omega_s^2}{\omega_{s0}^2} \right) \tau' + <\tau> - \frac{\eta F_0(\tau')}{E_0 T_0 \omega_{s0}^2} \right]. \qquad (3.80)$$

Introduce the polar coordinates

$$\tau' = r \cos \phi,$$

$$\frac{\eta}{\omega_s} \delta = r \sin \phi,$$

and the Vlasov equation reduces to

$$\frac{\partial \psi_1}{\partial t} + \omega_s \frac{\partial \psi_1}{\partial \phi} + g(\tau') \frac{\partial \psi_1}{\partial \delta} - \frac{F_1(\tau')}{E_0 T_0} \frac{\partial \psi_0}{\partial \delta} = 0. \qquad (3.81)$$

The first two terms in Eq. 3.81 are familiar. They are the Vlasov equation in polar coordinates when the bunch current is zero, or when the wake field is neglected. The time dependence in these two terms can be easily factored away if we assume the system is in the l synchrotron mode:

$$\psi_1 = \sum_{l'=-\infty}^{+\infty} R_{l'}(r) \exp(il'\phi - i\Omega t), \qquad (3.82)$$

75

then after projection into the l synchrotron mode, the contributions from the first two terms are:

$$- i(\Omega - l\omega_s)R_l(r). \tag{3.83}$$

The third and the fourth terms are the direct result of the wake field. We will investigate them in detail. From the expression for $g(\tau')$, we can break the third term into

$$g(\tau')\frac{\partial \psi_1}{\partial \delta} = A + B + C, \tag{3.84}$$

with

$$A = \frac{\omega_{s0}^2}{\eta} < \tau > \frac{\partial \psi_1}{\partial \delta}, \tag{3.85}$$

$$B = \frac{\omega_{s0}^2}{\eta}\left(1 - \frac{\omega_s^2}{\omega_{s0}^2}\right)\tau'\frac{\partial \psi_1}{\partial \delta}, \tag{3.86}$$

and

$$C = -\frac{F_0(\tau')}{E_0 T_0}\frac{\partial \psi_1}{\partial \delta}. \tag{3.87}$$

To proceed further, we need the relationship between the partial derivatives with respect to the polar coordinate variables r and φ to the partial derivatives with respect to the rectangular coordinates τ' and δ:

$$\frac{\partial \psi_1}{\partial \delta} = \frac{\eta}{\omega_s}\left(\frac{\partial \psi_1}{\partial r}\sin\phi + \frac{\partial \psi_1}{\partial \phi}\frac{\cos\phi}{r}\right). \tag{3.88}$$

Substituting the synchrotron mode decomposition of ψ_1 (Eq. 3.25) into Eq. 3.88 gives

$$\frac{\omega_s}{\eta}\frac{\partial \psi_1}{\partial \delta} = \sum_{l'=-\infty}^{+\infty} R'_{l'}(r)\exp(il'\phi)\sin\phi + \sum_{l'=-\infty}^{+\infty}\frac{R_{l'}(r)}{r}\exp(il'\phi)il'\cos\phi, \tag{3.89}$$

where we suppressed the factor $\exp(-i\Omega t)$ which is common to all terms in the first order Vlasov equation 3.21. So that

$$A = \frac{\omega_{s0}^2}{\omega_s} < \tau > \left[\sum_{l'=-\infty}^{+\infty} R'_{l'}(r)\exp(il'o)\sin\phi + \sum_{l'=-\infty}^{+\infty}\frac{R_{l'}(r)}{r}\exp(il'\phi)il'\cos\phi\right]. \tag{3.90}$$

76

Next we need to decompose this term into its l'th synchrotron mode,

$$A_l = \frac{1}{2\pi} \int d\phi \exp(-il\phi)A. \tag{3.91}$$

Noting that

$$\frac{1}{2\pi} \int d\phi \exp\left(i(l'-l)\phi\right)\sin\phi$$

$$= \frac{1}{2i}\frac{1}{2\pi} \int d\phi \exp\left(i(l'-l+1)\phi\right) - \frac{1}{2i}\frac{1}{2\pi} \int d\phi \exp\left(i(l'-l-1)\phi\right)$$

$$= \frac{i}{2}\left[\delta_{l'-l-1} - \delta_{l'-l+1}\right], \tag{3.92}$$

and

$$\frac{1}{2\pi} \int d\phi \exp\left(i(l'-l)\phi\right)\cos\phi$$

$$= \frac{1}{2}\frac{1}{2\pi} \int d\phi \exp\left(i(l'-l+1)\phi\right) + \frac{1}{2}\frac{1}{2\pi} \int d\phi \exp\left(i(l'-l-1)\phi\right)$$

$$= \frac{1}{2}\left[\delta_{l'-l-1} + \delta_{l'-l+1}\right], \tag{3.93}$$

we obtain

$$A_l = \frac{i}{2}\frac{\omega_{s0}^2}{\omega_s} < \tau > \left[R'_{l+1}(r) - R'_{l-1}(r) + (l-1)\frac{R_{l-1}(r)}{r} + (l+1)\frac{R_{l+1}(r)}{r}\right]. \tag{3.94}$$

There is no contribution to A_l from the l synchrotron mode. Since we will neglect the contributions from the neighboring modes, we have

$$A_l = 0, \tag{3.95}$$

in our improved Sacherer equation.

From Eq. 3.89,

$$B = \frac{\omega_{s0}^2}{\omega_s}\left(1 - \frac{\omega_s^2}{\omega_{s0}^2}\right) \sum_{l'=-\infty}^{+\infty} \frac{r}{2}R'_{l'}(r) \exp(il'\phi)\sin 2\phi$$

$$+ \frac{\omega_{s0}^2}{\omega_s}\left(1 - \frac{\omega_s^2}{\omega_{s0}^2}\right) \sum_{l'=-\infty}^{+\infty} R_{l'}(r) \exp(il'\phi)il'\cos^2\phi. \tag{3.96}$$

Using the integral identity

$$\frac{1}{2\pi} \int d\phi \exp\left(i(l'-l)\phi\right)\sin 2\phi$$

$$= \frac{1}{2i}\frac{1}{2\pi}\int d\phi \exp\left(i(l'-l+2)\phi\right) - \frac{1}{2i}\frac{1}{2\pi}\int d\phi \exp\left(i(l'-l-2)\phi\right)$$

$$= \frac{i}{2}\left[\delta_{l'-l-2} - \delta_{l'-l+2}\right], \tag{3.97}$$

and

$$\frac{1}{2\pi}\int d\phi \exp\left(i(l'-l)\phi\right)\cos^2\phi$$

$$= \frac{1}{2\pi}\int d\phi \exp\left(i(l'-l)\phi\right)\frac{1+\cos 2\phi}{2}$$

$$= \frac{1}{2}\delta_{l'-l} + \frac{1}{4}\frac{1}{2\pi}\int d\phi \exp\left(i(l'-l+2)\phi\right) + \frac{1}{4}\frac{1}{2\pi}\int d\phi \exp\left(i(l'-l-2)\phi\right)$$

$$= \frac{1}{2}\delta_{l'-l} + \frac{1}{4}\left[\delta_{l'-l+2} + \delta_{l'-l-2}\right]. \tag{3.98}$$

we can decompose the term B into its l'th synchrotron mode:

$$B_l = \frac{1}{2\pi}\int d\phi \exp(-il\phi)B$$

$$= \frac{i}{4}\frac{\omega_{s0}^2}{\omega_s}\left(1 - \frac{\omega_s^2}{\omega_{s0}^2}\right)\left[rR'_{l+2}(r) - rR'_{l-2}(r)\right]$$

$$+ \frac{i}{2}\frac{\omega_{s0}^2}{\omega_s}\left(1 - \frac{\omega_s^2}{\omega_{s0}^2}\right)lR_l(r) + \frac{i}{4}\frac{\omega_{s0}^2}{\omega_s}\left(1 - \frac{\omega_s^2}{\omega_{s0}^2}\right)\left[(l+2)R_{l+2}(r) + (l-2)R_{l-2}(r)\right]. \tag{3.99}$$

Neglecting the contributions from the neighboring synchrotron modes gives

$$B_l = \frac{i}{2}\frac{\omega_{s0}^2}{\omega_s}\left(1 - \frac{\omega_s^2}{\omega_{s0}^2}\right)lR_l(r). \tag{3.100}$$

Using

$$F_0(\tau') = Ne^2L_0\int_{\tau'}^{+\infty}d\tau''\rho_0(\tau'')W(\tau''-\tau')$$

$$= Ne^2\int d\omega\tilde{\rho}_0(\omega)Z(\omega)\exp(i\omega\tau'), \tag{3.101}$$

and Eq. 3.89, we find

$$C = -\frac{\eta Ne^2}{E_0T_0\omega_s}\int d\omega\tilde{\rho}_0(\omega)Z(\omega)\exp(i\omega r\cos\phi)$$

$$\times\left[\sum_{l'=-\infty}^{+\infty}R'_{l'}(r)\exp(il'\phi)\sin\phi + \sum_{l'=-\infty}^{+\infty}\frac{R_{l'}(r)}{r}\exp(il'\phi)il'\cos\phi\right]. \tag{3.102}$$

78

In deriving Eq. 3.101, we have used the definition of the longitudinal impedance given in Ch. 2,

$$Z(\omega) = L \int_{-\infty}^{+\infty} d\tau' e^{i\omega\tau'} W(\tau'), \tag{3.103}$$

and the Fourier transformation of the equilibrium density function ρ_0 given by

$$\tilde{\rho}_0(\omega) = \int \frac{d\tau'}{2\pi} e^{-i\omega\tau'} \rho_0(\tau'). \tag{3.104}$$

In order to decompose the term C into its l'th synchrotron mode, we need the integral identities

$$\int \frac{d\phi}{2\pi} \exp\left(i(l'-l)\phi + i\omega r \cos\phi\right) \sin\phi = -i^{l-l'} \frac{l-l'}{\omega r} J_{l-l'}(\omega r), \tag{3.105}$$

and

$$\int \frac{d\phi}{2\pi} \exp\left(i(l'-l)\phi + i\omega r \cos\phi\right) \cos\phi = -i^{l-l'+1} J'_{l-l'}(\omega r). \tag{3.106}$$

Here J_l is the Bessel function. With Eqs. 3.105 and 3.106, we find

$$C_l = \frac{1}{2\pi} \int d\phi \exp(-il\phi) C$$

$$= -\frac{\eta N e^2}{E_0 T_0 \omega_s} \int d\omega \tilde{\rho}_0(\omega) Z(\omega)$$

$$\times \left[-\sum_{l'=-\infty}^{+\infty} R'_{l'}(r) i^{l-l'} \frac{l-l'}{\omega r} J_{l-l'}(\omega r) + \sum_{l'=-\infty}^{+\infty} \frac{R_{l'}(r)}{r} l' i^{l-l'} J'_{l-l'}(\omega r) \right] \tag{3.107}$$

Once again we neglect the contributions from neighboring modes and arrive at

$$C_l = \frac{\eta N e^2}{E_0 T_0 \omega_s} l \int d\omega \tilde{\rho}_0(\omega) Z(\omega) \frac{J_1(\omega r)}{r} R_l(r). \tag{3.108}$$

Finally we are left with the last term of Eq. 3.81. Since

$$\psi_0 \propto \exp\left(-\frac{\delta^2}{2\sigma_{\delta 0}^2}\right) \rho_0(\tau), \tag{3.109}$$

then

$$\frac{\partial \psi_0}{\partial \delta} = -\frac{\delta}{\sigma_{\delta 0}^2} \psi_0. \tag{3.110}$$

This leads us to

$$-\frac{F_1(\tau')}{E_0 T_0}\frac{\partial \psi_0}{\partial \delta} = \frac{F_1(\tau')}{E_0 T_0}\frac{\delta}{\sigma_{\delta 0}^2}\psi_0 = \frac{\omega_s}{\eta E_0 T_0 \sigma_{\delta 0}^2}F_1(\tau')r\sin\phi\psi_0. \qquad (3.111)$$

From Eq. 3.42,

$$\psi_0(r,\phi) = \sum_{n=0}^{+\infty} f_n(r)\cos n\phi, \qquad (3.112)$$

we have

$$r\sin(\phi)\psi_0 = r f_0(r)\sin\phi + \sum_{n=1}^{+\infty} r f_n(r)\sin\phi\cos n\phi$$

$$= r f_0(r)\sin\phi + \sum_{n=1}^{+\infty}\frac{r}{2}f_n(r)\left[\sin(n+1)\phi - \sin(n-1)\phi\right]$$

$$= -\sigma^2 \sum_{n=1}^{+\infty} g_n(r)\sin n\phi. \qquad (3.113)$$

Here the functions $g_n(r)$ are related to the functions $f_n(r)$ by

$$g_1(r) = \frac{r}{2\sigma^2}\left(f_2(r) - 2f_0(r)\right), \qquad (3.114)$$

$$g_n(r) = \frac{r}{2\sigma^2}\left(f_{n+1}(r) - f_{n-1}(r)\right)\ n \geq 2. \qquad (3.115)$$

On the other hand, proceeding as in Eq. 3.101, we have

$$F_1(\tau') = N\epsilon^2 \int d\omega \tilde{\rho}_1(\omega)Z(\omega)\exp(i\omega r\cos\phi). \qquad (3.116)$$

The last term in the first order Vlasov equation 3.21 then becomes:

$$-\frac{F_1(\tau')}{E_0 T_0}\frac{\partial \psi_0}{\partial \delta} = -\frac{\eta N\epsilon^2}{\omega_s E_0 T_0}\int d\omega \tilde{\rho}_1(\omega)Z(\omega)\exp(i\omega r\cos\phi)\sum_{n=1}^{+\infty} g_n(r)\sin n\phi. \qquad (3.117)$$

In order to decompose this term into its l'th synchrotron mode, we must evaluate the integral

$$\int \frac{d\phi}{2\pi}\exp(-il\phi + i\omega r\cos\phi)\sin n\phi$$

$$= \frac{1}{2i}\int \frac{d\phi}{2\pi}\exp\left(-i(l-n)\phi + i\omega r\cos\phi\right) - \frac{1}{2i}\int \frac{d\phi}{2\pi}\exp\left(-i(l+n)\phi + i\omega r\cos\phi\right)$$

$$= \frac{1}{2i}i^{l-n}J_{l-n}(\omega r) - \frac{1}{2i}i^{l+n}J_{l+n}(\omega r), \qquad (3.118)$$

and express $\tilde{\rho}_1(\omega)$ in terms of the longitudinal synchrotron modes given by Eq. 3.30:

$$\tilde{\rho}_1(\omega) = \frac{\omega_s}{\eta} \sum_{l'} i^{-l'} \int_0^{+\infty} r'dr' R_{l'}(r') J_{l'}(\omega r'). \tag{3.119}$$

Then

$$\frac{1}{2\pi} \int d\phi \exp(-il\phi) \left(-\frac{F_1(\tau')}{E_0 T_0} \frac{\partial \psi_0}{\partial \delta} \right)$$

$$= -\frac{Ne^2}{E_0 T_0} \int d\omega \sum_{l'} i^{-l'} \int r'dr' R_{l'}(r') J_{l'}(\omega r') Z(\omega)$$

$$\times \sum_{n=1}^{+\infty} g_n(r) \left(\frac{1}{2i} i^{l-n} J_{l-n}(\omega r) - \frac{1}{2i} i^{l+n} J_{l+n}(\omega r) \right). \tag{3.120}$$

Neglecting the contributions from neighboring synchrotron modes result in

$$\frac{1}{2\pi} \int d\phi \exp(-il\phi) \left(-\frac{F_1(\tau')}{E_0 T_0} \frac{\partial \psi_0}{\partial \delta} \right)$$

$$= -\frac{Ne^2}{2i E_0 T_0} \sum_{n=1}^{+\infty} g_n(r) \int r'dr' G_l^{(n)}(r, r') R_l(r'). \tag{3.121}$$

Here $G_l^{(n)}(r, r')$ is given by

$$G_l^{(n)}(r, r') = \frac{1}{i^n} \int d\omega Z(\omega) \left(J_{l-n}(\omega r) - (-1)^n J_{l+n}(\omega r) \right) J_l(\omega r'). \tag{3.122}$$

It will be particularly illuminating to calculate the $n = 1$ term. Using the following recursion relation for the Bessel functions:

$$J_{l-1}(\omega r) + J_{l+1}(\omega r) = \frac{2l}{\omega r} J_l(\omega r), \tag{3.123}$$

we can simplify

$$G_l^{(1)}(r, r') = \frac{2l}{ir} \int d\omega \frac{Z(\omega)}{\omega} J_l(\omega r) J_l(\omega r')$$

$$= \frac{2l}{r} \int d\omega \frac{\mathrm{Im} Z(\omega)}{\omega} J_l(\omega r) J_l(\omega r') = \frac{2l}{r} G_l(r, r'). \tag{3.124}$$

Also noting that

$$g_1(r) = \frac{r}{2\sigma^2} \left(f_2(r) - 2f_0(r) \right)$$

$$= -\frac{r}{\sigma^2} \psi_0(r) \left[1 + \frac{\gamma_2}{8} \left(\frac{r^4}{24\sigma^4} - \frac{r^2}{2\sigma^2} + 1 \right) \right], \tag{3.125}$$

81

we find that the $n = 1$ term in Eq. 3.121 can be written as

$$-i\frac{Ne^2}{E_0 T_0}l\frac{1}{\sigma^2}\psi_0(r)\left[1 + \frac{\gamma_2}{8}\left(\frac{r^4}{24\sigma^4} - \frac{r^2}{2\sigma^2} + 1\right)\right]\int r'dr'G_l(r,r')R_l(r'). \qquad (3.126)$$

Comparing this with Eq. 3.32, we see that they are identical if $\gamma_2 = 0$ in Eq. 3.126. Thus the $n = 1$ term is proportional to the bunch current and alone would yield a generalized Sacherer equation (with a correction from the excess $\gamma_2 \neq 0$).

It is instructive to examine terms with $n \geq 2$ under the assumption that the wake field is linear. In this case the equilibrium bunch shape will be fully described by a Gaussian distribution. Thus the equilibrium distribution function in the phase space $\psi_0(\delta, \tau)$ depends only on r. In this limit we can expect

$$f_1(r) = f_2(r) = \cdots = 0. \qquad (3.127)$$

From the relation between functions $g_n(r)$ and $f_n(r)$,

$$g_n(r) = \frac{r}{2\sigma^2}\left(f_{n+1}(r) - f_{n-1}(r)\right), \qquad (3.128)$$

we know that $f_n(r) = 0$, $n \geq 2$ implies

$$g_2(r) = g_3(r) = \cdots = 0. \qquad (3.129)$$

All terms $g_n(r)$ with $n \geq 2$ vanish if we neglect the nonlinearity of the wake. They are the direct result of the corrections introduced by the *nonlinearity* of the wake force. From the above discussions, it is clear that these terms are the desired correction terms to the the original Sacherer equation.

Combining Eqs. 3.95, 3.100, 3.108 and 3.121 gives the improved Sacherer equation:

$$(\Omega - l\omega_s)R_l(r)$$

$$= \frac{l}{2}\frac{\omega_{s0}^2}{\omega_s}\left(1 - \frac{\omega_s^2}{\omega_{s0}^2}\right)R_l(r)$$

$$-il\frac{\eta Ne^2}{E_0 T_0\omega_s}\int d\omega\,\tilde{\rho}_0(\omega)Z(\omega)\frac{J_1(\omega r)}{r}R_l(r)$$

$$+\frac{Ne^2}{E_0T_0}l\frac{g_1(r)}{r}\int r'dr'G_l(r,r')R_l(r')$$

$$+\frac{Ne^2}{2E_0T_0}\sum_{n=2}^{+\infty}g_n(r)\int r'dr'G_l^{(n)}(r,r')R_l(r'). \qquad (3.130)$$

Eq. 3.130 is a significant result of this thesis. It gives, for the first time, an equation for an uncoupled synchrotron mode which includes the contributions from the static nonlinear wake force and predicts instability at a threshold current.

In the Sec. 3.4, we proved that since $G_l(r,r')$ is real and symmetric, and we can always absorb the remaining asymmetric parts $g_1(r)r'$ into a redefined weight function. This will lead to a real and symmetric Sacherer operator. The eigenvalues of this operator must all be real. Of interest here are the correction terms to the real and symmetric Sacherer operator given by the improved Sacherer equation 3.130. Although $G_l^{(n)}(r,r')$ is real, it is apparently asymmetric with respect to the variables r and r'. And we cannot use the same weight function redefinition technique to eliminate this asymmetry. We can conclude that in general, the correction terms are asymmetric real operators. Another important difference between the Sacherer operator and the asymmetric perturbations is their dependence on the current. As we have just shown in Eq. 3.125, $g_1(r)$ is equal to $\psi_0'(r)/r$ as the current approaches zero. So the Sacherer operator is proportional to the current. Since $g_2(r)$, $g_3(r)$, etc are zero when the nonlinearity of the wake is negligible, or when the current is zero, they are proportional to the current. Thus the asymmetric perturbation terms are proportional to the *square* of the current. This leads us to the mechanism of the single mode bunch lengthening instability: When the current is small, the real and symmetric Sacherer operator dominates. The system has only real eigenvalues. When the current reaches a threshold value, the asymmetric perturbations driven by nonlinearity in the wake force start to push the eigenvalues of the system into the complex plane and the bunch exhibits the bunch lengthening instability.

3.9 Frequency Shift of the Synchrotron Modes

Before we discuss the numerical solution of the improved Sacherer equation, we can get some physical insight by studying its behavior when the current is small (much less that the critical current). For this purpose, we will neglect all the terms proportional to the square of the current in Eq. 3.130, namely all the asymmetric perturbation terms. In this limit, the improved Sacherer equation becomes

$$(\Omega - l\omega_s)R_l(r)$$

$$= \frac{l}{2}\frac{\omega_{s0}^2}{\omega_s}\left(1 - \frac{\omega_s^2}{\omega_{s0}^2}\right)R_l(r)$$

$$-il\frac{\eta N e^2}{E_0 T_0 \omega_s}\int d\omega \tilde{\rho}_0(\omega)Z(\omega)\frac{J_1(\omega r)}{r}R_l(r)$$

$$+\frac{N e^2}{E_0 T_0}l\frac{\psi_0'(r)}{r}\int r'dr' G_l(r,r')R_l(r'). \tag{3.131}$$

In order to obtain an analytic solution, we choose a simplified model for the equilibrium distribution for the ψ_0,

$$\psi_0(r) = \begin{cases} 0 & \text{if } r > \hat{\tau}, \\ \frac{\eta}{\pi\hat{\tau}^2\omega_s} & \text{if } r < \hat{\tau}. \end{cases}$$

This distribution is called the water-bag model [29, 13]. Any perturbation on a water-bag beam will have to occur around the edge of the bag, i.e., around $r = \hat{\tau}$. As a result, all R_l's are δ-functions, i.e.

$$R_l(r) = \delta(r - \hat{\tau}). \tag{3.132}$$

This result also follows from Eq. 3.131 by inspection if we note that

$$\psi_0' = -\frac{\eta}{\pi\hat{\tau}^2\omega_s}\delta(r - \hat{\tau}). \tag{3.133}$$

Having obtained the eigenfunctions given by the equation 3.132, Eq. 3.131 reduces to an algebraic equation that determine the frequency for the l'th coherent synchrotron

mode:

$$(\Omega - l\omega_s) = \frac{l}{2}\frac{\omega_{s0}^2 - \omega_s^2}{\omega_s} - il\frac{\eta Ne^2}{E_0 T_0 \omega_s \hat{\tau}} \int d\omega \hat{\rho}_0(\omega) Z(\omega) J_1(\omega\hat{\tau})$$

$$- \frac{\eta Ne^2}{\pi \hat{\tau}^2 E_0 T_0 \omega_s} l \int d\omega \frac{ImZ(\omega)}{\omega} J_l^2(\omega\hat{\tau}). \tag{3.134}$$

In deriving Eq. 3.134, we have substituted the the kernel $G_l(r,r')$ by its explicit expression given by Eq. 3.33. To proceed further, we need to calculate the $\hat{\rho}_0(\omega)$.

$$\hat{\rho}_0(\omega) = \int \frac{d\tau}{2\pi} e^{-i\omega\tau} \rho_0(\tau) = \frac{1}{2\pi} \int d\tau d\delta e^{-i\omega\tau} \psi_0$$

$$= \frac{1}{\pi\hat{\tau}^2} \int_0^{\hat{\tau}} r dr \int \frac{d\phi}{2\pi} e^{-i\omega r \cos\phi} = \frac{1}{\pi\hat{\tau}^2} \int_0^{\hat{\tau}} r dr J_0(\omega r). \tag{3.135}$$

Using the integral identity for the Bessel function,

$$\int dx\, x^n J_{n-1}(x) = x^n J_n(x), \tag{3.136}$$

we obtain

$$\hat{\rho}_0(\omega) = \frac{1}{\pi\hat{\tau}\omega} J_1(\omega\hat{\tau}). \tag{3.137}$$

With $\hat{\rho}_0(\omega)$ given by Eq. 3.137, Eq. 3.134 simplifies to

$$\Omega - l\omega_{s0} = \frac{l}{2}\frac{\omega_{s0}^2 - \omega_s^2}{\omega_s} + l\frac{\eta Ne^2}{E_0 T_0 \omega_s \pi \hat{\tau}^2} \int d\omega \frac{ImZ(\omega)}{\omega} \left(J_1^2(\omega\hat{\tau}) - J_l^2(\omega\hat{\tau})\right). \tag{3.138}$$

This formula gives an explicit expression for the frequency shifts of different synchrotron modes. Since we have neglected all the terms proportional to the square of the current, we expect this formula to work well only when the current is small.

When $l = 1$, Eq. 3.138 has a particularly simple form:

$$\Omega - l\omega_{s0} = \frac{l}{2}\frac{\omega_{s0}^2 - \omega_s^2}{\omega_s}. \tag{3.139}$$

Since ω_s is very close to ω_{s0} when the current is small, we can neglect the right hand side of Eq. 3.139. This leads us to,

$$\Omega^{(1)} \approx \omega_{s0}. \tag{3.140}$$

85

Namely, the frequency of the dipole mode remains fixed as the current increases. This phenomenon has been verified experimentally. Results from our multiparticle multiperiod tracking simulation, which we will discuss in detail in Ch. 5, verify the same conclusion. In fact, our simulations show that the frequency of the dipole mode stays fixed even as the current is reaching its threshold value.

The absence of a frequency shift for the dipole mode can be easily understood physically. The dipole mode oscillation corresponds to the particle bunch sliding as a whole, together with its potential well deformation. Since we have neglected the nonlinearity of the RF bucket, the bunch slides up and down on an RF voltage with a constant slope. Therefore the coherent synchrotron frequency, which is proportional to the square root of this slope, remains unchanged, and is independent of the bunch distribution.

While shifts of $l = 1$ mode are not observed, tune spreads associated with this and other synchrotron modes have been seen both in the experiments and in the simulations when the bunch current approaches threshold. The source of these spreads has been omitted when we made the assumption of the water-bag equilibrium distribution. By using the water-bag distribution, we limited ourselves to a delta function perturbation. This restriction forces the degeneracy of radial modes (modes in the r variable) within a particular synchrotron mode. In the next section, we will use the equilibrium distribution given by the Haissinski equation and develop a numerical algorithm to solve the improved Sacherer equation, and thereby obtain the full spectrum of the radial modes.

3.10 A Numerical Algorithm for the Improved Sacherer Equation

In this section we develop a numerical algorithm to solve the eigenvalue problem presented by the improved Sacherer equation 3.130. In the process, we will identify two important parameters for the bunch-lengthening instability.

We will first demonstrate the whole process of discretization through the simpler case of Sacherer equation given by Eq. 3.32. For the improved Sacherer equation, the discretization procedure is identical.

The Sacherer equation is

$$(\Omega - l\omega_s)R_l(r) = \frac{Ne^2}{E_0 T_0} l \frac{\psi_0'(r)}{r} \int r' dr' G_l(r, r') R_l(r'). \qquad (3.141)$$

Since

$$\psi_0(r) = \frac{\eta}{2\pi\omega_s \sigma^2} \exp(-\frac{r^2}{2\sigma^2}), \qquad (3.142)$$

we can rewrite the Sacherer equation in the form

$$(\frac{\Omega}{\omega_s} - l)R_l(r) = -\frac{\eta Ne^2}{2\pi\omega_s^2 E_0 T_0 \sigma^2} l \exp(-\frac{r^2}{2\sigma^2}) \int \frac{r'}{\sigma} d\frac{r'}{\sigma} G_l(r, r') R_l(r'). \qquad (3.143)$$

Introduce a dimensionless parameter

$$x = \frac{r}{\sigma}, \qquad (3.144)$$

and Sacherer equation becomes

$$(\frac{\Omega}{\omega_s} - l)R_l(x) = -\frac{\eta Ne^2}{2\pi\omega_s^2 E_0 T_0 \sigma^2} l e^{-\frac{x^2}{2}} \int d\frac{x'^2}{2} G_l(x\sigma, x'\sigma) R_l(x'). \qquad (3.145)$$

Introduce the normalized quantities

$$R_l(x) = e^{-\frac{x^2}{2}} F_l(x), \qquad (3.146)$$

$$\xi = \frac{\eta Ne^2 R}{2\pi\omega_s^2 E_0 T_0 \sigma^2} l, \qquad (3.147)$$

87

$$\lambda = (\frac{\Omega}{\omega_s} - l)/\xi, \tag{3.148}$$

so that Sacherer equation simplifies to

$$\lambda F_l(x) = -\int d\frac{x'^2}{2} e^{-\frac{x'^2}{2}} [\int d\omega \frac{Im Z(\omega)}{R\omega} J_l(\omega\sigma x) J_l(\omega\sigma x')] F_l(x'). \tag{3.149}$$

Finally, changing variable once again,

$$y = \frac{x^2}{2}, \tag{3.150}$$

yields a dimensionless Sacherer equation:

$$\lambda F_l(y) = -\int dy' e^{-y'} [\int d\omega \frac{Im Z(\omega)}{R\omega} J_l(\omega\sigma\sqrt{2y}) J_l(\omega\sigma\sqrt{2y'})] F_l(y'). \tag{3.151}$$

In order to solve this integral operator eigenvalue problem, we need to approximate it by a matrix eigenvalue problem. Thus, we need to approximate the integral with respect to y' by a summation. We will use Gauss-Laguerre quadruture technique for this purpose.

We will not go into the details of the Gauss-Laguerre quadruture. The analysis here follows well-known methods. In particular, the readers can consult Numerical Recipes [47]. The technique shows that, if we choose the weight function to be

$$w(y) = e^{-y} y^l, \tag{3.152}$$

where l is a non-negative integer, then the following approximation of an integral by a summation is valid:

$$\int_0^{+\infty} dy w(y) f(y) \approx \sum_{j=1}^{N} w_j f(y_j). \tag{3.153}$$

Here the Gauss-Laguerre abscissas y_j and weights w_j can be obtained numerically [47].

With the help of the Gauss-Laguerre quadruture, the integral in Eq. 3.151 reduces to the summation:

$$\lambda F_l(y) = -\sum_j \frac{w_j}{y_j^l} [\int d\omega \frac{Im Z(\omega)}{R\omega} J_l(\omega\sigma\sqrt{2y}) J_l(\omega\sigma\sqrt{2y_j})] F_l(y_j). \tag{3.154}$$

If we set $y = y_i$, we have succeed transforming the eigenvalue problem with integral operator into a regular eigenvalue problem:

$$\lambda F(y_i) = \sum_j K^s_{ij} F(y_j), \tag{3.155}$$

with the matrix elements given by

$$K^s_{ij} = -\frac{w_j}{y^l_j} \int d\omega \frac{Im Z(\omega)}{R\omega} J_l(\omega\sigma\sqrt{2y_i}) J_l(\omega\sigma\sqrt{2y_j}). \tag{3.156}$$

The same discretization procedure can be used on the improved Sacherer equation 3.130. The only difference is that we obtain a new matrix element K_{ij}:

$$K_{ij} = \left[1 + \frac{\gamma_2}{8}\left(\frac{y_i^2}{6} - y_i + 1\right)\right] K^s_{ij}$$

$$+\frac{\gamma_1}{4}\left(\frac{y_i^2}{3} - y_i\right)\sqrt{\frac{w_i w_j}{y_i^l y_j^l}}\frac{\sigma}{l}\int d\omega \frac{Re Z(\omega)}{R}\left(J_{l-2}(\omega\sigma\sqrt{2y_i}) - J_{l+2}(\omega\sigma\sqrt{2y_i})\right) J_l(\omega\sigma\sqrt{2y_j})$$

$$-\frac{\gamma_1}{24}y_i^2\sqrt{\frac{w_i w_j}{y_i^l y_j^l}}\frac{\sigma}{l}\int d\omega \frac{Re Z(\omega)}{R}\left(J_{l-4}(\omega\sigma\sqrt{2y_i}) - J_{l+4}(\omega\sigma\sqrt{2y_i})\right) J_l(\omega\sigma\sqrt{2y_j})$$

$$+\frac{\gamma_2}{64}\left(y_i^2 - 4y_i\right)\sqrt{\frac{w_i w_j}{y_i^l y_j^l}}\frac{\sqrt{2y_i}\sigma}{l}\int d\omega \frac{Im Z(\omega)}{R}\left(J_{l-3}(\omega\sigma\sqrt{2y_i}) + J_{l+3}(\omega\sigma\sqrt{2y_i})\right) J_l(\omega\sigma\sqrt{2y_j})$$

$$-\frac{\gamma_2}{192}y_i^2\sqrt{\frac{w_i w_j}{y_i^l y_j^l}}\frac{\sqrt{2y_i}\sigma}{l}\int d\omega \frac{Im Z(\omega)}{R}\left(J_{l-5}(\omega\sigma\sqrt{2y_i}) + J_{l+5}(\omega\sigma\sqrt{2y_i})\right) J_l(\omega\sigma\sqrt{2y_j})$$

$$+\sigma^2 \int d\omega 2\pi\hat{\rho}_0(\omega)\frac{Im Z(\omega)}{R}\frac{J_1(\omega\sigma\sqrt{2y_i})}{\omega\sigma\sqrt{2y_i}}\delta_{ij}.$$

Here, $\hat{\rho}_0(\omega)$ is the Fourier transformation of the parameterized equilibrium distribution of particle density given by Eq. 3.59:

$$\hat{\rho}_0(\omega) = \int \frac{d\omega}{2\pi} \exp(-i\omega\tau')\rho_0(\tau')$$

$$= \int \frac{d\omega}{2\pi} \exp(-i\omega\tau')\left[1 + \frac{\gamma_1}{6}\left(\frac{\tau'^3}{\sigma^3} - 3\frac{\tau'}{\sigma}\right) + \frac{\gamma_2}{24}\left(\frac{\tau'^4}{\sigma^4} - 6\frac{\tau'^2}{\sigma^2} + 3\right)\right]\frac{1}{\sqrt{2\pi}\sigma}\exp(-\frac{\tau'^2}{2\sigma^2})$$

$$= \left\{1 + \frac{\gamma_1}{6}\left[\left(\frac{i}{\sigma}\frac{d}{d\omega}\right)^3 - 3\left(\frac{i}{\sigma}\frac{d}{d\omega}\right)\right] + \frac{\gamma_2}{24}\left[\left(\frac{i}{\sigma}\frac{d}{d\omega}\right)^5 - 6\left(\frac{i}{\sigma}\frac{d}{d\omega}\right)^2 + 3\right]\right\}\frac{1}{2\pi}\exp(-\frac{\omega^2\sigma^2}{2})$$

$$= \left(1 + i\frac{\gamma_1}{6}\sigma^3\omega^3 + \frac{\gamma_2}{24}\sigma^4\omega^4\right)\frac{1}{2\pi}\exp(-\frac{\omega^2\sigma^2}{2}), \tag{3.157}$$

89

and the frequency of the l'th synchrotron mode Ω is related to the eigenvalue λ by

$$\frac{\Omega}{\omega_{s0}} = \frac{\sigma_0}{\sigma}\xi\lambda + \frac{l}{2}(\frac{\sigma_0}{\sigma} + \frac{\sigma}{\sigma_0}).$$ (3.158)

It is rather obvious that the matrix elements K_{ij} are completely determined by parameter $\omega_r\sigma$ and γ_1 and γ_2. γ_1 and γ_2 are determined by the equilibrium particle density, which in turn is given by the Haissinski equation 2.86. Since the Haissinski equation is determined by two parameters, $\omega_r\sigma$ and ξ, there are, for the case of a broadband resonator wake, only two parameters in our analysis of the bunch lengthening instability. This observation is very important in our analysis of the bunch lengthening instability. In Ch. 5, we will determine the critical coupling ξ_c as a function of $\omega_r\sigma$.

From Eq. 3.147, the threshold peak current I_p is given by

$$I_p = \frac{Ne}{\sigma} = \frac{(2\pi)^3\nu_s^2 E_0\sigma}{\eta e T_0 R}\xi_c.$$ (3.159)

Thus, at fixed tune ν_s and momentum compaction η, the threshold peak current increases with a decrease in either the ring impedance, ring circumference or an increase in bunch energy.

90

Chapter 4

Multiparticle Tracking Simulation

With the advance of computational technology, simulations have become important tools in studying accelerator physics. In this thesis, an efficient multiparticle, multiperiod tracking simulation code is developed to investigate the bunch lengthening instability. The motivation is to verify the new instability mechanism presented in the previous chapter, in particular the determination of the critical current based on the instability analysis of the improved Sacherer equation. Unlike other areas in experimental physics, there are only very small sets of experimental results on the bunch lengthening instability. This is mostly due to the fact that many of the important parameters in the bunch lengthening instability are machine parameters, which are difficult to change. Furthermore, there are numerous factors present in the experimental results, which makes it hard to identify the core mechanism underlying the bunch lengthening instability. By using Monte Carlo simulations, we can control the factor (i.e., the physics) to be included and thereby pinpoint the key physics which determines the onset of the bunch lengthening instability.

In Sec. 4.1, we investigate the single particle longitudinal dynamics discussed in Ch. 2. We focus on the stability of the iteration given by Eqs. 2.6 and 2.7. In Sec. 4.2, we discuss a particle's trajectory in longitudinal phase space. It is a tilted ellipse rather than a circle as previously assumed. This observation has led to a new quiet

loading scheme. In Sec. 4.3, we describe how to incorporate the radiation damping and quantum emission into the longitudinal single particle dynamics. In Sec. 4.4, we include wake fields in our multiparticle simulation code. We discuss two fast algorithms to compute the wake force experienced by each macroparticle. In Sec. 4.5, we point out that the wake used in our multiparticle simulation is a local wake, while, in contrast, the wake is distributed all around the the real ring. The impact of the localized wake on the equilibrium bunch shape can have very different from that of a distributed wake. In order to simulate the ring, we employ a multiperiod multiparticle simulation, which distributes the wake over many periods. Finally, in Sec. 4.6, we introduce several new diagnostics into our multiparticle multiperiod simulation code. These new diagnostics are more powerful than most of the widely-used diagnostics.

4.1 Discrete Longitudinal Dynamics Revisited

The discrete longitudinal dynamics for a single particle are given by Eq. 2.6,

$$\tau_{n+1} = \tau_n - \frac{\eta T_0}{E_0} \delta E_{n+1}, \tag{4.1}$$

$$\delta E_{n+1} = \delta E_n - eV \cos(\phi_s) \omega_{rf} \tau_n. \tag{4.2}$$

A natural question arises: Why should one use E_{n+1} rather than E_n in Eq. 4.1? If we review the physical arguments leading to Eq. 2.6, it seems that the difference between the two are very small: both of them provide an approximation to the real synchrotron oscillation dynamics, and it is hard to tell which one is better. But, from the perspective of the stability analysis, the difference is huge.

First, consider

$$\tau_{n+1} = \tau_n - \frac{\eta T_0}{E_0} \delta E_n, \tag{4.3}$$

$$\delta E_{n+1} = \delta E_n - eV \cos(\phi_s) \omega_{rf} \tau_n. \tag{4.4}$$

92

The stability of the iteration depends on the eigenvalues of the transfer matrix [48]:

$$M = \begin{pmatrix} 1 & -\frac{\eta T_0}{\beta^2 E_0} \\ -eV\cos(\phi_s)\omega_{rf} & 1 \end{pmatrix}.$$

(4.5)

The eigenvalues of the 2 × 2 matrix M are given by

$$\lambda^2 - \text{Tr}M\lambda + \det M = 0.$$

(4.6)

Since Tr $M = 2$, one has

$$\lambda^2 - 2\lambda + \det M = 0.$$

(4.7)

Furthermore,

$$\det M = 1 - \frac{\eta T_0}{\beta^2 E_0} eV\cos(\phi_s)\omega_{rf} > 1.$$

(4.8)

if the synchrotron phase is in the range of $\frac{\pi}{2} < \phi_s < \pi$. As explained in Sec. 2.1, this is the desired range of the synchrotron phase (from the consideration of the stability of the longitudinal oscillation). Thus, with the iteration given by Eqs. 4.3 and 4.4, we have

$$|\lambda|^2 = \det M > 1.$$

(4.9)

The iteration is unstable.

Next, we investigate the iteration in Eqs. 2.6 and 2.7:

$$\tau_{n+1} = \tau_n - \frac{\eta T_0}{E_0}\delta E_{n+1},$$

(4.10)

$$\delta E_{n+1} = \delta E_n - eV\cos(\phi_s)\omega_{rf}\tau_n.$$

(4.11)

Substituting the second equation into the first one, we have

$$\tau_{n+1} = \left(1 + \frac{\eta T_0}{E_0}eV\cos(\phi_s)\omega_{rf}\right)\tau_n - \frac{\eta T_0}{E_0}\delta E_n,$$

(4.12)

$$\delta E_{n+1} = \delta E_n - eV\cos(\phi_s)\omega_{rf}\tau_n.$$

(4.13)

In this case, the transfer matrix is given by

$$N = \begin{pmatrix} 1 + \frac{\eta T_0}{E_0}eV\cos(\phi_s)\omega_{rf} & -\frac{\eta T_0}{E_0} \\ -eV\cos(\phi_s)\omega_{rf} & 1 \end{pmatrix}.$$

(4.14)

Its determinant is

$$\det N = 1, \tag{4.15}$$

and trace is

$$\mathrm{Tr}N = 2 + \frac{\eta T_0}{E_0} eV \cos(\phi_s)\omega_{rf} < 2, \tag{4.16}$$

for the desired range of the synchrotron phase, $\frac{\pi}{2} < \phi_s < \pi$. From the eigenvalue equation:

$$\lambda^2 - \mathrm{Tr}N\lambda + \det N = 0, \tag{4.17}$$

since $(\mathrm{Tr}N)^2 - 4 < 0$, we can conclude that its eigenvalues are imaginary. Furthermore, since

$$|\lambda|^2 = \det N = 1, \tag{4.18}$$

the iteration given by Eqs. 2.6 and 2.7 is stable. This is the reason that Eqs. 2.6 and 2.7 are used in the single particle longitudinal dynamics.

4.2 Tilted Ellipse and Quiet Loading

In this section, we study the particle trajectory in the longitudinal phase space. Since the iteration given by Eqs. 2.6 and 2.7 is similar to the particle's transverse linear motion, we follow the results there to derive the equation for the particle's trajectory. A useful reference on this subject can be found in the summer school lecture notes by D.A. Edwards and M.J. Syphers [49]. In their notes, the transfer matrix is given by

$$TM = \begin{pmatrix} \cos\psi + \alpha\sin\psi & \beta\sin\psi \\ -\frac{1+\alpha^2}{\beta}\sin\psi & \cos\psi - \alpha\sin\psi \end{pmatrix}. \tag{4.19}$$

The particle trajectory is completely determined by the two parameters α and b. γ is related to them by

$$\gamma = \frac{1+\alpha^2}{\beta}. \tag{4.20}$$

94

Let's compute these parameters from the transfer matrix for the longitudinal dynamics. Comparing the trace of the matrix TM with that of the transfer matrix N gives

$$\cos\psi = 1 + \frac{\eta T_0}{2E_0}eV\cos(\phi_s)\omega_{rf}. \tag{4.21}$$

Introducing the synchrotron tune,

$$\nu_{s0} = \frac{\omega_{s0}}{\omega_0}, \tag{4.22}$$

from Eq. 2.11, gives

$$2\pi\nu_{s0} = \sqrt{-\frac{\eta T_0}{E_0}eV\cos(\phi_s)\omega_{rf}}. \tag{4.23}$$

Thus, we obtain the phase advance:

$$\cos\psi = 1 - \frac{1}{2}(2\pi\nu_{s0})^2. \tag{4.24}$$

β is determined by equating $TM_{12} = N_{12}$:

$$\beta = -\frac{\eta T_0}{E_0}\frac{1}{\sin\psi}. \tag{4.25}$$

By equating TM_{21} to N_{21}, we find

$$\gamma = \frac{eV\cos(\phi_s)\omega_{rf}}{\sin\phi}. \tag{4.26}$$

Finally, from

$$TM_{11} - TM_{22} = N_{11} - N_{22}, \tag{4.27}$$

we obtain

$$2\alpha\sin\psi = \frac{\eta T_0}{E_0}eV\cos(\phi_s)\omega_{rf} = -(2\pi\nu_{s0})^2. \tag{4.28}$$

Thus

$$\alpha = -\frac{2\pi^2\nu_{s0}^2}{\sin\psi}. \tag{4.29}$$

The trajectory given by the transfer matrix TM is an ellipse. Its equation is given by [49]:

$$\gamma\tau^2 + \alpha\tau\delta E + \beta(\delta E)^2 = \text{constant}. \tag{4.30}$$

95

Substituting the parameters we just calculated,

$$eV\cos(\phi_s)\omega_{rf}\tau^2 - (2\pi\nu_{s0})^2\tau\delta E - \frac{\eta T_0}{E_0}(\delta E)^2 = \text{constant}. \qquad (4.31)$$

It is illuminating to normalize τ and δE by the natural bunch length σ_0 and the natural energy spread $\sigma_{\epsilon 0}$. Since they are related by

$$\frac{\sigma_0}{\sigma_{\epsilon 0}} = \frac{\eta T_0}{2\pi\nu_{s0}E_0}, \qquad (4.32)$$

Eq. 4.31 can be simplified to

$$\left(\frac{\tau}{\sigma}\right)^2 + 2\pi\nu_{s0}\frac{\tau}{\sigma}\frac{\delta E}{\sigma_{\epsilon 0}} + \left(\frac{\delta E}{\sigma_{\epsilon 0}}\right)^2 = \text{constant}. \qquad (4.33)$$

This is an ellipse that is tilted 45 degrees. One example is shown in Figure 4.1. The ratio of its major axis to its minor axis is $1 + \pi\nu_{s0}$. Since for most of the electron storage rings synchrotron tune is usually very small (less than 0.1), there is only small difference between the tilted ellipse and a circle, which was previously considered to be the particle's trajectory in the phase space.

However, there is an important application of this small effect in the particle loading for our multiparticle multiperiod simulation code. Most simulation codes for bunch lengthening load the macroparticles around a circle. This introduces an artificial dipole motion which does not correspond to the longitudinal dynamics of a real bunch. By loading macroparticles along the ellipse, we eliminate this loading noise. This is clearly demonstrated in Fig. 4.2.

4.3 Radiation Damping and Quantum Emission

4.3.1 Preliminaries

Synchrotron radiation is the dominant factor in the design of high-energy electron synchrotron and is the primary obstacle to building circular electron accelerators at
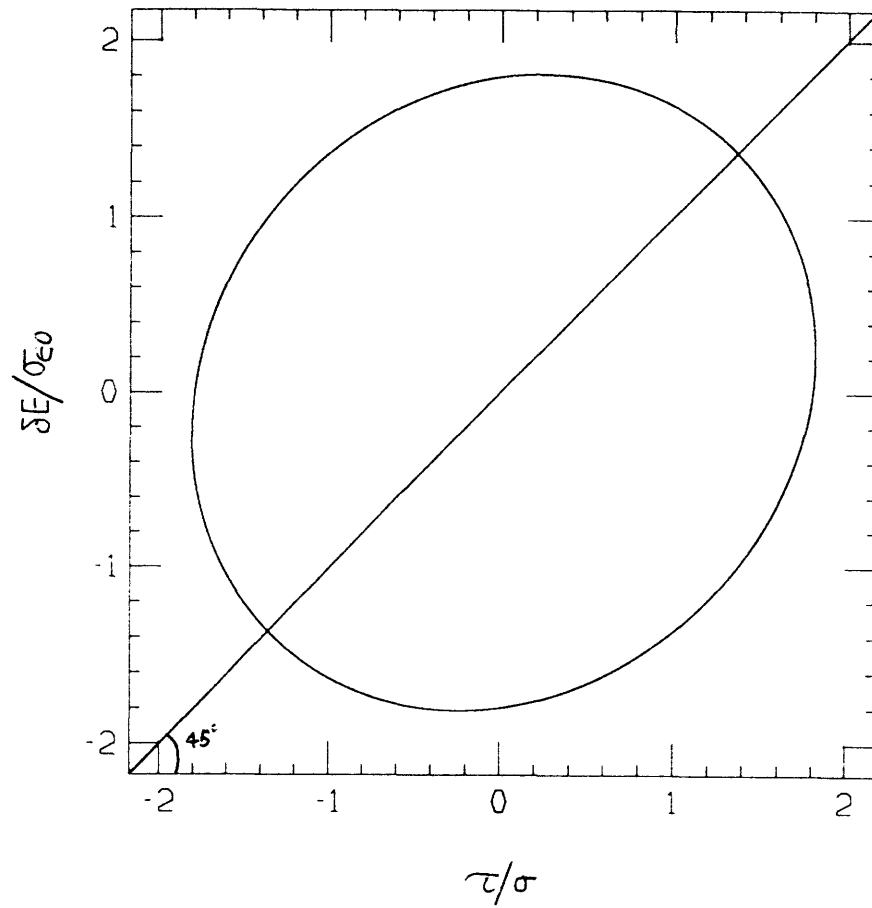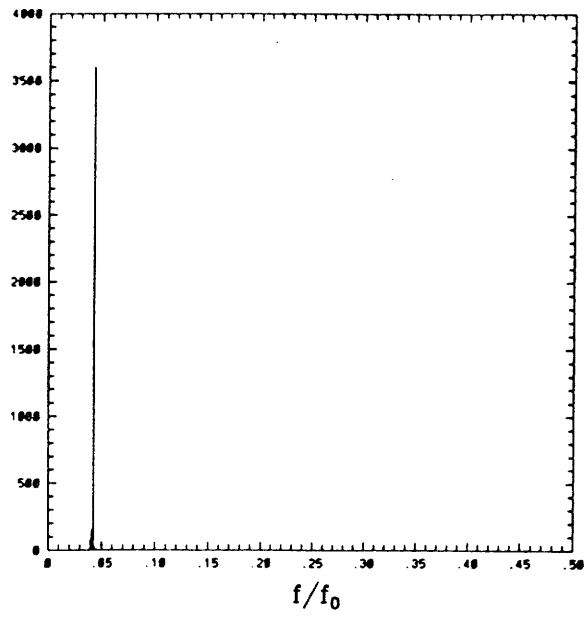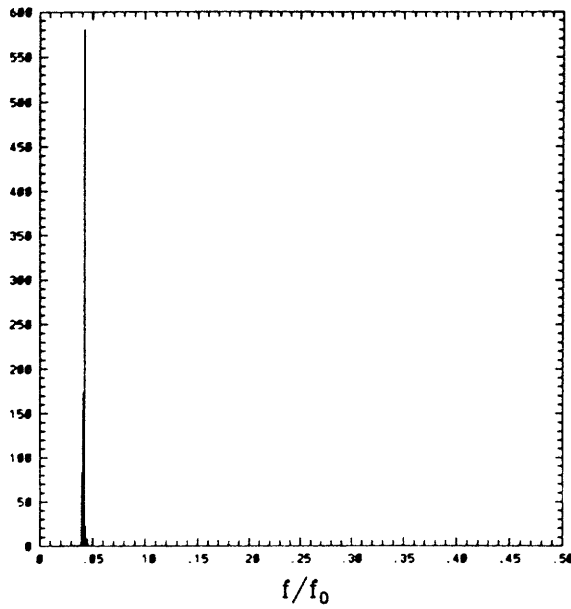
Figure 4.1: The longitudinal phase space trajectory of a particle is a tilted ellipse.

97

Figure 4.2: Results from our multiparticle simulation. (a) Mode amplitude without quiet loading. (b) With quiet loading. Note that the quiet loading reduces noise by a factor of 7.

energies exceeding 100-GeV. It has also brought about the spectacular success of synchrotron light sources. In this section, we look at two counter-balancing effects of synchrotron radiation: Classical synchrotron radiation provides damping to the longitudinal phase space and the quantum nature of the synchrotron radiation provides diffusion in the phase space. The balance between these two aspects of synchrotron radiation gives rise to the equilibrium bunch shape. We mentioned these above in the discussion on the static potential well distortion (Sec. 2.3). There it was treated phenomenologically by introducing a diffusion term in the Vlasov equation. Here we will start microscopically and try to incorporate these effects into the iteration given by Eqs. 2.6 and 2.7

As is well known from classical electrodynamics [39], electrons radiate when they accelerate or decelerate. For a highly relativistic electron, the most significant synchrotron radiation comes from the components of acceleration that are perpendicular to the electron's velocity. In the circular accelerator, this is simply the bending acceleration, or the centripetal acceleration given by

$$a = \frac{c^2}{\rho}. \tag{4.34}$$

Here we assume the electron is moving close to the speed of the light. As a result, the power of synchrotron radiation is [39]:

$$P = \frac{2}{3} \frac{e^2 a^2}{c^3} \gamma^4 = \frac{2}{3} \frac{e^2 c}{\rho^2} \gamma^4. \tag{4.35}$$

The total energy loss of an electron in one revolution is:

$$U(E) = \oint dt P = \frac{1}{c} \oint ds P = C_\gamma E^4 R < \frac{1}{\rho^2} >, \tag{4.36}$$

where

$$C_\gamma = \frac{4\pi}{3} \frac{r_e}{(mc^2)^3} = 8.85 \times 10^{-5} \text{ meters/GeV}^{-3}, \tag{4.37}$$

and the square of the curvature $1/\rho$ is averaged over the circumference $2\pi R$ of the ring:

$$< \frac{1}{\rho^2} > = \frac{1}{2\pi R} \oint ds \frac{1}{\rho^2}. \tag{4.38}$$

From Eq. 2.71, we need dU/dE in order to calculate the radiation damping time. Since

$$U(E) = \oint dt P(E) = \oint ds \frac{dt}{ds} P(E), \tag{4.39}$$

not only dP/dE contributes to the dU/dE; dt/ds also has contribution. This is due to the momentum dispersion. When the electron's energy is differs slightly from that of the design particle's energy E_0, it will travel along a slightly different trajectory. The radius of curvature of an electron with energy $E_0 + \delta E$ is different from that of the design particle's by the small amount:

$$x_p = D \frac{\delta E}{E_0}. \tag{4.40}$$

For ds traversed by the design particle, the off-energy electron will move

$$dl = \frac{\rho + x_p}{\rho} ds. \tag{4.41}$$

Thus, w

$$\frac{dt}{ds} = \frac{1}{c} \frac{dl}{ds} = \frac{1}{c}(1 + \frac{D}{\rho} \frac{\delta E}{E_0}). \tag{4.42}$$

Substituting Eq. 4.42 into Eq. 4.39 yields

$$U(E) = \frac{1}{c} \oint ds P(E)(1 + \frac{D}{\rho} \frac{P}{E_0}), \tag{4.43}$$

and

$$\frac{dU(E)}{dE} = \frac{1}{c} \oint ds(\frac{dP(E)}{dE} + \frac{D}{\rho} \frac{P}{E_0}). \tag{4.44}$$

Since

$$\rho = \frac{E}{eB}, \tag{4.45}$$

where B is the magnetic field, we have

$$P \propto E^2 B^2, \tag{4.46}$$

and

$$\frac{dP}{dE} = 2\frac{P}{E} + 2\frac{P}{B}\frac{dB}{dE} = 2\frac{P}{E} + 2\frac{P}{B}\frac{dB}{dx}\frac{dx}{dE}$$
$$= 2\frac{P}{E} + 2\frac{P}{B}\frac{dB}{dx}\frac{D}{E_0}. \tag{4.47}$$

In the last equality, we have used Eq. 4.40. Finally, substitution of Eq. 4.47 into Eq. 4.44, gives

$$\frac{dU(E)}{dE}|_{E=E_0} = \frac{1}{c}\oint ds(2\frac{P}{E_0} + 2\frac{P}{B}\frac{dB}{dx}\frac{D}{E_0} + \frac{D}{\rho}\frac{P}{E_0})$$
$$= \frac{2U(E_0)}{E_0}(1 + \frac{\alpha}{2}), \tag{4.48}$$

where

$$\alpha = \frac{1}{cU(E_0)}\oint DP(E_0)(\frac{1}{\rho} + \frac{2}{B}\frac{dB}{dx}). \tag{4.49}$$

The radiation damping time is thus

$$\frac{1}{t_r} = \frac{1}{2T_0}\frac{dU}{dE}|_{E=E_0} = \frac{<P>}{2E_0}(2 + \alpha). \tag{4.50}$$

If the results of the preceding discussion were the end of the subject, we could design an electron storage ring in which the longitudinal phase space is damped, and the longitudinal emittance shrinks to zero. But such is not the case. The radiation process proceeds through the emission of discrete quanta, and the fluctuations in this random process excite synchrotron oscillations.

To see how this excitation comes about, let us suppose that a particle travels on its synchrotron orbit and emits a photon of energy ϵ. The position of the particle doesn't change, so it suddenly finds itself starting a synchrotron oscillation with an initial energy offset $-\epsilon$. Because of the random character of the photon emission, synchrotron radiation contributes a constant term to the growth of the emittance. This

101

can be understood by first considering a linear synchrotron oscillation in a stationary bucket without radiation damping:

$$\delta E = A \cos(\omega_{s0} t + \Delta), \tag{4.51}$$

$$\delta \phi = -A \left(\frac{h \omega_0 \eta}{\omega_{s0} E_0} \right) \sin(\omega_{s0} t + \Delta). \tag{4.52}$$

Here the amplitude of oscillation is

$$A^2 = (\delta E)^2 + \left(\frac{\omega_{s0} E_0}{h \omega_0 \eta} \right)^2 (\delta \phi)^2, \tag{4.53}$$

and h is equal to ω_{rf}/ω_0. Suppose at time $t = t_\epsilon$, the energy $E = E_0 + \delta E$ of the electron is suddenly decreased by amount ϵ due to the emission of a quanta, the synchrotron oscillation is now given by

$$\delta E = A \cos(\omega_{s0} t + \Delta) - \epsilon \cos[\omega_{s0}(t - t_\epsilon)], \tag{4.54}$$

$$\delta \phi = -A \left(\frac{h \omega_0 \eta}{\omega_{s0} E_0} \right) \sin(\omega_{s0} t + \Delta) - \epsilon \left(\frac{h \omega_0 \eta}{\omega_{s0} E_0} \right) \sin[\omega_{s0}(t - t_\epsilon)]. \tag{4.55}$$

The new amplitude is

$$A_\epsilon^2 = (\delta E)^2 + \left(\frac{\omega_{s0} E_0}{h \omega_0 \eta} \right)^2 (\delta \phi)^2 = A^2 + \epsilon^2 - 2 A \epsilon \cos(\omega_{s0} t_\epsilon + \Delta). \tag{4.56}$$

Since the radiation of the quanta can be assumed to occur with equal probability at any time, Δ is a random number with equal probability taking values from 0 to 2π. Averaging with respect to Δ yields

$$< \delta A_\epsilon^2 > = < A_\epsilon^2 - A^2 > = < \epsilon^2 > . \tag{4.57}$$

If we denote $n(\epsilon) d\epsilon$ to be the number of photons emitted between energy ϵ and $\epsilon + \delta \epsilon$ per unit time, we have

$$\frac{d < A^2 >}{dt} = \dot{Q}_E, \tag{4.58}$$

with

$$Q_E = \int_0^{+\infty} d\epsilon \, n(\epsilon) \epsilon^2 = \frac{55}{24\sqrt{3}} e^2 c^2 \left(\frac{h}{2\pi} \right)^2 \frac{\gamma^7}{\rho^2 R}. \tag{4.59}$$

A good derivation of the expression for Q_E can be found in the paper by J. Schwinger [50].

Including longitudinal radiation damping, the longitudinal phase space area occupied by the beam evolves according to

$$\frac{d<A^2>}{dt} = Q_E - \frac{2}{t_r}<A^2>.$$ (4.60)

The first term is the constant term contributing to the growth of the longitudinal emittance and the second term is the damping term which will reduce the emittance to zero. Equilibrium energy spread is obtained by balancing these two effects. Setting $d<A^2>/dt = 0$ yields the equilibrium energy spread:

$$\sigma_{\epsilon 0} = \frac{<A^2>}{2} = \frac{Q_E t_r}{4}.$$ (4.61)

4.3.2 Implementation of Radiation Damping and Quantum Emission

Finally, let us consider how to incorporate the effect of the quantum emission into the iteration given by Eqs. 2.6 and 2.7. For a macroscopically measurable change of the energy ϵ due to synchrotron radiation, there are many quanta involved:

$$\epsilon(t) = \sum_i \epsilon_i e^{-(t-t_i)/t_r} \cos[\omega_{s0}(t - t_i)]$$ (4.62)

Here t_i are randomly distributed, and the summation is over all the quanta contributing to the change of energy by ϵ. According to the central limit theorem [51], the distribution of ϵ is a Gaussian distribution:

$$p(\epsilon) = \frac{1}{\sqrt{2\pi}\sigma_{\epsilon 0}} \exp(-\frac{\epsilon^2}{2\sigma_{\epsilon 0}^2}).$$ (4.63)

Thus, we get the iteration equations for the longitudinal synchrotron oscillation which have incorporated the effect of the radiation damping and the energy fluctuation due to the quantum nature of the radiation:

$$\tau_{n+1} = \tau_n - \frac{\eta T_0}{E_0}\delta E_{n+1},$$ (4.64)

$$\delta E_{n+1} = \delta E_n - eV\cos(\phi_s)\omega_{rf}\tau_n - \frac{2T_0}{t_r}\delta E_n + 2\sigma_{\epsilon 0}\sqrt{\frac{T_0}{t_r}}R(n).$$ (4.65)

Here $R(n)$ is a Gaussian distributed random number with mean 0 and standard deviation 1.

In the next chapter, we will discuss simulation results based upon these equations. With an arbitrary initial phase space distribution, we run the simulation for a few damping times. The asymptotic distribution in phase space becomes a normal distribution with energy spread given by $\sigma_{\epsilon 0}$ and the bunch length σ_0 related to the energy spread by

$$\sigma_0 = \frac{\eta}{\omega_{s0} E_0} \sigma_{\epsilon 0}. \tag{4.66}$$

4.4 Full Equations for the Multiparticle Simulation

In this section, we add the wake field into Eq. 4.65 and derive the complete equations for the multiparticle simulation for the bunch lengthening instability.

Typically, there are many billions of electrons in a bunch, and it is computationally impractical to simulate such a large number of particles. One approximation is to represent many electrons by a single macroparticle. By considering only the dynamics of these macroparticles, we significantly reduce the number of the degrees of freedom in our system. Since the bunch lengthening instability is related to the low-frequency collective motion of the electrons in the bunch, we do not expect problems from this truncation of the degrees of freedom in our approximation. Should we consider modes of order of the total number of macroparticles, our truncation approximation breaks down.

The motion in phase space of each of the macroparticles is given by:

$$\tau_{n+1}(m) = \tau_n(m) - \frac{\eta T_0}{E_0} \delta E_{n+1}(m), \tag{4.67}$$

$$\delta E_{n+1}(m) = \delta E_n(m) - eV \cos(\phi_s)\omega_{rf}\tau_n(m)$$
$$- \frac{2T_0}{t_r}\delta E_n(m) - \frac{2T_0}{t_D}\delta \bar{E}_n$$

104

$$+2\sigma_{\epsilon 0}\sqrt{\frac{T_0}{t_r}}R(n,m)+V_n(m). \tag{4.68}$$

In these equations $m = 1, \ldots, M$ specifies the macroparticle number, and the argument n specifies the number of revolutions the particles have made in the storage ring. Eqs. 4.67 and 4.68 are the central equations in the existing multiparticle tracking simulation codes [8, 19, 54, 55, 56] Compared with Eq. 4.65, we note a new term that characterizes the effect of Robinson damping [10]. Since motions of the center of the bunch, or dipole oscillations are damped by Robinson damping, we expect the damping term to be proportional to the center of the bunch $\delta\bar{E}_n$. The damping times t_D are taken from measurements. The wake field term, $V_n(m)$, gives the wake force on the macroparticle m from all particles which precede it in the bunch:

$$V_n(m) = Ne^2 L_0 \int_\tau^{+\infty} d\tau' \rho(\tau') W(\tau' - \tau). \tag{4.69}$$

$$= \frac{Ne^2 L_0}{M} \sum_{j(t_j \geq t_m)} W(t_j - t_m). \tag{4.70}$$

Whenever the longitudinal impedance of the ring can be approximated by a resonator impedance, the wake function is given by:

$$W(t)L_0 = \begin{cases} 0 & \text{if } t < 0, \\ \frac{\omega_r R}{Q}\exp(-vt)(\cos\Omega t - \frac{v}{\Omega}\sin\Omega t) & \text{if } t > 0. \end{cases} \tag{4.71}$$

This wake function provides us with a special algorithm for computing the wake field term $V_n(m)$ given by Eq. 4.70. To see this, rewrite the non-zero part of the wake function as:

$$W(t)L_0 = C\exp(-vt)\cos(\Omega t + \Delta), \quad \text{for } t \geq 0, \tag{4.72}$$

with C and Δ given by

$$C = \frac{\omega_r R}{Q}\sqrt{1 + \frac{v^2}{\Omega^2}}, \tag{4.73}$$

and

$$\Delta = \arctan\frac{v}{\Omega}. \tag{4.74}$$

Furthermore, the wake function can be written as:

$$W(t)L_0 = Im \ C \exp(-vt + i\Omega t + i\Delta), \quad \text{for } t \geq 0. \tag{4.75}$$

With this result, the wake field computation can proceed in the following way. First, arrange the arrival times of the macroparticles, $\tau_m, m = 1, \ldots, M$, into an ascending array, with later elements of the array corresponding to the particles which arrive earlier. The purpose of this arrangement is to take advantage of the causality of the wake function: $W(t)$ vanishes when $t < 0$. For a particular macroparticle m, we need only calculate the wake fields left behind from all those macroparticles with $m' > m$. Quick Sort is an excellent algorithm to sort any array into an orderly array. For large M, on average, it is the fastest known sorting algorithm [52].

Next, with $\Delta t = t_{m+1} - t_m$, we can easily calculate the wake from the $(m+1)$'th macroparticle by computing

$$CW = C \exp(-v\Delta t + i\Omega\Delta t + i\Delta), \tag{4.76}$$

and the wake is the imaginary part of CW. The wake from the $(m+2)$'th macroparticle can be found by using $\Delta t_1 = t_{m+2} - t_{m+1}$, and noting

$$W(t_{m+2} - t_m)L_0 = Im \ \exp\left(-v(\Delta t + \Delta t_1) + i\Omega(\Delta t + \Delta t_1) + i\Delta\right)$$

$$= Im \ \exp(-v\Delta t_1 + i\Omega\Delta t_1)CW. \tag{4.77}$$

The calculation of the wake including the $(m+2)$'th macroparticle is thus reduced to multiplying the complex wake CW by the complex number

$$\exp(-v\Delta t_1 + i\Omega\Delta t_1),$$

and then taking the imaginary part. The wake from other macroparticles can be calculated similarly. This procedure has the important advantage that it can be used to calculate the wake from previous turns without keeping track of the actual arrival

time of a particle. This technique is very useful for the coupled-bunch instability. For the bunch lengthening instability, the relevant impedance is broadband impedance of the ring. After one turn, the wake corresponding to the broadband impedance has decayed to a negligible level and the bunch lengthening instability is mostly a single-turn effect. In the case of a single turn wake, this technique does not improve the computation speed much when compared with the brute force method of summing the wakes together.

The most time consuming part of the multiparticle simulation is the wake field calculation. For each macroparticle m, we must compute the wakes left behind by all the particles ahead of it, and this calculation must be repeated for for all the macroparticles. The number of computations relating to the wake field is thus proportional to M^2. Since we need to increase M to distinguish the noise from the real collective motion (noise amplitude goes down with M as $1/\sqrt{M}$ while the amplitude of a collective mode does not change much with respect to M), the M^2 dependence will increase our computation times significantly. Fortunately, a simple observation saves us from this problem. Instead of computing the wake by the summation, or Eq. 4.70, we compute it by integration, or Eq. 4.69:

$$V_n(m) = Ne^2 L_0 \int_{\tau_n(m)}^{+\infty} d\tau' \rho(\tau') W(\tau' - \tau_n(m)). \qquad (4.78)$$

To calculate $\rho(\tau)$ at each turn we simply bin the macroparticles in τ, without smoothing, and count on the use of a very large number of macroparticles to give us a sufficiently smooth distribution. The number of computations for the integral of Eq. 4.78 is then proportional to the number of bins we use. Repeating this procedure for all the macroparticles results in the computation being proportional to the product of the number of bins and the number of macroparticles. Since the number of bins is fixed, this method will have a great advantage when we need to increase the number of macroparticles much more than the number of bins.

4.5   Localized Wake and Multiperiod Simulation

As pointed out in Sec. 2.2.4, the bunch lengthening instability is typically modeled by a ring broadband impedance. The major sources of the wake force, i.e., the vacuum beam pipe, bellows, etc., are distributed throughout the ring. This distributed wake is the model used in Ch. 3 when we developed the analytical theory of the bunch lengthening instability. On the other hand, existing multiparticle tracking simulation codes [8, 19, 54, 55, 56] always treat the wake force as working at one point in a ring. It is natural to wonder under what circumstances modeling a distributed wake by a localized wake leads to an accurate description of the bunch lengthening instability.

In App. A, we show that these two methods can give very different results. For example, in the case of a localized constant wake function, the energy spread of the bunch increases with the bunch current and the mixing between the energy deviation and the arrival time also increases with the bunch current. From Sec. 2.3, we know that under a distributed wake, the equilibrium energy spread does not depend on the current and there is no mixing between the energy deviation and the arrival time.

Until the present work, the importance of localized vs. distributed wakes in the multiparticle simulation has not been appreciated. We have solved the problem of modeling the distributed wake with a localized wake breaking the iteration given by Eqs. 4.67 and 4.68 into many periods. This is done straightforwardly by replacing T_0 with T_0/N_s, eV with eV/N_s and $V_n(m)$ with $V_n(m)/N_s$. Here, N_s is the number of periods within one revolution. In this way the wake field induced voltage drop is only one N_s'th of its value without the introduction of multiperiods. The resulting equations for the multiparticle multiperiod bunch lengthening simulation is given by:

$$\tau_{n+1}(m) = \tau_n(m) - \frac{\eta T_0}{N_s E_0}\delta E_{n+1}(m), \tag{4.79}$$

$$\delta E_{n+1}(m) = \delta E_n(m) - \frac{1}{N_s}eV\cos(\phi_s)\omega_{rf}\tau_n(m)$$

$$-\frac{2T_0}{N_s t_r}\delta E_n(m) - \frac{2T_0}{N_s t_D}\delta\bar{E}_n$$

$$+2\sigma_{\epsilon 0}\sqrt{\frac{T_0}{N_s t_r}}R(n,m) + \frac{V_n(m)}{N_s}. \tag{4.80}$$

It is obvious that as the number of periods N_s increases, the multiparticle multiperiod code simulates the distributed wake force more accurately. But how many periods are enough? From our experience with the multiparticle multiperiod simulation, we choose the number of periods N_s in the following way. We count the number of iterations in which the wake field kick exceeds ten percent of the natural energy spread. If the count is less than one percent of the total number of iterations, N_s is accepted. Otherwise we increase N_s until the count is less than one percent of the total number of iterations.

4.6   Diagnostics

The most common diagnostic tool in existing multiparticle simulation codes, including ours, is the temporal evolution of the center of the bunch, bunch length, center of the energy deviation, and energy spread. Numerically, we evaluate

$$< \tau_n > = \frac{1}{M}\sum_{m=1}^{M}\tau_n(m), \tag{4.81}$$

$$\sigma_n^2 = \frac{1}{M}\sum_{m=1}^{M}[\tau_n(m) - <\tau_n>]^2, \tag{4.82}$$

$$< \delta E_n > = \frac{1}{M}\sum_{m=1}^{M}\delta E_n(m), \tag{4.83}$$

$$\sigma_{\epsilon n}^2 = \frac{1}{M}\sum_{m=1}^{M}[\delta E_n(m) - <\delta E_n>]^2. \tag{4.84}$$

Here, the summation over m is a sum over macroparticles. When the tracking code is run with many periods, these quantities are sampled at one particular period each full revolution in the ring. This corresponds to the fact that bunch length, energy spread and phase shift are observed experimentally at a fixed location in the ring.

In any simulation run, we track the bunch revolution four damping times. We start to sample the above four quantities for the length of one damping time after the initial three damping times. The numerical value for the center of the bunch, bunch length, center of the energy deviation and energy spread are obtained by averaging $< \tau_n >$, σ_n^2, $< \delta E_n >$ and $\sigma_{\epsilon n}^2$ over all the data points gathered over one damping time.

The amplitude of the Fast Fourier Transformation (FFT) of $< \tau_n >$, σ_n^2, $< \delta E_n >$ and $\sigma_{\epsilon n}^2$ serve as an important diagnostic for identifying low order coherent synchrotron modes and determining that these modes are not coupled at the threshold currents.

In our multiparticle multiperiod simulation code, we have sample five additional quantities at each turn compared with the existing codes:

$$< \tau_n^3 > = \frac{1}{M} \sum_{m=1}^{M} [\tau_n(m)]^3, \tag{4.85}$$

$$< \tau_n^4 > = \frac{1}{M} \sum_{m=1}^{M} [\tau_n(m)]^4, \tag{4.86}$$

$$< \delta E_n^3 > = \frac{1}{M} \sum_{m=1}^{M} [\delta E_n(m)]^3, \tag{4.87}$$

$$< \delta E_n^4 > = \frac{1}{M} \sum_{m=1}^{M} [\delta E_n(m)]^4, \tag{4.88}$$

and

$$corr_n = \frac{1}{M} \sum_{m=1}^{M} [\tau_n(m) - < \tau_n >][\delta E_n(m) - < \delta E_n >]. \tag{4.89}$$

Using the relationship between the cummulant moments and the ordinary moments given by Eq. 3.49 and 3.50, we have:

$$< \tau_n^3 >_c = < \tau_n^3 > -3 < \tau_n > \sigma_n^2 - < \tau_n >^3, \tag{4.90}$$

$$< \tau_n^4 >_c = < \tau_n^4 > -3\sigma_n^4 - 4 < \tau_n > < \tau_n^3 >_c -6 < \tau_n >^2 \sigma_n^2 - < \tau_n >^4, \tag{4.91}$$

$$< \delta E_n^3 >_c = < \delta E_n^3 > -3 < \delta E_n > \sigma_{\epsilon n}^2 - < \delta E_n >^3, \tag{4.92}$$

110

$$< \delta E_n^4 >_c = < \delta E_n^4 > -3\sigma_{\epsilon n}^4 - 4 < \delta E_n >< \delta E_n^3 >_c -6 < \delta E_n >^2 \sigma_{\epsilon n}^2 - < \delta E_n >^4 \ .$$

$$(4.93)$$

Averaging all these quantities over one damping time yields γ_1, γ_2 for the distribution in τ; $\gamma_{1\epsilon}$, $\gamma_{2\epsilon}$ for the distribution in δE; and $corr$ for the mixing between τ and ϵ. We can thus make detailed comparison between simulation and theory.

The turbulent threshold is determined in the following way: Since the equilibrium distribution in τ is given by the theory of the potential well distortion, we can compute $< \tau >$, σ, γ_1 and γ_2 from the numerical solution of the Haissinski equation and compare them with the values obtained from the simulation. This serves as a first test of simulation and theory. We expect differences to arise at or near the turbulent threshold. The most sensitive measure of nearness to the threshold is the distribution at δE. According to the potential well distortion theory, σ_ϵ must be constant, and $\gamma_{1\epsilon} = \gamma_{2\epsilon} = corr = 0$ below the turbulent threshold. Thus we must find only the current at which $\gamma_{1\epsilon}$, $\gamma_{2\epsilon}$, and $corr$ become non-zero.

Chapter 5

Comparison of Theory, Experiment and Simulation

In this chapter, we present the results from the instability analysis based on the improved Sacherer equation 3.130 and the multiparticle multiperiod simulation, and compare them with the experimental results of Wilson et al. [8] and Brandt et al. [36].

Most of the results are based on the parameters of SPEAR II given by Table 5.1. There are two primary motivations for choosing the SPEAR II data [8, 55] as a benchmark for our theoretical and numerical study. One is that the impedances and the bunch lengthening measurements on SPEAR II are the most comprehensive, and data are readily available. The second one results from the scaling behavior of the bunch lengthening instability. In Sec. 3.10, we noted that there are only two parameters, namely $\omega_r \sigma$ and ξ, which need to be specified to determine the turbulent threshold. Therefore, whether we use the SPEAR II parameter set or other parameter sets is not important; $\omega_r \sigma$ and ξ are the only relevant parameters for the bunch lengthening instability. In Sec. 5.2, we also compare the instability analysis with the experimental results from LEP.

ring circumference	L_0	234m
bending radius	ρ	12.7m
RF frequency	f_{rf}	358.54Mhz
beam energy	E_0	3GeV
peak RF voltage	V	2.9 MeV
momentum compaction	α	0.0418
eta	η	0.0418
synchrotron tune	ν_{s0}	0.042
energy loss per turn		0.564MeV
revolution period	T_0	0.78μs
radiation damping time	t_r	3.91ms
natural bunch length	σ_0	2.59cm
natural energy spread	$\sigma_{\epsilon0}$	2.1Mev
Robinson damping time	t_D	0.6/I(mA)

Table 5.1: SPEAR II parameters.

5.1 Simulation Results

1024 macroparticles were tracked using Eqs. 4.79 and 4.80 to calculate the longitudinal phase space motion. The initial distributions in both arrival time and energy deviation were bivariate normal distributions with bunch length and energy spread equal to their natural values. After running three damping times, we start the diagnostic process (see Sec. 4.6) for one damping time.

On each turn we calculate the four lower cummulant moments of the distributions. By averaging over the last damping time, we obtain the average properties of the distribution: center of the bunch $< \tau >$, bunch length σ, skewness γ_1 and excess γ_2. In Fig. 5.1, we plot the center of the bunch and bunch length as a function of current. The solid lines are computed from the potential well distortion theory. The dotted lines are simulation results. We can identify 45mA as the threshold current, since this is where the sold lines and dotted lines start to diverge. In Fig. 5.2, we plot γ_1 and γ_2 as a function of current. We can still identify 45mA as the threshold current, although the difference in γ_1 is not obvious.

From Fig. 5.3 to Fig. 5.5, the center of the bunch vs. turn number n, bunch length vs. turn number n and their Fast Fourier Transforms (FFT) are plotted for a current I=15mA, well-below the threshold. Fig. 5.3(a) shows the FFT amplitude of $< \tau_n >$ vs. n. Fig. 5.3(b) is the logarithm of this amplitude. The excitation of several synchrotron modes is apparent. As expected, the dipole mode is the strongest. In Fig. 5.4(a), the FFT amplitude of σ_n^2 vs. n is plotted. In Fig. 5.4(b), its logarithm is plotted. In this case, the quadrupole mode is stronger than the dipole mode. In Fig. 5.5, both τ_n and σ_n^2 are plotted for one damping time.

From Fig. 5.6 to Fig. 5.8, simulation results are plotted for the 50mA bunch current. In Fig. 5.6(a), the FFT amplitude of $< \tau_n >$ vs. n is plotted. Fig. 5.6(b) plots the logarithm of this amplitude. The tune spread of the dipole mode is apparent.

Compared with Fig. 5.3, it is clear that the frequency of the center of the dipole mode remains unchanged. This is exactly what is proved in Sec. 3.9. Although there is some overlap between sidebands of the dipole mode and quadrupole mode, the centers of these two modes remain widely separated. Fig. 5.7(a) is the FFT amplitude of σ_n^2 vs. n, and Fig. 5.7(b) is its logarithm. In Fig. 5.8, both τ_n and σ_n^2 vs. n are plotted for one damping time. Compared with Fig. 5.5, Fig. 5.8 are noisier. This is due to the strong excitation of dipole and quadrupole modes.

In conclusion, our multiparticle multiperiod tracking simulation has identified the turbulent threshold of 45mA. At this current, the dipole mode and quadrupole mode are still widely separated. Thus we see no indication of mode coupling, which was previously considered as a likely cause of the instability.

The turbulent threshold measured from SPEAR II by Wilson et. al. [8] for the 3GeV beam energy is 20mA. It is significantly lower than the 45mA threshold found with our simulation. We attribute this discrepancy to details of the model used for the wake field. Indeed, Siemann [55] used the impedance calculated from the loss factor measurement at SPEAR II rather than a broadband resonator impedance (which only approximates the real wake), and obtained a threshold from his simulation that agreed with the experiment. The purpose of our multiparticle multiperiod simulation code is to test our new explanation of the mechanism for the bunch lengthening instability, and not to directly simulate SPEAR II.

It would be very useful if we could identify the dependence of the collective mode amplitude on M, the number of macroparticles. We expect the scaling to be $1/\sqrt{M}$ below the threshold current and independent of M when the mode becomes unstable. Unfortunately, detailed scaling studies are computationally prohibitive, but are of interest for the future.

5.2 Comparison of the Improved Sacherer Equation with Experiments and Numerical Studies

In Sec. 3.10, we developed a numerical algorithm to analyze the instability threshold of the improved Sacherer equation. By discretizing in r, we transform the improved Sacherer equation into an eigenvalue problem of an asymmetric real matrix. The instability threshold corresponds to the bunch current at which the matrix starts to have complex eigenvalues. We use the powerful and efficient Gauss-Laguerre scheme [47] for discretization. Our instability analysis for the onset of bunch lengthening with $l = 1$, $N_d = 5$ predicts that the dipole mode becomes unstable around 50mA. (Here N_d is the number of points used for the discretization.) Increasing N_d to 40 does not change the conclusion. The quadrupole mode is predicted to become unstable at slightly higher current: 52mA. All these results are in good agreement with our multiparticle multiperiod tracking simulation.

Since the instability threshold is determined by two dimensionless scaling parameters: $\omega_r \sigma$ and ξ, we have also run our instability code to determine the critical coupling ξ_c as a function of $\omega_r \sigma$. Using a full-scale numerical Vlasov analysis, Oide and Yokoya [34] also calculated $\xi_c(\omega_r \sigma)$. In Fig. 5.9, we compare our results (dashed line) with that of Oide and Yokoya (solid line). We only plots our result for $\omega_r \sigma$ less than 0.7. In this range, results from both methods are in good agreement.

When $\omega_r \sigma$ is larger than 0.7, our instability code is not useful. The reason is due to the our parameterization scheme which uses the four lowest-order cummulants to approximate the real equilibrium particle density. Fig. 5.10 shows a typical case with $\omega_r \sigma = 0.8$. In Fig. 5.10, the solid line is from the solution of the Haissinski equation and the dashed line is from our four-parameter cummulant expansion. It is clear that the parameterization scheme needs to be improved. Developing an improved

parameterization scheme including the region $\omega_r\sigma > 0.7$ is left to future study.

In summary, the bunch lengthening threshold calculation based on the instability analysis of the improved Sacherer equation is seen to work well for short bunches and impedances described by a single broadband resonator.

Brandt and Hofmann [36] measured the bunch lengthening instability at LEP. They found that the dipole mode becomes unstable first at a threshold current of 0.1mA. With a 1.4GHz ring broadband impedance, they inferred a longitudinal impedance Z/n of 0.4Ω from the measured frequency shift of the quadrupole mode. The equilibrium bunch length is 1cm, $\omega_r\sigma$ is 0.29. This is a short bunch and our theory should work well. Our instability analysis identifies the dipole mode to be the first unstable synchrotron mode with threhold current of 0.113mA. Once again, the instability analysis agrees with the experimental results.
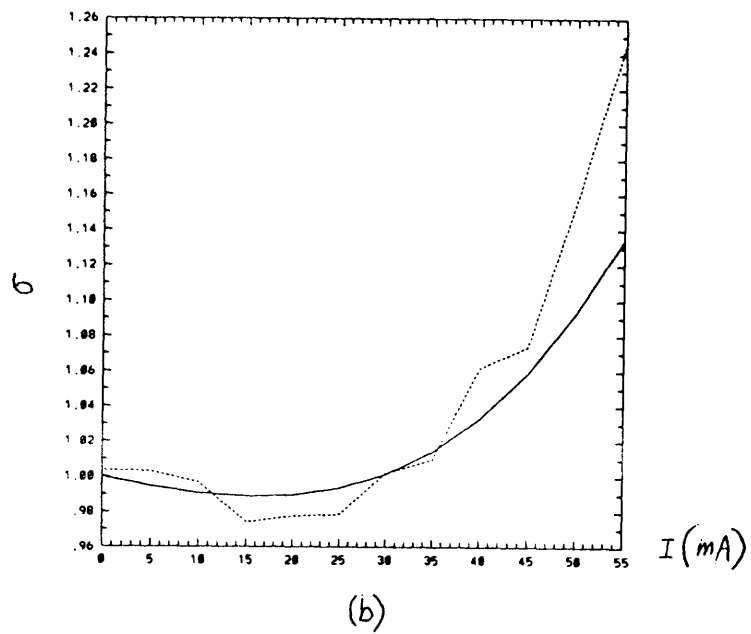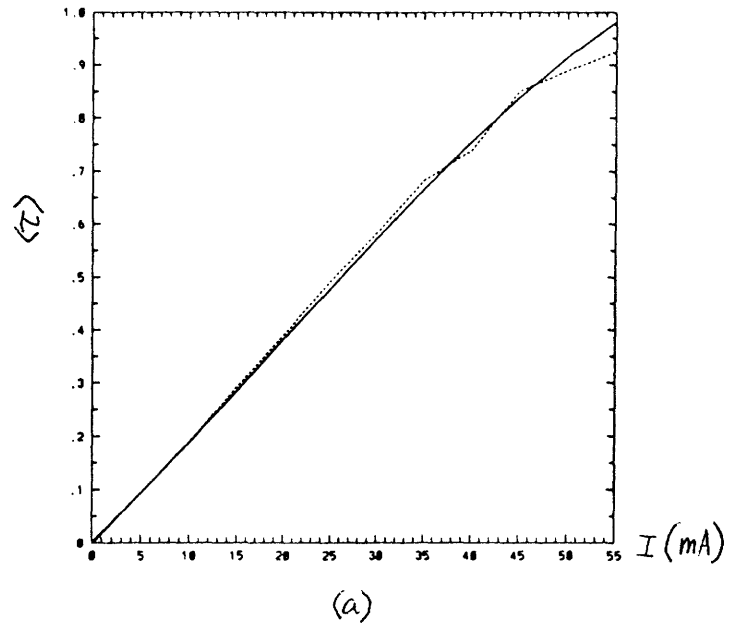
Figure 5.1: (a) $< \tau >$ as a function of current, (b) σ as a function of current. Solid lines are computed from the Haissinski equation 2.86, dashed lines are simulation results. At I=45mA, solid lines and dotted lines start to diverge.
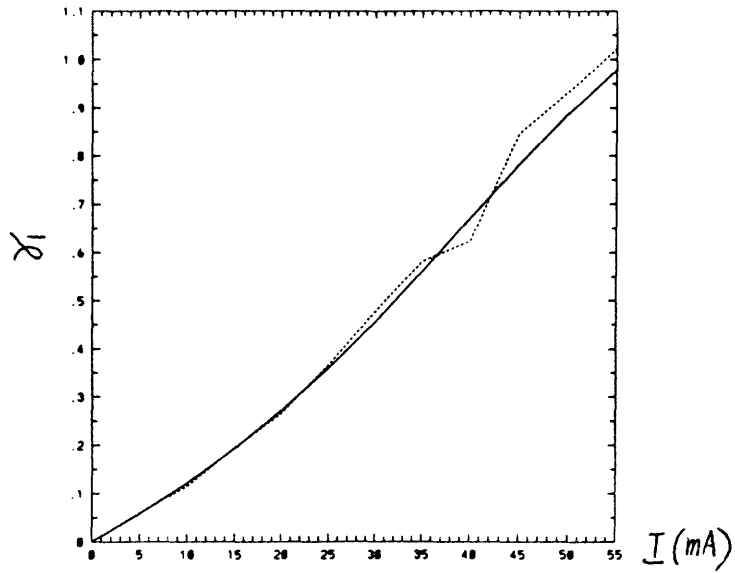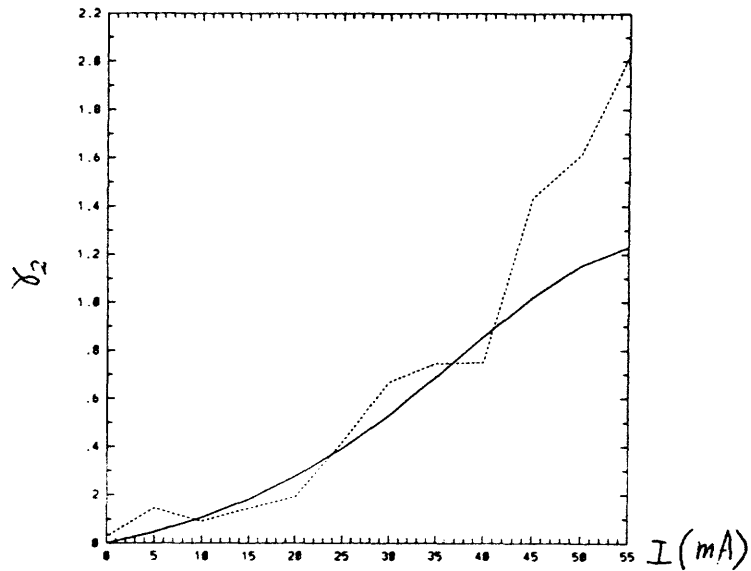
Figure 5.2: (a) γ_1 as a function of current, (b) γ_2 as a function of current. Solid lines are computed from Haissinski equation 2.86, dashed lines are simulation results. At I=45mA, solid lines and dotted lines start to diverge.
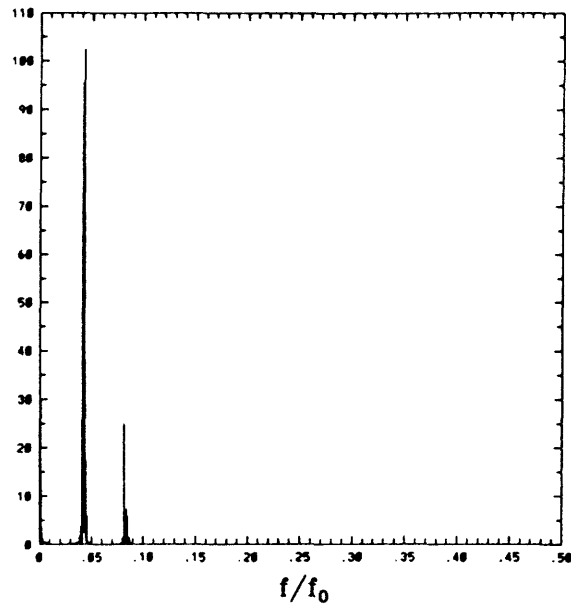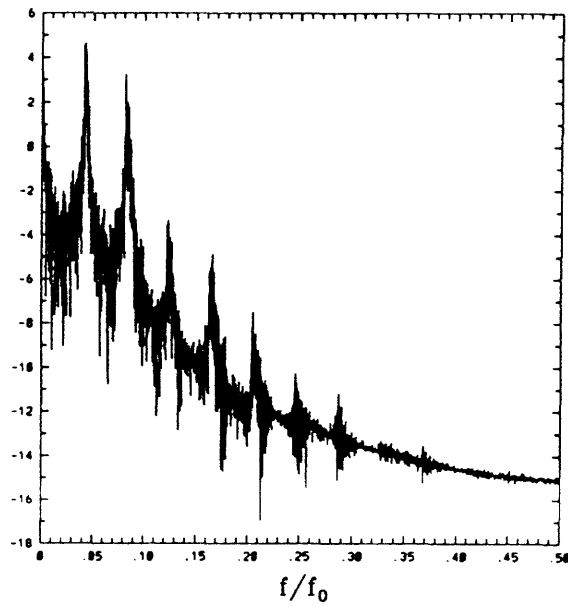
Figure 5.3: (a) FFT amplitude of $< \tau_n >$. (b) Logarithm of the FFT amplitude. Bunch current is 15mA (well-below threshold). Clear peaks are seen at the first few synchrotron harmonics $f/f_0 = l\nu_{s0}$. Here $l = 1, 2, \ldots$; $\nu_{s0} = 0.042$.
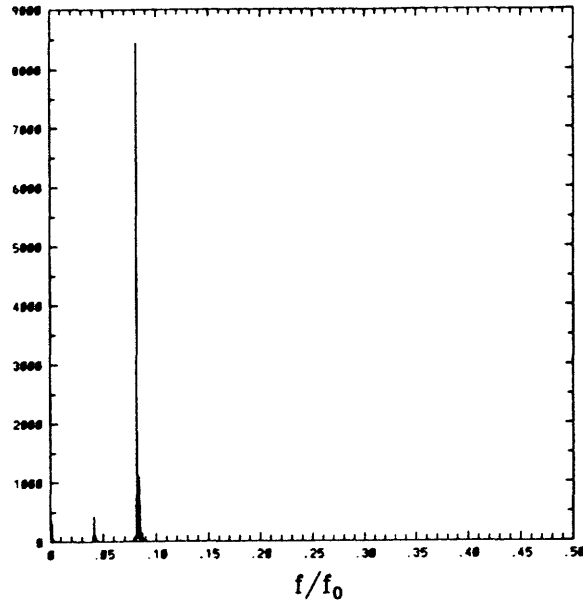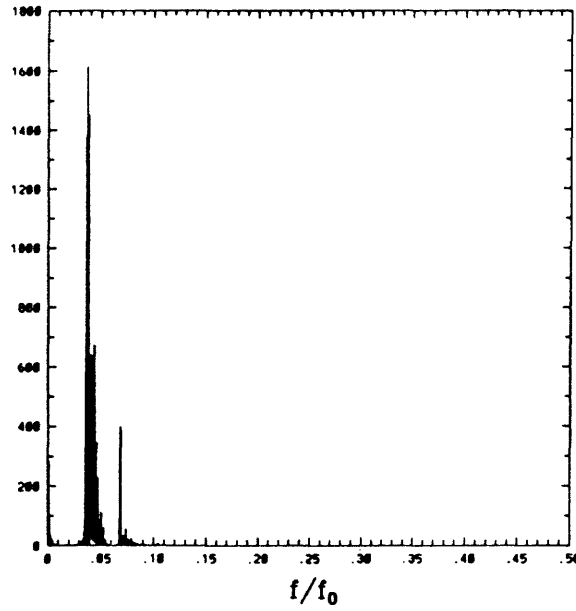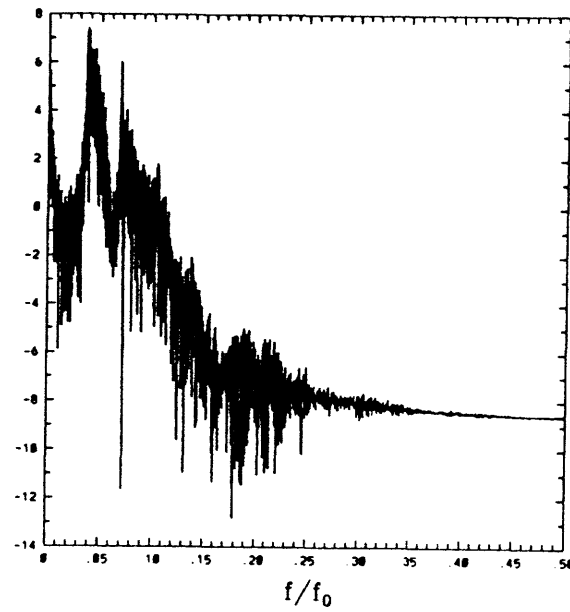
(a)
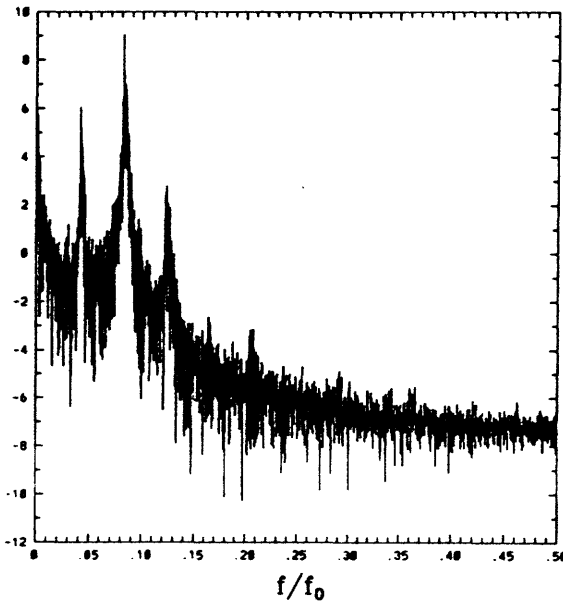
(b)

Figure 5.4: (a) FFT amplitude of σ_n^2. (b) Logarithm of the FFT amplitude. Bunch current is 15mA (well-below threshold). Clear peaks are seen at the first few synchrotron harmonics $f/f_0 = l\nu_{s0}$. Here $l = 1, 2, \ldots$; $\nu_{s0} = 0.042$.
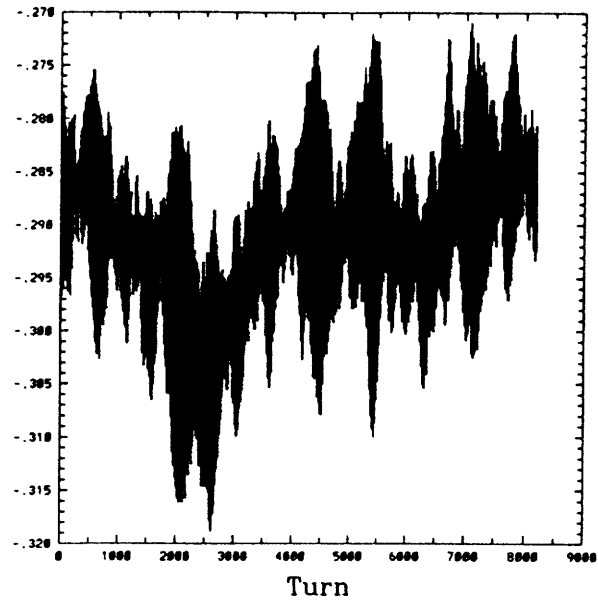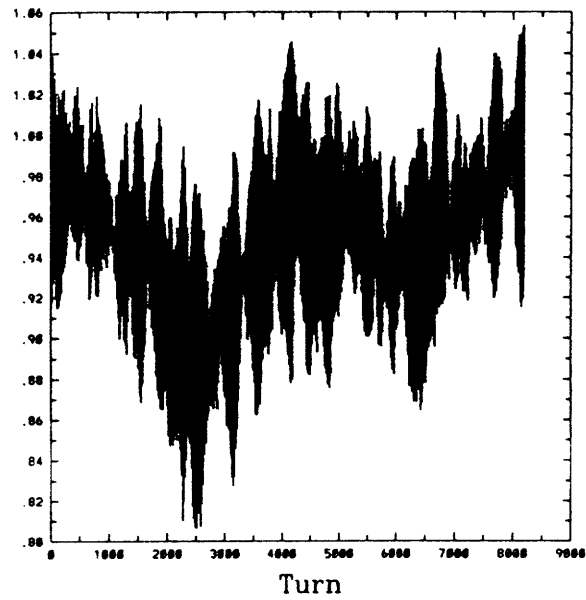
Figure 5.5: (a) Center of bunch vs. turn number. (b) Bunch length squared vs. turn number. Bunch current is 15mA (well below threshold).

(a)

(b)

Figure 5.6: (a) FFT amplitude of $< \tau_n >$. (b) Logarithm of the FFT amplitude. Bunch current is 50mA (slightly above threshold). Note that (1) The dipole and quadrupole mode are clearly separated. (2) The frequency of the dipole mode is not shifted. (3) Higher and broader peaks compared to the 15mA case seen in Fig. 5.3
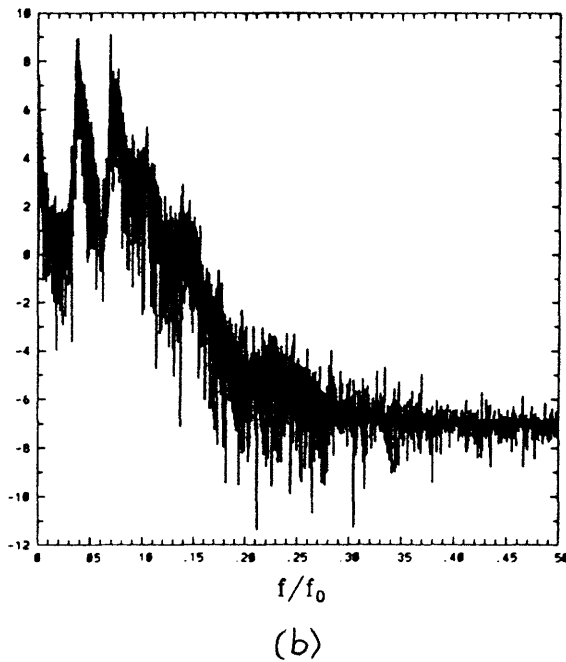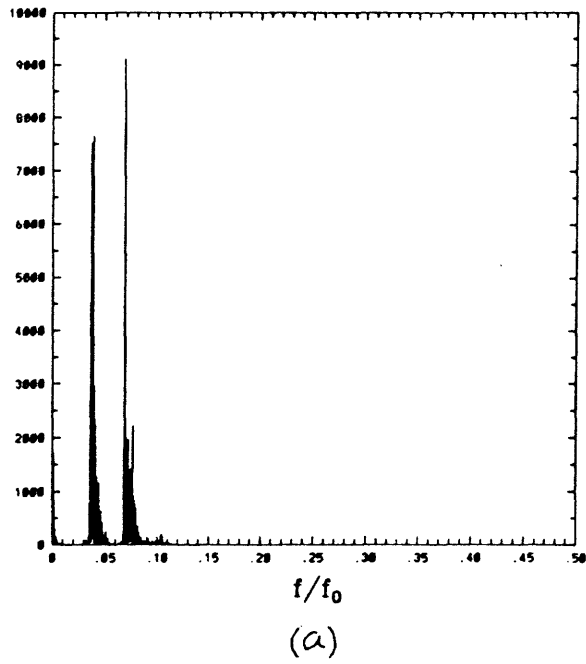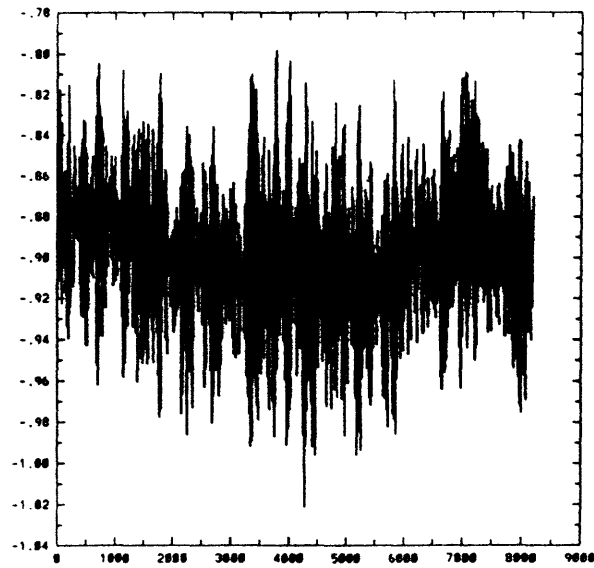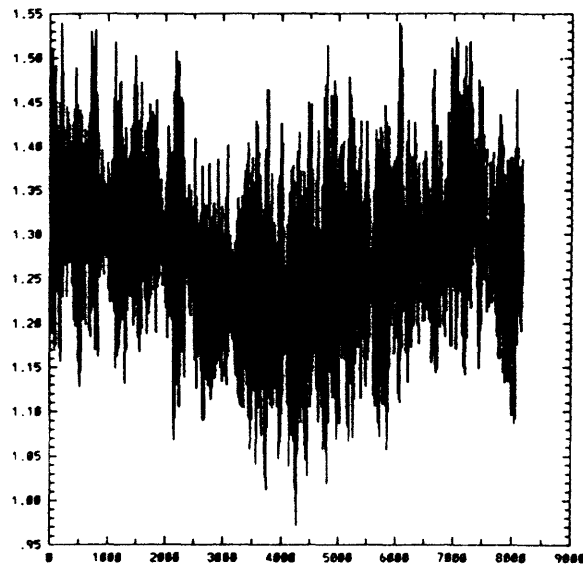
123

(a)

(b)

Figure 5.7: (a) FFT amplitude of σ_n^2. (b) Logarithm of the FFT amplitude. Bunch current is 50mA (slightly above threshold). Note that (1) The dipole and quadrupole mode are clearly separated. (2) The frequency of the dipole mode is not shifted. (3) Higher and broader peaks compared to the 15mA case seen in Fig. 5.4

124

(a)

(b)

Figure 5.8: (a) Center of bunch vs. turn number. (b) Bunch length square vs. turn number. Bunch current is 50mA (slightly above threshold). Compared with 15mA case seen in Fig. 5.5, signals are noisier due to the strong excitation of dipole and quadrupole modes.
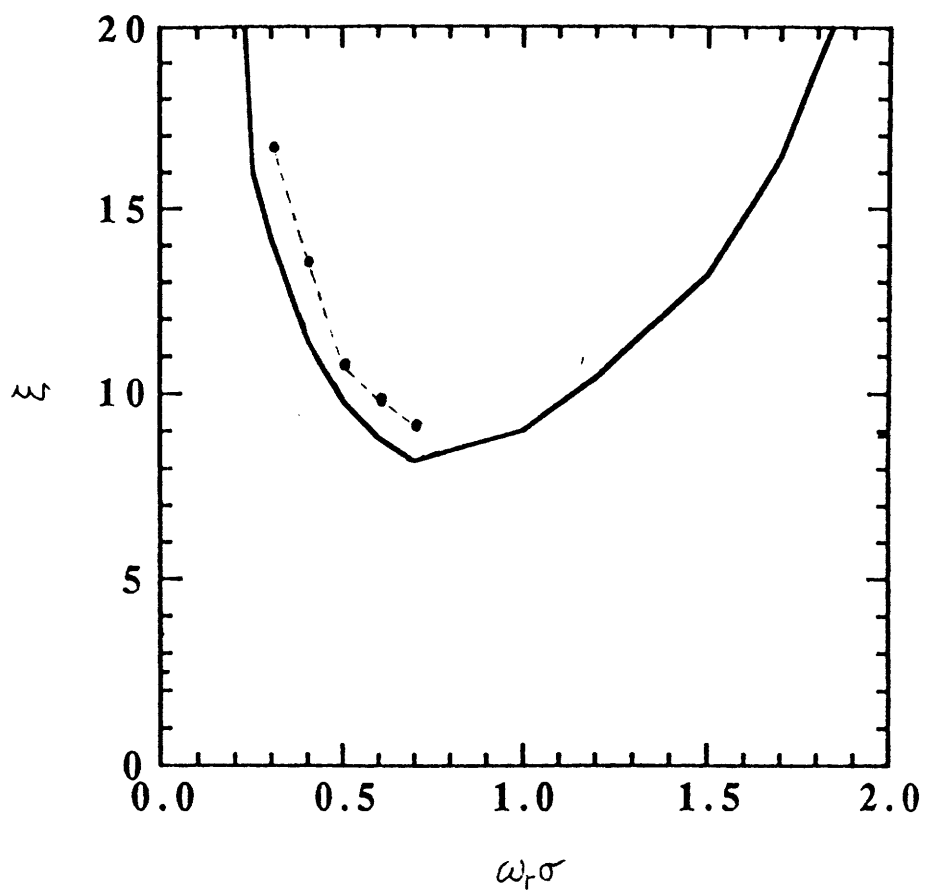
Figure 5.9: Critical coupling ξ_c vs. $\omega_r\sigma$. Dashed line is obtained from our theory for $\omega_r\sigma < 0.7$, solid line is obtained by Oide and Yokoya [34].
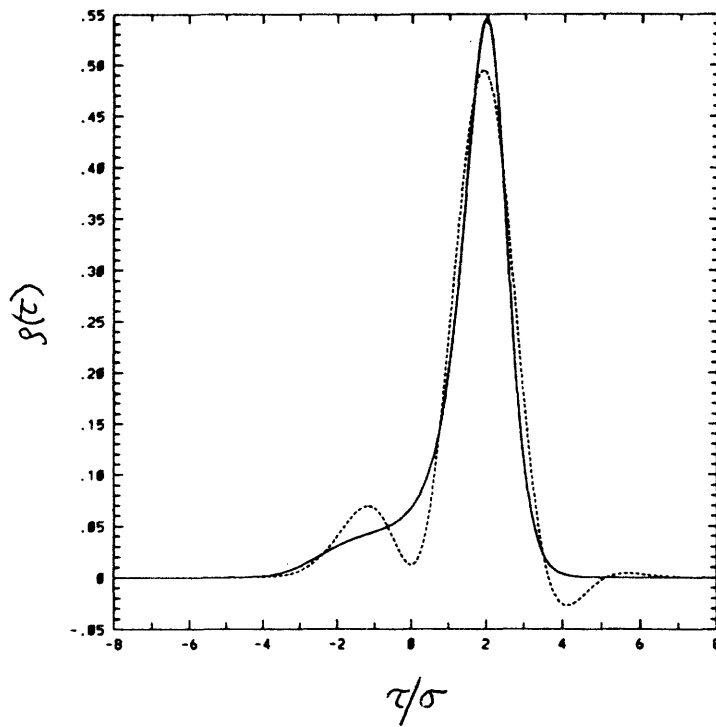
Figure 5.10: Equilibrium bunch shape when $\omega_r \sigma = 0.8$. Solid line is computed from Haissinski equation 2.86, dashed line is from our approximate distribution 3.60.

Chapter 6

Summary

In this thesis, an instability mechanism for turbulent bunch lengthening has been identified. Traditionally, the bunch lengthening instability has been explained by the coupling of two adjacent synchrotron modes. However, both simulation and experimental results exclude the possibility of the coupling of lower-order synchrotron modes. Coupling of higher-order synchrotron modes is unlikely since it requires strong impedances at frequencies well beyond the vacuum chamber cutoff. Starting from the assumption that the instability of an uncoupled synchrotron mode is sufficient to drive the turbulent bunch lengthening, we have found that a critical role is played by the nonlinearity of the static wake force. Without the nonlinearity of the static wake force, the Sacherer equation does not have an unstable eigenmode. We show that the nonlinearity of the static wake force distorts the equilibrium density from its Gaussian shape, and derive an improved Sacherer equation which includes asymmetric terms proportional to the square of the current. This improved Sacherer equation is unstable when the bunch current reaches a threshold value.

This is the most important result of this thesis, and is presented in Sec. 3.5. The successful prediction of the turbulent threshold requires an accurate parameterization of the equilibrium distribution, given by the Haissinski equation 2.78. We use the cummulant expansion technique for this purpose. By using only four lowest order

cummulants, we are able to approximate the equilibrium distribution to great accuracy for short bunches. This greatly reduces the number of correction terms needed for the instability analysis.

In order to verify the theoretical predictions based on the instability analysis of the improved Sacherer equation, we developed a multiparticle multiperiod simulation code. We have three improvements over the existing multiparticle tracking code: (1) We point out that the trajectory given by the iteration equations of longitudinal synchrotron motion is a tilted ellipse, rather than a circle as previously assumed. By loading the particles along the ellipses, we eliminate a source of loading noise. (2) Since the equilibrium distribution for a bunch under the influence of a localized wake is drastically different from that of a distributed wake, we distribute the wake force into many periods in our multiparticle simulation code. We use a counter in our code to make sure that we have used an optimal number of periods for any simulation run. (3) We have introduced new diagnostics into our multiparticle multiperiod simulation code. These new diagnostics verify our new understanding of the importance of nonlinearity in the bunch lengthening instability.

Instability analysis based on the improved Sacherer equation gives a threshold current very close to the simulation result and identifies the same unstable mode as seen in the experiment. The threshold scaling parameter ξ_c as a function of $\omega_r \sigma$ determined by the improved Sacherer equation agrees very well with the results from the numerical multimode Vlasov treatment of Oide and Yokoya [34]. Future work includes extending the comparison to other rings and impedances, taking into account the nonlinearity of the RF bucket, and devising a good parameterization scheme for long bunches.

Appendix A

Equlibrium Bunch Shape for a Localized Wake

The bunch lengthening instability is driven by the beam broadband impedance. The major sources of the corresponding wake force are distributed throughout the ring. This is the reason that we focus exclusively on the distributed wake in our analytical theory of the bunch lengthening instability. Although the multiparticle tracking simulation employs the localized wake, we try to break it up into many periods to approximate the distributed nature of the wake. In this appendix, we discuss the equilibrium phase space distribution for a localized wake. For the sake of analytical tractability, we consider a constant wake. We will discover that the equilibrium phase space distribution for a localized wake has very different characteristics from that of a distributed wake given by the potential well distortion theory of Sec. 2.3. This appendix presents a clear and simplified derivation of many of the results previously obtained by Hirata [35].

A.1   Synchrotron Oscillation

First, let's consider the iteration for the synchrotron oscillation:

$$
\begin{pmatrix} x_1' \\ x_2' \end{pmatrix} = \begin{pmatrix} \cos \Delta\phi & \sin \Delta\phi \\ -\sin \Delta\phi & \cos \Delta\phi \end{pmatrix} \begin{pmatrix} x_1 \\ x_2 \end{pmatrix},
\tag{A.1}
$$

where, compared to the same iteration given by Eq. 2.6 and Eq. 2.7, we have changed the notation: here $x_1 = \tau/\sigma_{\tau 0}$ and $x_2 = \delta E/\sigma_{\epsilon 0}$. We have also ignored the effect of a tilted ellipse as described by Eq. 4.33.

With

$$U = \begin{pmatrix} \cos \Delta\phi & \sin \Delta\phi \\ -\sin \Delta\phi & \cos \Delta\phi \end{pmatrix}, \tag{A.2}$$

the iteration equations for the center of the bunch are:

$$< x_i' > = U_{ij} < x_j >, \quad \text{for } i = 1, 2. \tag{A.3}$$

We have used $< x_i >$ to denote the average of x_i with respect to the particle phase space distribution, namely, the center of the bunch in both coordinates. To obtain the fixed point of the center of the bunch, x_1^∞ and x_2^∞, we solve

$$\begin{pmatrix} x_1^\infty \\ x_2^\infty \end{pmatrix} = \begin{pmatrix} \cos \Delta\phi & \sin \Delta\phi \\ -\sin \Delta\phi & \cos \Delta\phi \end{pmatrix} \begin{pmatrix} x_1^\infty \\ x_2^\infty \end{pmatrix}, \tag{A.4}$$

and find the fixed point:

$$x_i^\infty = 0, \quad \text{for } i = 1, 2. \tag{A.5}$$

Next, consider the second-order moment

$$\sigma_{ij} = < x_i x_j > - < x_i >< x_j > . \tag{A.6}$$

The iteration equations for σ_{ij} are given by

$$\sigma_{ij}' = < x_i' x_j' > - < x_i' x_j' >$$

$$= U_{il} U_{jm} \left(< x_i x_j > - < x_i >< x_j > \right) = U_{il} \sigma_{lm} (U^T)_{mj}. \tag{A.7}$$

In matrix notation,

$$\sigma' = U \sigma U^T, \tag{A.8}$$

where U^T is the transpose of U. The fixed point for the second-order moment, σ^∞ is given by

$$\sigma^\infty = U \sigma^\infty U^T, \tag{A.9}$$

131

or, equivalently

$$\sigma^\infty U = U \sigma^\infty. \tag{A.10}$$

One solution is

$$\sigma^\infty = \begin{pmatrix} 1 & 0 \\ 0 & 1 \end{pmatrix}. \tag{A.11}$$

This is the usual solution where the bunch length is σ_{r0}, the energy spread is $\sigma_{\epsilon 0}$ and there is no mixing between the two coordinates (i.e., σ_{r0} and $\sigma_{\epsilon 0}$ are not coupled by the synchrotron oscillation in the linear RF bucket.)

A.2 Radiation Damping and Energy Fluctuation

In the absence of any synchrotron motion in the RF bucket, the radiation damping and the energy fluctuation due to the quantum nature of the synchrotron radiation can be described by the following iteration:

$$x_1' = x_1, \tag{A.12}$$

$$x_2' = \xi x_2 + \sqrt{1 - \xi^2} R. \tag{A.13}$$

Here R is a Gaussian random number with mean 0 and variance 1, and ξ is given by

$$\xi = \exp(-\frac{2T_0}{t_0}). \tag{A.14}$$

In most storage rings, the radiation damping time is much longer than the revolution time, $t_0 \gg T_0$. Expanding Eq. A.13 to first order with respect to the small quantity T_0/t_0 recovers the "old" damping and the energy fluctuation term in Eq. 4.65.

Averaging Eq. A.12 and Eq. A.13 gives iteration equations for the the center of the bunch:

$$< x_1' >=< x_1 >, \tag{A.15}$$

$$< x_2' >= \xi < x_2 > . \tag{A.16}$$

The fixed point for the center of the bunch is found from

$$x_1^\infty = x_1^\infty, \tag{A.17}$$

$$x_2^\infty = \xi x_2^\infty. \tag{A.18}$$

Since $\xi < 1$, the fixed point for the center of the bunch is:

$$x_1^\infty = \quad \text{arbitrary}, \tag{A.19}$$

$$x_2^\infty = 0. \tag{A.20}$$

Next, consider the iteration equations for the second-order moments σ_{ij}. For σ_{11}, we have

$$\sigma_{11}' =< x_1'^2 > - < x_1' >^2 =< x_1^2 > - < x_1 >^2 = \sigma_{11}. \tag{A.21}$$

For $\sigma_{12} = \sigma_{21}$, the result is

$$\sigma_{12}' =< x_1' x_2' > - < x_1' >< x_2' >=< x_1 \left(\xi x_2 + \sqrt{1 - \xi^2} R \right) > - \xi < x_1 >< x_2 >$$

$$= \xi \left(< x_1 x_2 > - < x_1 >< x_2 > \right) = \xi \sigma_{12}. \tag{A.22}$$

And finally, for σ_{22},

$$\sigma_{22}' =< x_2'^2 > - < x_2' >^2 =< \left(\xi x_2 + \sqrt{1 - \xi^2} R \right)^2 > - \xi^2 < x_2 >^2$$

$$= \xi^2 < x_2^2 > +1 - \xi^2 - \xi^2 < x_2 >^2 = \xi^2 \sigma_{22} + 1 - \xi^2. \tag{A.23}$$

In summary,

$$\sigma_{11}' = \sigma_{11}, \tag{A.24}$$

$$\sigma_{12}' = \xi \sigma_{12}, \tag{A.25}$$

$$\sigma_{22}' = \xi^2 \sigma_{22} + 1 - \xi^2. \tag{A.26}$$

The fixed point for the second order moment is given by

$$\sigma_{11}^\infty = \sigma_{11}^\infty, \tag{A.27}$$

133

$$\sigma_{12}^{\infty} = \xi \sigma_{12}^{\infty}, \tag{A.28}$$

$$\sigma_{22}^{\infty} = \xi^2 \sigma_{22}^{\infty} + 1 - \xi^2. \tag{A.29}$$

The fixed point is given by

$$\sigma_{11}^{\infty} = \quad \text{arbitrary}, \tag{A.30}$$

$$\sigma_{12}^{\infty} = 0, \tag{A.31}$$

$$\sigma_{22}^{\infty} = 1. \tag{A.32}$$

Radiation damping and quantum emission determine the equilibrium energy spread $\sigma_{\epsilon 0}$. Without the synchrotron oscillation, there is no coupling between the arrival time and the energy deviation. Thus, the bunch length can be arbitrary.

A.3   The Wake Field and the Full Iteration

We first examine the iteration equations for an idealized constant wake,

$$W(t) = \begin{cases} 0 & \text{if } t < 0, \\ W_0 & \text{if } t > 0. \end{cases} \tag{A.33}$$

From Eqs. 2.6 and 2.7,

$$x_1' = x_1, \tag{A.34}$$

$$x_2' = x_2 - \frac{Ne^2 L_0 W_0}{\sigma_{\epsilon 0}} \int_0^{+\infty} dy \, \rho(x_1 + y). \tag{A.35}$$

The iteration equations for the center of the bunch are

$$< x_1' > = < x_1 >, \tag{A.36}$$

$$< x_2' > = < x_2 > - \frac{Ne^2 L_0 W_0}{\sigma_{\epsilon 0}} \int_0^{+\infty} dy < \rho(x_1 + y) > . \tag{A.37}$$

Using an integral identity (which we will prove in the last section of this appendix,)

$$\int_0^{+\infty} dy < \rho(x_1 + y) > = \frac{1}{2}, \tag{A.38}$$

134

the iteration equations for the center of the bunch become

$$< x_1' >=< x_1 >, \tag{A.39}$$

$$< x_2' >=< x_2 > -g. \tag{A.40}$$

Here, g is defined by

$$g = \frac{N e^2 L_0 W_0}{2\sigma_{\epsilon 0}}. \tag{A.41}$$

Instead of finding the fixed point of the center of the bunch under the wake field alone, now consider the fixed point for the complete iteration. The complete iteration equations are given by:

$$< x_i > \text{(Radiation)} \longrightarrow < x_i' > \text{(Wake)} \longrightarrow < x_i'' > \text{(Oscillation)} \longrightarrow < x_i''' > . \tag{A.42}$$

The radiation contribution to the iteration is given by Eqs. A.15 and A.16; The wake field contribution to the iteration is given by Eq. A.39 and A.40 and the oscillation contribution to the iteration is given by Eq. A.3. Combining these yields

$$\begin{pmatrix} < x_1''' > \\ < x_2''' > \end{pmatrix} = \begin{pmatrix} \cos \Delta\phi & \sin \Delta\phi \\ -\sin \Delta\phi & \cos \Delta\phi \end{pmatrix} \begin{pmatrix} < x_1 > \\ \xi < x_2 > -g \end{pmatrix}. \tag{A.43}$$

The fixed point is found by setting

$$< x_1''' >=< x_1 >, \tag{A.44}$$

$$< x_2''' >=< x_2 > . \tag{A.45}$$

Simple algebraic manipulations yield

$$x_1^\infty = \frac{g}{(1 + \xi)\tan \frac{\Delta\phi}{2}}, \tag{A.46}$$

$$x_2^\infty = \frac{g}{(1 + \xi)}. \tag{A.47}$$

Note that x_1^∞ is the fixed point for the center of the bunch and x_2^∞ is the fixed point for the center of the energy deviation. While Eq. A.46 may still be consistent

with the results of the theory of potential well distortion, Eq. A.47 definitely is not. According to the potential well distortion theory of Sec. 2.3, the wake force does not have any effect on the bunch distribution in the energy deviation. The center of the energy deviation should always equal to zero, rather than be proportional to the bunch current as given by Eq. A.47. This shows that the equilibrium phase space distribution from distributed wakes and localized wakes are qualitatively different.

Next, we study the iteration for the second order moments σ_{ij} under a constant wake. One easily finds

$$\sigma'_{11} = <x'^2_1> - <x'_1>^2 = <x^2_1> - <x_1>^2 = \sigma_{11}, \qquad (A.48)$$

and, after a little algebra,

$$\sigma'_{12} = <x'_1 x'_2> - <x'_1><x'_2>$$

$$= <x_1 x_2> - \frac{Ne^2 L_0 W_0}{\sigma_{\epsilon 0}} \int_0^{+\infty} dy <x_1 \rho(x_1 + y)>$$

$$- <x_1><x_2> + \frac{Ne^2 L_0 W_0}{\sigma_{\epsilon 0}} <x_1> \int_0^{+\infty} dy <\rho(x_1 + y)>$$

$$= \sigma_{12} - \frac{Ne^2 L_0 W_0}{\sigma_{\epsilon 0}} \int_0^{+\infty} dy <(x_1 - <x_1>)\rho(x_1 + y)> . \qquad (A.49)$$

Using another integral identity proved in the last section of this appendix,

$$\int_0^{+\infty} dy <(x_1 - <x_1>)\rho(x_1 + y)> = \frac{\sqrt{\sigma_{11}}}{2\sqrt{\pi}}, \qquad (A.50)$$

we obtain

$$\sigma'_{12} = \sigma_{12} - \frac{g\sqrt{\sigma_{11}}}{\sqrt{\pi}}. \qquad (A.51)$$

Finally,

$$\sigma'_{22} = <x'^2_2> - <x'_2>^2$$

$$= <x^2_2> - \frac{2Ne^2 L_0 W_0}{\sigma_{\epsilon 0}} \int_0^{+\infty} dy <x_2 \rho(x_1 + y)>$$

$$+ \left(\frac{Ne^2 L_0 W_0}{\sigma_{\epsilon 0}}\right)^2 <\left(\int_0^{+\infty} dy \rho(x_1 + y)\right)^2> - <x_2>^2$$

$$+ \frac{2Ne^2 L_0 W_0}{\sigma_{\epsilon 0}} <x_2> \int_0^{+\infty} dy <\rho(x_1 + y)>$$

$$- \left(\frac{Ne^2 L_0 W_0}{\sigma_{\epsilon 0}} \right)^2 \left(\int_0^{+\infty} dy <\rho(x_1 + y)> \right)^2 .$$

$$= \sigma_{22} - \frac{2Ne^2 L_0 W_0}{\sigma_{\epsilon 0}} \int_0^{+\infty} dy <(x_2 - <x_2>)\rho(x_1 + y)>$$

$$+ \left(\frac{Ne^2 L_0 W_0}{\sigma_{\epsilon 0}} \right)^2 < \left(\int_0^{+\infty} dy \rho(x_1 + y) \right)^2 > -g^2. \qquad (A.52)$$

Using two identities from the last section of the appendix,

$$< \left(\int_0^{+\infty} dy \rho(x_1 + y) \right)^2 > = \frac{1}{3}, \qquad (A.53)$$

$$< \int_0^{+\infty} dy (x_2 - <x_2>)\rho(x_1 + y) > = \frac{\sigma_{12}}{2\sqrt{\pi \sigma_{11}}}, \qquad (A.54)$$

gives

$$\sigma_{22}' = \sigma_{22} - \frac{2g\sigma_{12}}{\sqrt{\pi \sigma_{11}}} + \frac{1}{3}g^2. \qquad (A.55)$$

Thus,

$$\sigma_{11}' = \sigma_{11}, \qquad (A.56)$$

$$\sigma_{12}' = \sigma_{12} - \frac{g\sqrt{\sigma_{11}}}{\sqrt{\pi}}, \qquad (A.57)$$

$$\sigma_{22}' = \sigma_{22} - \frac{2g\sigma_{12}}{\sqrt{\pi \sigma_{11}}} + \frac{1}{3}g^2. \qquad (A.58)$$

The full iteration equations for the second-order moments σ_{ij} are:

$$\sigma_{ij}(\text{Radiation}) \longrightarrow \sigma_{ij}'(\text{Wake}) \longrightarrow \sigma_{ij}''(\text{Oscillation}) \longrightarrow \sigma_{ij}'''. \qquad (A.59)$$

The radiation contribution to the iteration is given by Eqs. A.24, A.25 and A.26; the wake field contribution to the iteration is given by Eqs. A.56, A.57 and A.58; and the oscillation contribution to the iteration is given by Eq. A.8. These are the central results of this appendix. While they have been previously obtained by Hirata [35], our derivations are simpler and more straightforward.

The fixed points for the second-order moments are given by equation:

$$\sigma_{ij}''' = \sigma_{ij}.$$

$$(A.60)$$

After a lengthy calculations, we get

$$\sqrt{\sigma_{11}^\infty} = -ag + \sqrt{1 + (a^2 + b)g^2},$$

$$(A.61)$$

$$\sigma_{22}^\infty = 1 + bg^2,$$

$$(A.62)$$

$$\sigma_{12}^\infty = \frac{g}{\sqrt{\pi}(1 + \xi)}\sqrt{\sigma_{11}^\infty}.$$

$$(A.63)$$

Here,

$$a = \frac{1}{\sqrt{\pi}(1 + \xi)\tan\Delta\phi},$$

$$(A.64)$$

$$b = \frac{\pi(1 + \xi) - 6\xi}{3\pi(1 + \xi)(1 - \xi^2)}.$$

$$(A.65)$$

In Fig. A.1, we have plotted normalized bunch length $\sqrt{\sigma_{11}}$, normalized energy spread $\sqrt{\sigma_{22}}$, and normalized correlation coefficient $\sqrt{\sigma_{12}}$ as a function of g, which is proportional to the bunch current. The result is very different from the particle phase space distribution for the case of a distributed wake given by the theory of potential well distortion. According to the theory of potential well distortion, only the bunch length depends on the current. Energy spread does not depend on the current and is always equal to the value given by balancing the radiation damping and the quantum fluctuation of the synchrotron radiation. For a constant localized wake, Fig A.1 tells a different story. The energy spread increases monotonically as the bunch current increases, as does the mixing in the phase space between the arrival time and the energy deviation.

It is illuminating to see the transition from a localized wake to a distributed wake. In the multiparticle multiperiod tracking simulation discussed in Ch. 4, we break the iteration into many periods. We expect that as we increase the number of periods, we recover the result of a distributed wake. If we denote by N_s the number of periods
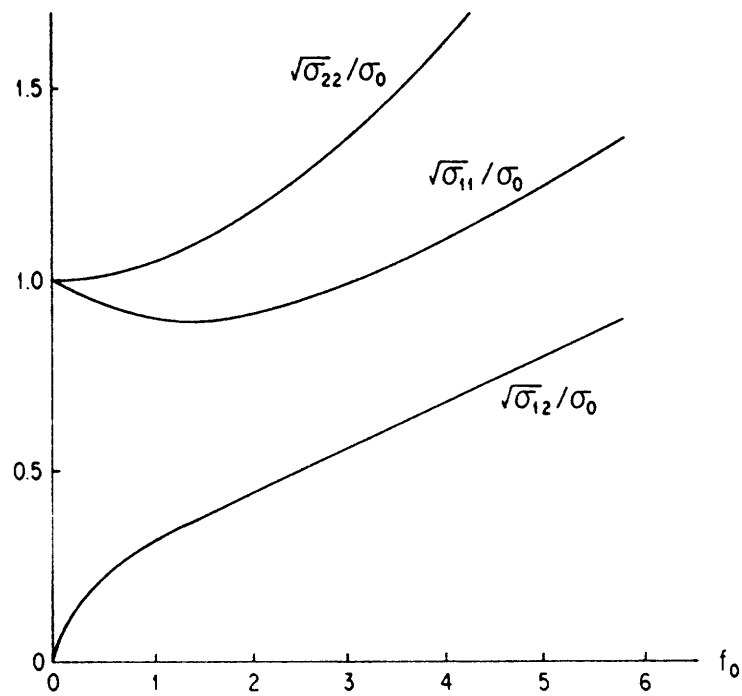
Figure A.1: Normalized bunch length $\sqrt{\sigma_{11}}/\sigma_0$, normalized energy spread $\sqrt{\sigma_{22}}/\sigma_{\epsilon 0}$ and the arrival time energy deviation mixing $\sqrt{\sigma_{12}}/\sqrt{\sigma_0\sigma_{\epsilon 0}}$ as functions of the strength of the wake force. The abscissa is labeled in units of 10^{-3}. (from Hirata, 1987.)

into which a constant wake is divided, all of the results in this appendix are still valid under the substitutions:

$$\Delta\phi \longrightarrow \Delta\phi/N_s, \tag{A.66}$$

$$\xi \longrightarrow \xi^{\frac{1}{N_s}}, \tag{A.67}$$

$$g \longrightarrow g/N_s. \tag{A.68}$$

As N_s approaches infinity, we find:

$$\lim_{N_s \to \infty} x_1^\infty = \frac{g}{\Delta\phi}, \tag{A.69}$$

$$\lim_{N_s \to \infty} x_2^\infty = 0. \tag{A.70}$$

Eq. A.70 is exactly what is expected from the theory of potential well distortion: The wake field does not have any influence on the bunch's distribution in the energy deviation. Eq. A.69 also agrees with the result of the potential well distortion when the bunch current is small. The restriction that the bunch current must be small comes from the the assumption we used to derive the iteration equations for the second order moments. We assume that the particle distribution in the phase space is always a bivariate normal distribution. Obviously this assumption is only valid when the bunch current is small. As shown in Sec. 3.6, higher moments can not be neglected when the bunch current is large. The assumption that the particle phase space distribution is always a bivariate normal distribution is critical for the several integral identities we have used (those derived in the last section of this appendix).

Now consider the limit of the second-order moments:

$$\lim_{N_s \to \infty} \sigma_{11}^\infty = -A + \sqrt{1 + A^2}, \tag{A.71}$$

$$\lim_{N_s \to \infty} \sigma_{22}^\infty = 1, \tag{A.72}$$

$$\lim_{N_s \to \infty} \sigma_{12}^\infty = 0. \tag{A.73}$$

Here

$$A = \frac{g}{2\sqrt{\pi}\Delta\phi}.$$ (A.74)

Equations A.72 and A.73 agree with the theory of potential well distortion: Energy spread does not depend on the bunch current and is equal to its natural value. There is also no mixing between the arrival time and the energy deviation. Eq. A.71 agrees with the result of the potential well distortion. It can be shown that when we assume a normal distribution in the arrival time and neglect all of the higher-order moments, the Haissinski equation 2.86 will reduce to an algebraic equation for the bunch length. The solution for the equation is identical to Eq. A.71.

The analysis of this appendix gives us a strong foundation for the introduction of periods in the multiparticle simulation. Most of the earlier works [19, 53, 54, 55, 56] on bunch lengthening simulations did not consider the possible differences of a localized wake and a distributed wake. As we demonstrate in this appendix for the case of a constant wake, the differences are significant as long as the differences between two wakes are significant. Our analyses also suggest that by using many periods, we can simulate a distributed wake by distributing a localized wake into may periods. When the wake field kicks are small in each period, the simulation results are very close to the results of a distributed wake. This is exactly the criterion we used to pick an optimal N_s for our multiparticle multiperiod simulations.

We have not discussed the stability of the fixed point under the full iteration. It turns out that the equilibrium bunch length in electron storage rings with localized wake can have a cusp-catastrophe behavior. Contrary to the results of the conventional theory for a distributed wake force, the system becomes bistable and exhibits hysteresis in some region of the parameter space. Interested readers can find a good discussion on this subject in reference [58].

In the last section of this appendix, we will outline the procedures to prove several

integral identities which have been used to derive the iteration equations for the center of the bunch and the second-order moments.

A.4 Some Integral Identities

We assume that the particle's phase space distribution is a bivariate normal distribution with the following second-order moments:

$$\sigma = \begin{pmatrix} \sigma_{11} & \sigma_{12} \\ \sigma_{21} & \sigma_{22} \end{pmatrix}. \tag{A.75}$$

The bivariate normal distribution can be explicitly written as

$$\psi(x_1, x_2) = \frac{1}{2\pi\sqrt{\det\sigma}} \exp\left(-\frac{1}{2}(x_i - <x_i>)(\sigma^{-1})_{ij}(x_j - <x_j>)\right). \tag{A.76}$$

The $\rho(x_1)$ is given by

$$\rho(x_1) = \int dx_2 \psi(x_1, x_2) = \frac{1}{\sqrt{2\pi\sigma_{11}}} \exp\left(-\frac{(x_1 - <x_1>)^2}{2\sigma_{11}}\right). \tag{A.77}$$

Now we are ready to prove the following integral identity:

$$I_1 = \int_0^{+\infty} dy <\rho(x+y)>$$

$$= \frac{1}{\sqrt{2\pi\sigma_{11}}} \int_0^{+\infty} dy <\exp\left(-\frac{(x+y-<x_1>)^2}{2\sigma_{11}}\right)>$$

$$= \frac{1}{2\pi\sigma_{11}} \int_{-\infty}^{+\infty} dx \int_0^{+\infty} dy \exp\left(-\frac{(x-<x_1>)^2}{2\sigma_{11}} - \frac{(x+y-<x_1>)^2}{2\sigma_{11}}\right). \tag{A.78}$$

Performing the double integral, we obtain

$$I_1 = \frac{1}{2}. \tag{A.79}$$

Other integral identities can be proved similarly.

Appendix B

List of Important Symbols

c :   speed of light in vacuum
e :   positron charge
τ :   arrival time deviation
δE :   energy deviation
σ_0 :   natural bunch length (s)
σ :   bunch length (s)
$\sigma_{\epsilon 0}$:   natural energy spread
σ_ϵ :   energy spread
N :   number of particles in a bunch
E_0 :   bunch energy
L_0 :   ring circumference
T_0 revolution time
ω_0 :   angular revolution frequency
I :   average bunch current $(= Ne/T_0)$
ρ :   bending radius
f_{rf} :   RF frequency
V :   peak RF voltage
ϕ_s synchrotron phase
η :   momentum compaction factor
ν_{s0} :   unperturbed synchrotron tune
ω_{s0} :   unperturbed synchrotron frequency $(= \nu_{s0}\omega_0)$
ν_s :   synchrotron tune
ω_s :   synchrotron frequency $(= \nu_s\omega_0)$
$W(t)$:   longitudinal wake field
$Z(\omega)$:   longitudinal impedance
ω_r :   resonator frequency
R :   shunt impedance
ξ :   dimensionless coupling constant
t_r :   radiation damping time
t_D :   Robinson damping time

Bibliography

[1] A.W. Chao, *Physics of Collective Beam Instabilities in High Energy Accelerators* (John Wiley & Sons, New York, 1993).

[2] M.S. Zisman, S. Chattopadhyay and J.J. Bisognano, LBL-21270, Dec. (1986).

[3] *Frontiers of Particle Beams: Intensity Limitations*, ed. by M. Dienes, M. Month and S. Turner, (Springer-Verlag, New York, 1992).

[4] R. Belbeoch et al., Proc. Natl. Conf. Moscow, 129 (1968).

[5] P. Amman, *IEEE Trans. Nucl. Sci.*, **NS-16**, 1073 (1969).

[6] I. Grigoriev et al., Proc. Intl. Conf. Yerevan, 121 (1969).

[7] B. Richter et al., Proc. Part. Accel. Conf. San Francisco 753 (1973).

[8] P.B. Wilson et al., *IEEE Trans. Nucl. Sci.*, **NS-24**, 1211 (1977).

[9] C. Pellegrini and A. Sessler, *Nuovo Cimento*, **53B**, 198 (1968).

[10] K. Robinson, CEAL Report TM-183 (1969).

[11] A. Lebedev, Proc. School Enrico Fermi XLVI, 185 (1969).

[12] C. Pellegrini and A. Sessler, *Nuovo Cimento*, **3A**, 116 (1971).

[13] A. Chao and J. Gareyte, SLAC SPEAR-Note 197 (1975).

[14] K.L. Bane, SLAC-PUB-5177, Feb (1990).

[15] A. Burov, *Particle Accelerators*, **28** 525 (1990).

[16] D. Brandt et al., CERN/LEP Report MD-35, July (1990).

[17] J. Haissinski, *Nuovo Cimento*, **18 B**, 72 (1973).

[18] H. G. Hereward, SLAC Report PEP Note No. 53 (1973).

[19] A. Renieri, Laboratori Nazionali di Frascati Report No. LNF-75/11R (1975).

[20] D. Boussard, CERN Lab II/RF/Int 75-2 (1975).

[21] R.D. Ruth and J.M. Wang, *IEEE Trans. Nucl. Sci.*, **NS-28**, 2405 (1981).

[22] L.J. Laslett, V.K. Neil and A.M. Sessler, *Rev. Sci. Instrum.*, **32**, 276 (1961).

[23] E. Keil and W. Schnell, CERN-ISR/TH/RF/69-48 (1969).

[24] A. A. Vlasov, *J. Phys. USSR*, **9**, 25 (1945).

[25] L.D. Landau, *J. Phys. USSR*, **10**, 25 (1946).

[26] A.G. Ruggiero and V.G. Vaccaro, CERN-ISR-TH/68-33 (1968).

[27] J.M. Wang and C. Pellegrini, Proc. of the 11th Int. Conf. on High-Energy Accelerators, CERN, 554 (1980).

[28] F. Sacherer, *IEEE Trans. Nucl. Sci.*, **NS-22**, 1393 (1977).

[29] F. Sacherer, *IEEE Trans. on Nucl. Sci.*, **NS-20**, 825 (1973).

[30] M. Messerschmid and M. Month, *Nucl. Instr. Meth.*, **136** 473 (1976).

[31] B. Zotter, *IEEE Trans. on Nucl. Sci.*, **NS-28**, 2435 (1981).

[32] T. Suzuki, Y. Chin and K. Satoh, *Part. Accel.*, **13**, 179 (1983).

[33] L. Rivkin et al., *IEEE Trans. Nucl. Sci.*, **NS-32**, 634 (1985).

[34] K. Oide and K. Yokoya, KEK-Preprint-90-10 (1990).

[35] K. Hirata, *Particle Accelerators*, **22**, 57 (1987).

[36] D. Brandt and A. Hofmann, Proc. of the 3rd European Particle Accelerator Conference, Berlin, 345 (1992).

[37] H.G. Hereward, Proc. 1975 ISABELLE Summer Study, BNL 20550 Vol. II, 555 (1975).

[38] M. Sands, SLAC Report 121 (1970).

[39] J.D. Jackson, *Classical Electrodynamics, 2nd ed.* (John Wiley & Sons, New York, 1975).

[40] P.B. Wilson, *AIT Conf. Proc.*, **87**, 450 (1982).

[41] A. Hofmann and J.R. Maidment, CERN Report LEP-168 (1979).

[42] A. Chao, *AIP Conf. Proc.*, **105**, 353 (1983).

[43] S. Chandrasekhar, *Rev. Mod. Phys.*, **15**, 1 (1943).

[44] P. Germain and H. Hereward, CERN Div. Report MPS/DL-75/5 (1975).

[45] B. Zotter, *IEEE Trans. Nucl. Sci.*, **NS-28**, 2435 (1981).

[46] T. Suzuki et al., KEK Preprint 82-26 (1982).

[47] W.H. Press et al., *Numerical Recipes in C, 2nd ed.* (Cambridge University Press, 1992).

[48] K. Steffen, DESY HERA Report 85-10 (1985).

[49] D.A. Edwards and M.J. Syphers, *An Introduction to the Physics of High Energy Accelerators* (John Wiley & Sons, New York, 1993).

[50] J. Schwinger, *Phys. Rev.*, **75**, 1912 (1949).

[51] S.M. Ross, *Stochastic Processes* (John Wiley & Sons, New York, 1983).

[52] R. Sedgewick, *Communications of the ACM*, **21**, 847 (1978).

[53] P.B. Wilson, et al., *IEEE Trans. Nucl. Sci.*, **NS-28**, 2525 (1981).

[54] T. Weiland, DESY 81/088, Dec. (1981).

[55] R. Siemann, *Nucl. Instr. Meth.*, **203**, 57 (1982).

[56] D. Brandt, CERN-ISR-TH-89-09, May (1982).

[57] J.M. Hammersley and D.C. Handscomb, *Monte Carlo Methods* (Methuen, London, 1964).

[58] K. Hirata, *Phys. Rev. Lett.*, **66**, 1693 (1991).